Lateral Torsional Buckling Strength of Sinusoidal Corrugated Web Plate Girders

Lateral Torsional Buckling Strength of Sinusoidal Corrugated Web Plate Girders

By

PHILIP A. REINDERS, B. ENG.

A Thesis Submitted to the School of Graduate Studies in Partial Fulfillment of the Requirements for the Degree Master of Applied Science

McMaster University

MASTER OF APPLIED SCIENCE (2022) (Civil Engineering)

McMaster University Hamilton, Ontario

TITLE:	Lateral Torsional Buckling Strength of Sinusoidal Corrugated Web Plate Girders
AUTHOR:	Philip A. Reinders, B. Eng. (McMaster University)
SUPERVISOR:	Dr. Georgios Balomenos
NUMBER OF PAGES:	i-104

LAY ABSTRACT

Corrugated web plate girders (CWPG) have grown in popularity due to their economic efficiency. No research has been presented in Canada and very minimal research has been published on the lateral torsional strength of CWPGs with sinusoidally corrugated webs.

This research studied the lateral torsional buckling (LTB) strength of CWPGs through the experimental testing of physical members and a new equation for the calculation of the LTB strength is proposed. This equation and design process was then numerically tested to determine its viability as a design process.

ABSTRACT

Corrugated web plate girders (CWPGs) have become an increasingly popular structural member in Canada in recent years. This is because of their economic efficiency over standard wide flange members. Although the flexural performance of such has been increasingly studied in recent years there is still advancements that can be made in their design. No research has been completed in Canada on the subject of lateral torsional buckling (LTB) strength and very minimal research has been published on sinusoidal CWPGs. In order to examine the LTB strength of a CWPG with a sinusoidally shaped web, nine specimens were loaded and failed in simply supported arrangement that favours lateral torsional buckling. Specimens were chosen to observe the difference in strength due to web thickness, web depth and variation in identical beams. All of the specimens recorded strengths that exceeded the theoretical design strengths confirming that the current design procedure is conservative. A trend of ultimate capacity increasing was observed with the increase of web thickness. The depth of the web had no significant effect on the torsional strength besides what is gained from the increased flange distance. An equivalent web thickness equation was formulated based on the results for the purpose of calculating LTB strength. To test the proposed equation a numerical analysis was run on a wider range of beams and compared with the testing results. It was determined the physical testing results can be effectively captured by the proposed equation among more than just the tested beams. Two additional analyses were prepared to lay the foundation for further investigation of the proposed equation. The first was a Monte Carlo simulation to test the risk of using the proposed equation which requires additional data. Secondly, a preliminary finite element analysis (FEA) model was developed and presented for future use to expand this research.

ACKNOWLEDGEMENTS

Firstly, I would like to thank my supervisor Dr. Georgios Balomenos, his encouragement and guidance has continuously enhanced my education and research. He always provided advice on my research and support and encouragement when motivation was low.

I would also like to thank the fantastic technicians at the advanced dynamic laboratory. Kent Wheeler and Paul Heerema's advice and teaching was incredibly useful in the preparation, construction and testing of the experimental program and they were always ready to overcome the challenges that arose throughout the process of my research.

Additionally, I would like to thank my fellow graduate students who helped guide me in areas of which I had limited experience. Their advice helped the process of learning smooth and painless.

I would also like to thank the National Science and Engineering Research Council (NSERC) for the funding provided through their Discovery Grant as well as Steelcon Fabrication Incorporated for the materials and fabrication support to complete this research.

Finally, I would like to thank my family and friends for their continued prayer and support in my studies. Particularly to my wife, Jessica, who has supported me through all the difficult and exciting moments of this journey.

TABLE OF CONTENTS

LIST OF FIGURES

LIST OF TABLES

Chapter 1: Introduction

1.1 Motivation

Corrugated web plate girders (CWPGs) have recently become more popular in the structural engineering industry. This is mainly due to the weight savings that can be achieved when utilizing these members in design. Designing lighter beams is not only economically advantageous but also provides overall lighter structures and therefore more efficient designs. A CWPG much like a standard built up wide flange (WF) member consists of two flanges connected by a web. However, the CWPG uses a thin-walled web that is corrugated into a specific shape to connect the two flanges together rather than a flat web. Figure 1-1 shows the use of CWPGs in a commercial building application (Steelcon Fabrication Inc. 2019a).

Figure 1-1: CWPGs in Commercial Building

Although CWPGs have become popular in recent years there is still hesitation to use them, mainly either due to the lack of knowledge of their performance or whether they meet standard design codes, because of the lack of relevant research in Canada. Additionally, there are advancements that can be made to these members to create more efficient design procedures particularly in the design checks for lateral torsional buckling (LTB) strength. Therefore, the motivation of this research is to increase the awareness of these types of beams.

1.2 CWPG Design Summary

For a typical WF beam the flanges resist most of the moment forces and the web resists most of the shear forces. To increase the bending strength of such members the flange distance (beam depth) is increased. This creates a larger force couple to resist the load but also makes the web very slender and susceptible to buckling. To avoid these issues, the design codes adopt a slenderness limit that dictates the depth to thickness ratio of the web to prevent this buckling which leads to webs being thicker than necessary for the factored shear forces. Corrugating the web provides an additional stability against buckling, because the shape in the web provides a stiffer web system without the need for added plate stiffeners. Thus, the web can be designed much thinner than a standard flat web beam (Driver et al. 2006). This means that when designing CWPGs the designer can more efficiently design the flanges and web to meet the force requirements instead of being governed by shear or flexural design.

Although the corrugated web provides additional shear stiffness there is the drawback of not resisting axial load in the web. In a typical WF member the flanges provide most of the flexural strength with a small percentage being provided by the web material and vice versa the web provides most of the shear strength with a small portion of the flange that is in line with the web provides the shear strength. This is not the case with CWPGs as the corrugation in the web removes

the ability of resisting axial load. Therefore, the flanges of a CWPG must resist all of the axial forces on the beam including the moment induced axial forces. Then the web is left to resist all of the shear forces acting on the beam. This concept is shown graphically in Figure 1-2.

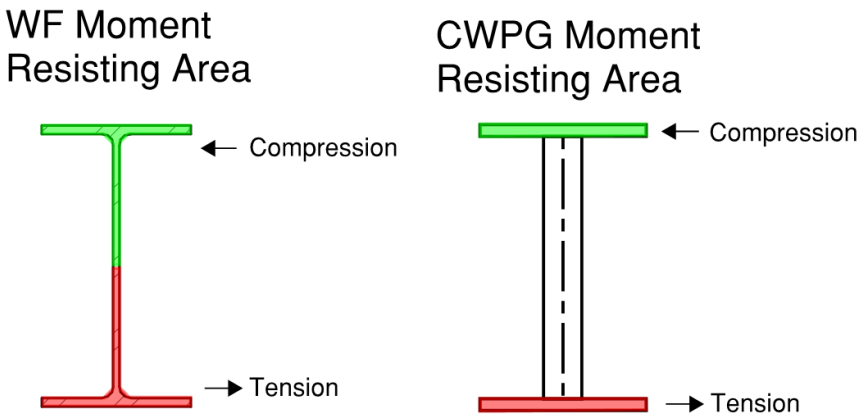

Figure 1-2: Moment Resisting Areas of Cross Sections

The moment resistance of CWPGs can easily be calculated then by following the S16 guidelines by calculating geometric constants like the section modulus utilizing the flange material alone (Canadian Standards Association 2014). This procedure can also be used to calculate the lateral torsional buckling (LTB) strength of a CWPG. Although the mechanics of CWPGs indicate that the web cannot contribute to the cross-sectional moment strength of the beam intuitively it can add strength to the LTB resistance of the beam. The web adds an additional rotational stability to the beam because of the corrugation's larger footprint on the flange (Sayed-Ahmed 2005; Nguyen et al. 2010; Elkawas et al. 2018). This means that by following the procedure of utilizing only the flange material to calculate the beam strength may be a conservative approach to the LTB design of a beam.

1.3 Summary of Past Research

CWPG's construction is made up of a corrugated web and two flat plate flanges. Several different methods can be used to achieve this configuration. The early process that was adopted was to bend a flat plate of steel using a brake press into a trapezoidal configuration. The trapezoidally corrugated web is then welded by hand to the upper and lower flanges (Figure 1-3). This configuration was useful for initial conceptual testing and to test the various moment and shear capacities (Elgaaly et al. 1997; Sause et al. 2003).

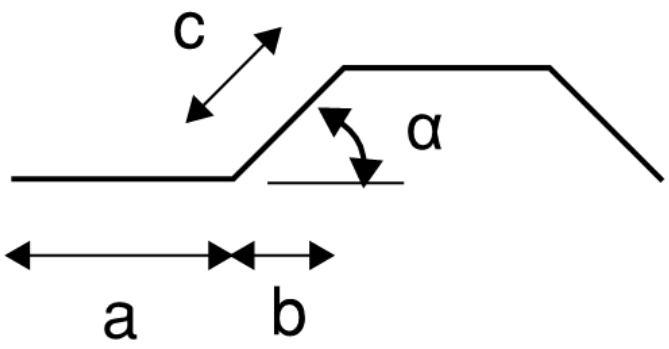

Figure 1-3: Corrugated Web Profile

These early tests showed the economic viability of such members and proved many of the initial assumptions of how a beam with a corrugated web would perform under shear and bending loads. Based on these early tests the current design process for designing such members was formulated. The flange material must resist all of the bending and axial forces and the corrugated web must resist all of the shear forces. Elgaaly et al. (1997) also established that there is no interaction between the bending resisted by the flanges and the shear resisted by the web, thus each portion of the beam can be designed very efficiently. Eq. (1) and Eq. (2) outline how to calculate elastic or plastic moduli, respectively, of the section for equal rectangles using the geometric properties

outlined in Figure 1-4. This geometric property can then be used to calculate the sectional moment resistance.

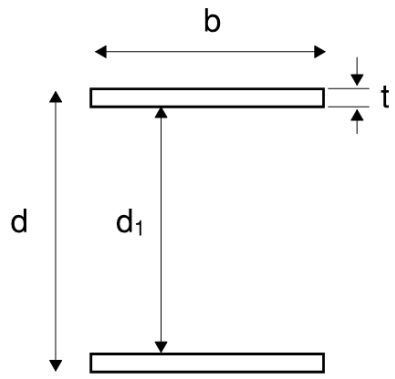

Figure 1-4: Equal Rectangles Geometric Parameters

$$S_x = \frac{b(d^3 - d_1^3)}{6d} \tag{1}$$

$$Z_x = bt(d - t) \tag{2}$$

This design procedure does accurately calculate the sectional moment strength, but it does not precisely estimate the LTB strength. For the simple sectional moment strength, the only material resisting bending load is the flanges; however, under unbraced long spans when bending is about the strong axis lateral torsional buckling can become the governing factor. Following the previously established design process all the by calculating the geometric constants with two floating flanges does provide a safe design. Eq. (3),(4) and (5) outline how to calculate the torsional constants C_w, J, and I_y.

$$C_w = \frac{(d - t)^2 b^3 t}{24} \tag{3}$$

$$J = \frac{2bt^3}{3} \tag{4}$$

$$I_y = \frac{tb^3}{6} \tag{5}$$

However, research into the LTB strength has revealed the previous procedure underestimates the actual LTB strength by anywhere from 15% to 30%. This is because the corrugation of the web provides a larger area of support to the flange preventing it from lateral buckling (Figure 1-5) (Sayed-Ahmed 2005; Nguyen et al. 2010; Elkawas et al. 2018).

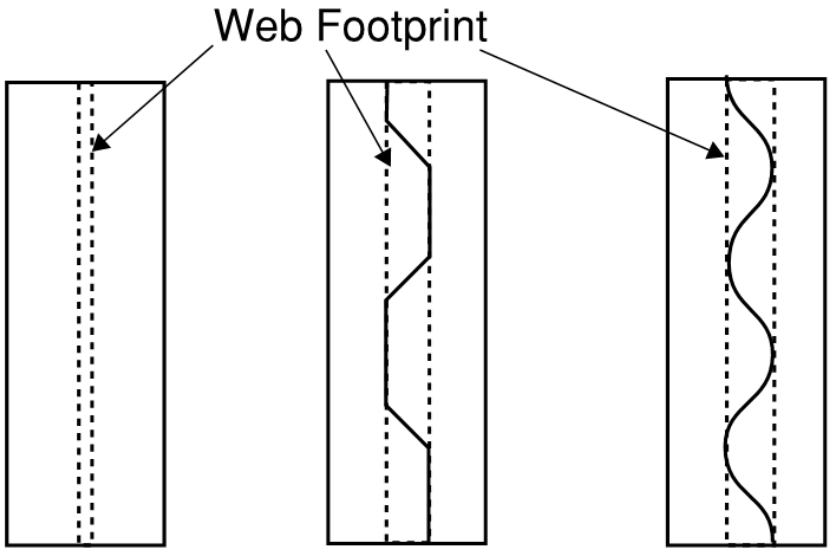

Figure 1-5: Web Footprint of a Wide Flange and CWPGs

To counter this overstrength one proposed solution has been to adjust the geometric properties of the beam to better estimate the LTB strength of a beam. Several models have been proposed to quantify the additional stiffness provided by the corrugated web. Lindner (1990) first studied the warping torsional constant C_w and the torsional constant J concluding that in comparison to a flat

web girder J remains the same and C_w is different, and thus proposed to adjust the warping torsional constant using the following formula and denoting it as I_w^* (Eq. (6))

$$I_w^* = I_w + \frac{c_w L^2}{E\pi^2} \tag{6}$$

$$c_w = \frac{(2d)^2 h_w^2}{8u_x(a+b)} \tag{7}$$

$$u_x = \frac{h_w}{2Gat_w} + \frac{h_w^2(a+b)^3}{25a^2Ebt_f^3} \tag{8}$$

In Eq. (6) I_w^* denotes the adjusted warping torsional constant of CWPG and I_w denotes unadjusted warping torsional constant. In Eq. (7) d is the total depth of the beam, h_w is the depth of the web and a and b are geometric properties of the web corrugation (Figure 1-3) In Eq. (8) G is the shear modulus of the steel, t_w is the thickness of the web material, E is the elastic modulus of the steel, b is the width of the flange and t_f is the thickness of the flange. Although Lindner (1990) did verify that the suggested method was valid through physical testing. The suggested method changed the warping torsional constant for different lengths of beams when typically, these constants are only based on sectional properties. Another proposed solution to the overstrength was to adjust the elastic critical moment (M_{cr}) that is utilized in most design codes for calculating LTB strength. Moon et al. (2009) proposed to calculate M_{cr} using Eq. (9) which then utilizes an adjusted reduced modulus (G_{co}) that accounts for the corrugation properties and a warping torsional constant $\overline{I}_w$ that uses the combination of unit warping values at different points of the corrugation. It should be noted the Canadian design code S16-14 simplifies Eq. (9) and Eq. (10) into one equation denoted by M_u (Canadian Standards Association 2014).

$$M_{cr} = \frac{\pi}{L}\sqrt{EI_y G_{co} J(1 + W^2)} \tag{9}$$

$$W = \frac{\pi}{L}\sqrt{E\frac{\bar{I}_w}{G_{co}J}} \tag{10}$$

$$G_{co} = \frac{a+b}{a+c}G \tag{11}$$

The drawback of proposed method by Moon et al. (2009) of adjusting M_{cr} with corrected shear modulus and warping torsional constant is that it does not take into account the additional stiffness in the moment of inertia in the weak axis (I_y) instead using the standard floating flange method. Other variations of this method were proposed in the following years (Nguyen et al. 2010; Zhang et al. 2011). The final proposed method to account for the overstrength caused by the increased stiffness of the web is to use an equation for equivalent web thickness. Sayed-Ahmed (2005) proposed that it is possible to quantify the increased stiffness through an equivalent web thickness method. By following the same procedure as a flat web beam, the CWPG web thickness would be increased with an equation that takes into account the geometric properties of the corrugation as proposed in Eq. (12) (Sayed-Ahmed 2005).

$$t_{eq} = t_w * \frac{s}{c} \tag{12}$$

Where t_{eq} is the resulting equivalent web thickness to be used in the remainder of the LTB calculations, t_w is the actual web thickness, s is the wavelength of the corrugation, and c is the projected length of the corrugation. Although this method makes sense intuitively it has only been proposed as a theory and has yet to be tested as a viable method of calculating the LTB resistance

of a CWPG. Other research has been published on the LTB strength of CWPGs used in a variety of configurations such as box girders, unsymmetrical flanges or using high strength steel for bridge design (Ibrahim 2014; Elkawas et al. 2018; Feng et al. 2019). Although these do provide insight into the performance of CWPGs as a whole, none of them propose solutions for beams being currently designed and used in Canada.

In Canada the major manufacturer of CWPGs fabricate these members with sinusoidal web profiles (Steelcon Fabrication Inc. 2019b). With the utilization of robotic automation the fabrication of such members can be done much more cost effectively. Using a sinusoidal profile allows the web to be cold rolled into the desired shape and a robotic welder can then provide a consistent fusion between the corrugated web and the flanges (Steelcon Fabrication Inc 2015). In comparison to the trapezoidal web configuration this is much more cost effective than hand bending plate and manually welding the flanges and web together. Although it is possible that the trapezoidal web configuration could be automated, as of writing this thesis the major manufacturers utilize the sinusoidal configuration. Since the majority of the past published research on CWPGs has been done on members with trapezoidal web profiles the previously proposed models for calculating LTB resistance may not apply to beams that have sinusoidal web profiles. There has been some research completed on CWPGs with sinusoidal web profiles outlining similar findings to the trapezoidal web profile beams showing that the flange carries all of the bending capacity and web carries all of the shear (Pasternak and Kubieniec 2010). As for the LTB resistance some physical testing was completed and many finite element simulations were completed in order to confirm that the current design approach of ignoring web contribution could be considered conservative (Hannebauer 2008). This physical testing of Hannebauers (2008) research focused primarily on the web thickness and other corrugation geometry and kept the depth

and flange size the same. Although the Hannebauers (2008) research provides useful information on sinusoidal beams, it examined beam sizes that are not common sizes used in Canada and the total selection was limited to just four beams. Finally, to the best of the author's knowledge, the Hannebauers (2008) research is published in German only, and thus, it might not be easily accessed by industry members looking at using these members.

1.4 Research Objectives

This research has three objectives. Firstly, this research studies experimentally the LTB resistance of a CWPG with a sinusoidally shaped web. The experimental program utilizes CWPGs with a variety of web thicknesses and depths that are available and utilized in the Canadian market to confirm the conservative nature and assumptions of the current design approach. Secondly, this thesis proposes a new method for the calculation of LTB strength of CWPGs that utilizes an equivalent web thickness method while calculating the critical elastic moment in typical LTB design procedures. The proposed methods viability is investigated through the numerical analysis of a full selection of common CWPGs that are available and determines the risk associated with adopting the new model for design. Finally, two numerical models are proposed and presented to be research further with a Monte Carlo simulation and a finite element analysis.

1.5 Thesis Outline

Chapter 1 of the thesis outlines the reasons that this research was undertaken outlining the gaps in previous research and the reasons that what has been completed is important to the academic community.

Chapter 2 outlines the experimental program that was completed. It discusses the development, construction and procedures for the laboratory testing of the LTB strength of CWPGs with sinusoidally shaped webs.

Chapter 3 discusses the results of the testing which will be used to develop the model for estimating the equivalent web thickness for the purpose of calculating LTB strength.

Chapter 4 develops and examines the capability of the proposed equation by investigating how it effects the strength of a large number of commonly used beams and the risk associated with adopting this equation into the design approach. It also provides the preliminary finite element modelling that was done and discusses the future development and use of the model to further this research.

Chapter 5 discusses the conclusions that can be drawn from all of the research and how future work could expand this research.

Chapter 2: Experimental Program

2.1 General

Nine CWPGs with sinusoidally corrugated webs, referred to hereinafter as SIN beams, were chosen to investigate their LTB resistance. The SIN beams that were selected were chosen to have a range of web thicknesses (t_w) and web depths (h_w) to examine the effects that the web properties have on their LTB strength. All of the chosen specimens are common sizes that are available in the Canadian market.

2.2 SIN Beam Specimens

All specimens were provided by Steelcon Fabrication Inc. (Brampton, ON, Canada) who is the major manufacturer and supplier of SIN beams in Canada. To indicate the cross sectional geometric properties the following designation will be used which is adopted from the SIN Beam Technical Guide (Steelcon Fabrication Inc. 2019b). WT[web thickness] [web height] / [flange width] x [flange thickness]. For example, specimen #1 is a WTA333/127x6 SIN Beam, and this means that it has a web thickness of 1.897 mm, a web depth of 333 mm and flanges that are 127 mm wide and 6 mm thick (Figure 2-1). Table 2-1 outlines the designation used for different SIN beam web thicknesses and Figure 2-1 graphically indicates the SIN beam cross sectional geometry.

Table 2-1: Designation for SIN Beams with Different Web Thicknesses

Web Thicknesses			
SIN Beam	gauge	mm	IN
WTA	14	1.897	0.075
WTB	12	2.657	0.105
WTC	11	3.038	0.12
WTF	8	4.176	0.164

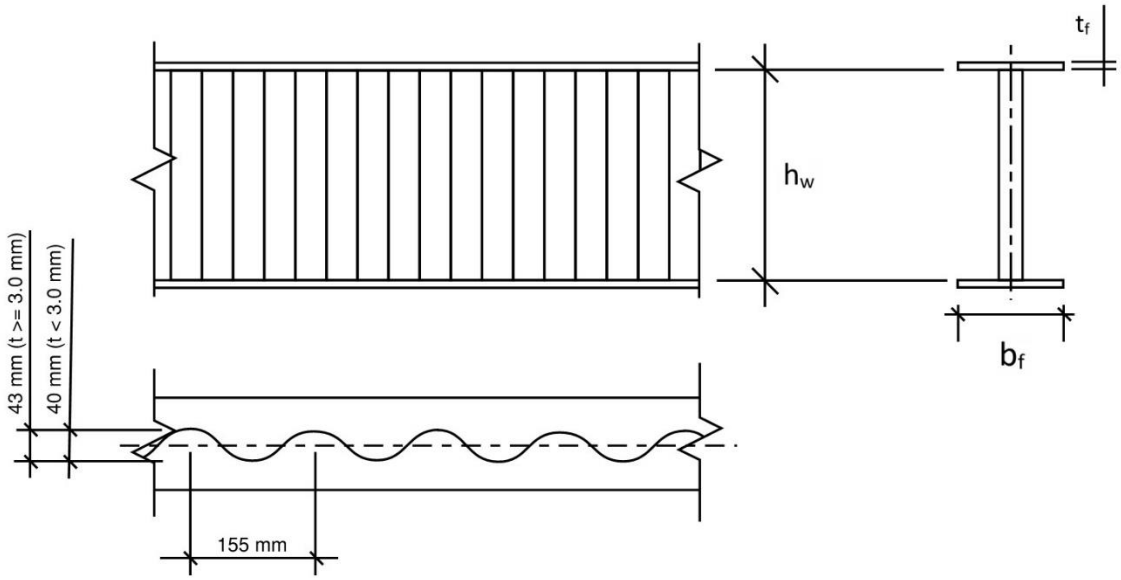

Figure 2-1: SIN Beam Geometric Parameters

All of the nine tested SIN beams have the same flange size of 127 mm width by 6 mm thickness. This standardizes the flange contribution to the moment strength isolating the web parameters as the cause of strength fluctuation. To investigate the effect of the corrugated web, two main groups of beams were chosen to examine a specific parameter. The first group of four SIN beams had the same web thickness (1.897 mm) but different web depths, i.e., 333 mm (WTA333), 500 mm (WTA500), 610 mm (WTA610), and 750 mm (WTA 750). The second group of four SIN beams had the same web depth (333 mm) but different web thicknesses, i.e., 1.897 mm (WTA333), 2.657 mm (WTB333), 3.038 mm (WTC333), and 4.176 mm (WTF333). Finally, one additional WTA333 beam was procured to create a small sample of identical beams to examine the fluctuation of strength in identical beams.

Table 2-2: SIN Beam Specimens

Test #	SIN Beam Size
1	WTA333/127x6
2	WTA333/127x6

3	WTA500/127x6
4	WTA610/127x6
4	WTA610/127x6
5	WTA750/127x6
6	WTB333/127x6
7	WTC333/127x6
8	WTF333/127x6
9	WTA333/127x6

Each SIN beam was procured at a length of 5250 mm in length. Utilizing the SIN Beam Technical Guide this length was chosen to ensure all of the beams would have a lateral torsional buckling failure mode prior to any other forms of failure. Mill test reports were obtained from the suppliers of the beams used in the testing and they show a yield strength of 408 MPa and an ultimate strength of 562 MPa.

To fabricate the SIN beam specimens a robotic fabrication system was used. The web was cold rolled to the shape outlined in Figure 2-1, the flanges are then placed alongside the web and a robot welder provided a consistent fillet weld along one side of the web. This ensures all beams were consistent in fabrication. To cap the ends of the beams a 10 mm plate was welded to the flanges and the web to prevent local buckling at the ends during the test.

2.3 Test Setup

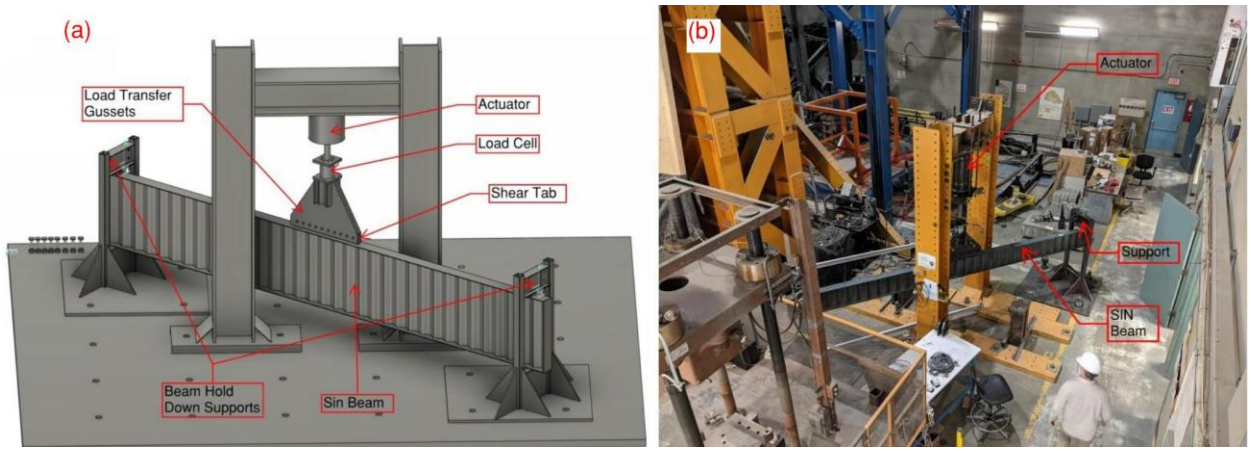

Figure 2-2: Testing Apparatus (a) 3D Rendering (b) Constructed Setup

Figure 2-2 shows the SIN beam test setup. To ensure that all the selected SIN beams fail under an LTB mode prior to a local buckling an unbraced length of 5000 mm is required. The main constraint when developing the testing apparatus was creating a 5000 mm unbraced length under the laboratory constraints and preventing the loading solution from bracing the compression flange. A traditional simply supported beam configuration would be sufficient in providing the internal moment required, however the hydraulic actuator applying the force to the beam would then provide bracing to the compression flange preventing LTB failure. To avoid this issue the applied load is flipped and provided as a tension force to the top of the beam. This creates an internal moment force placing the top flange in tension and the bottom flange in compression while also leaving the bottom flange to freely move as needed. Figure 2-3 shows graphically the beam configuration and beam response.

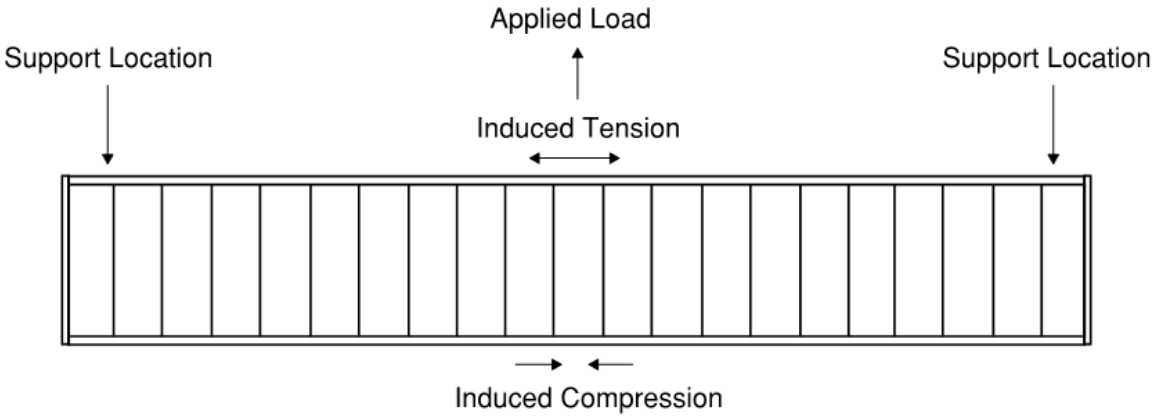

Figure 2-3: Beam Loading Configuration

Since the simply supported configuration is being used in an inverted manner the two ends of the beam are held down to the rigid floor of the lab by capture devices. The capture device consists of a 25 mm thick plate bolted to the floor with three large anchors. Two HSS columns are welded to the plate and stiffeners are added to transfer the load seamlessly from the columns down into the laboratory floor. A short W310x21 is spanned between the two columns and is used as the support to hold the end of the beam down. Figure 2-4 shows the constructed hold down supports. Since the connection at the ends of the beam are to simulate a shear connection there is no torsional restraint.

Figure 2-4: Beam Hold Down Supports

To apply the point load to the beam a hydraulic actuator is used to apply a tensile force to the top of the beam. To avoid a local flange failure at the location of loading a 1000 mm long plate was welded to the top of each beam. Ten, one inch diameter bolts are used to distribute the load evenly to the beam without overstressing either the flange or the web of the beam or any part of the load transfer system. This also allows the flange of the beam to rotate if needed during the test. Figure 2-5 shows the apparatus that transfers the load from the load cell to the top of the beam. The entire testing apparatus is designed to be able to apply 1000kN of applied force at the actuator location.

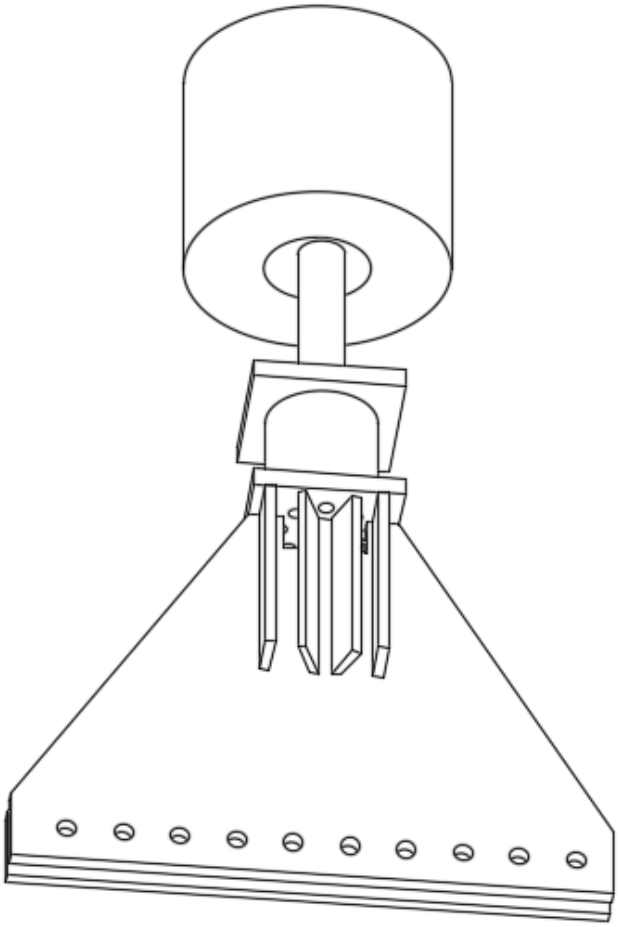

Figure 2-5: Load Distribution System

2.4 Test Instrumentation

A combination of strain gauges and displacement gauges are used to monitor and record the SIN beams responses throughout the experiments. Figure 2-6 illustrates the locations of all of the strain gauges on the SIN beam.

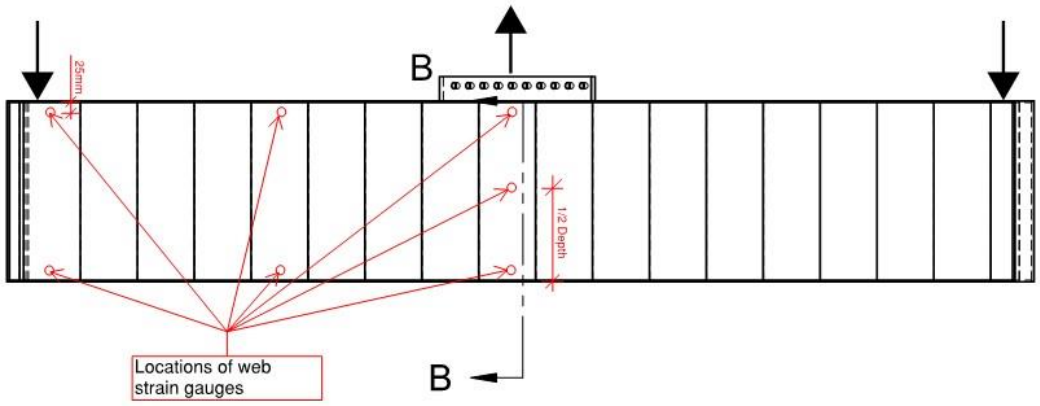

Figure 2-6: SIN Beam Strain Gauge Placement

Ten strain gauges are installed on every beam specimen to monitor the stress in each beam, seven of which are installed on the web and three of which are installed on the compression flange. From the seven gauges on the web two of the gauges are placed at the support location, three are placed at the center of the beam and the remaining two gauges are placed halfway between the support and center of the beam. This configuration was used to monitor the stress of the web across the height at the most critical point for LTB, the center. It also allows the stress in the web to be monitored across the length of the beam. A preliminary test was run with additional gauges installed in a rosette configuration; in this configuration the horizontal strain was 0 at all locations confirming the strain only acts in the vertical direction. Therefore, for the remaining tests all of the web strain gauges were installed in the vertical direction to record the shear strain. Three strain gauges were installed on the lower flange (compression flange) in the longitudinal direction to record the axial strain. Similar to the web gauges one is placed at the support location, one at the center of the beam and one halfway between the other two locations.

Ten displacement gauges are also installed on each beam. Figure 2-7 shows the locations of all ten displacement gauges.

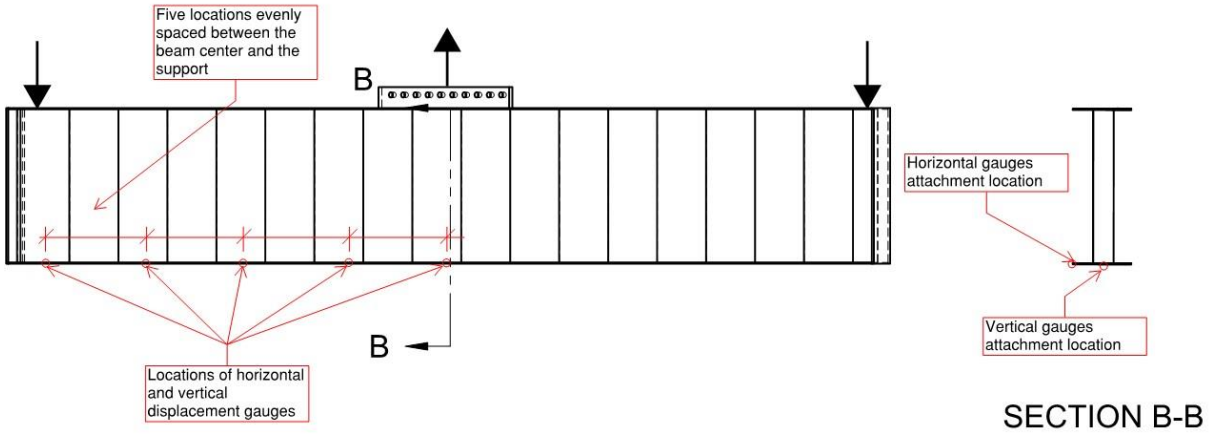

Figure 2-7: SIN Beam Displacement Gauge Placement

Two string pots are connected to the lower flange of each beam at five equidistant locations between the end support and the center of the beam. One string pot is connected to underside of the flange to measure the vertical displacement over the duration of the test. The second string pot is connected to the edge of the bottom flange to measure the horizontal displacement over the duration of the test. Finally, in between the beam shear tab and the hydraulic actuator is a load cell to record tensile force that applied to the beam over the duration of the test. The load cell is rated for loads up to 1000kN in tensile force which is greater than the maximum possible resistance of the chosen beams. Finally, the instrumentation was only placed on one side of the beam assuming that the beam response is symmetrical. Although symmetry of the beam is out of the scope of this study it should be examined in future studies.

2.5 Test Procedure

A static loading procedure is applied to all of the SIN beams using the hydraulic actuator. The applied static load is steadily increased using displacement control of the actuator. A rate of 5 mm per minute is used until the beam reaches 60% of the predicted ultimate capacity. From there the load rate is reduced to 0.5 mm per minute to better observe the beams performance. Throughout the test photographs and timelapse videos are recorded of the beams (Figure 2-8b). Once the beam reaches its failure point, a local buckling that occurs after an LTB failure (Figure 2-8c), or the deflection in the beam will impact the test apparatus (Figure 2-8a) then the test is ceased and final photographs of the beam are taken. The beam is then unloaded, and photographs of the beam's residual deformation are taken (Figure 2-8d).

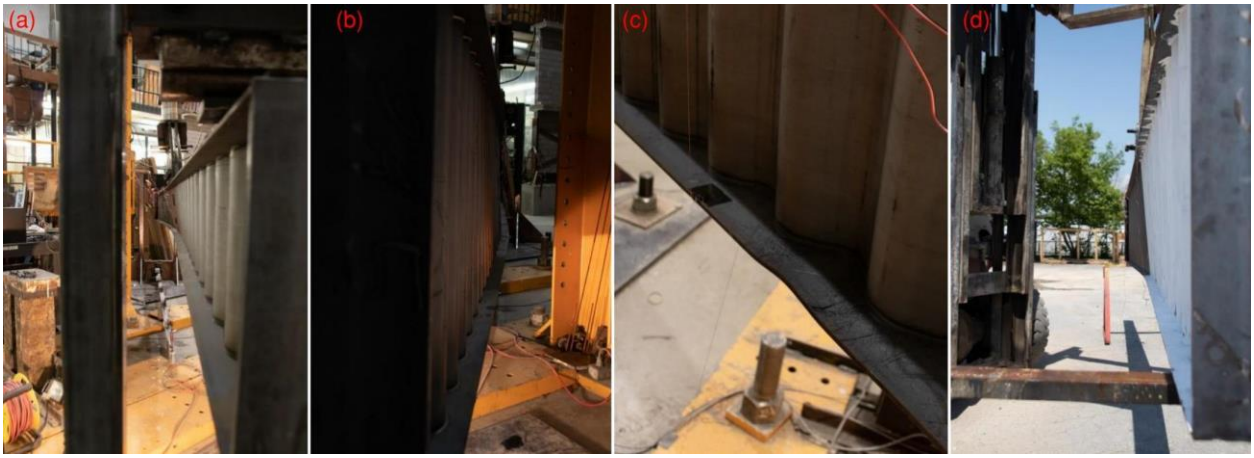

Figure 2-8: (a) Large Beam Deflection (b) 60% estimated Load (c) Local Flange Buckling (d) Residual Deformation

Chapter 3: Experimental Results

3.1 Summary of Tests

All nine SIN beams that were tested exhibited a higher capacity than the theoretical capacity that is calculated using the standard procedure outlined in the SIN Beam Technical Guide (Steelcon Fabrication Inc. 2019b). Photos of all the test can be found in Appendix A. The average overstrength in all of the beams was 49% with the smallest in all the tests coming from the WTA750/127x6 with an overstrength of 30%. This confirms the conservative nature of the current LTB design procedure of CWPGs. Table 3-1 summarizes the test results showing the peak deflections in both horizontal and vertical directions as well as the theoretically calculated moment strength using the conventional method ($Mr_{theoretical}$), and the peak or ultimate experimental moment strength (Mr_{ex}). The experimental moment strength is the induced moment in the beam resulting from the point load applied to the top of the beam. This was chosen as the comparable value as typically a moment value is used to define LTB strength. The calculation of $Mr_{Theoretical}$ can be found in Appendix B.

Table 3-1: SIN Beam Tests Summary

Test #	SIN Beam Size	$Mr_{theoretical}$ (kNm)	Mr_{ex} (kNm)	Corresponding Vertical Deflection (mm)	Corresponding Horizontal Deflection (mm)	Overstrength (%)
1	WTA333	39.86	103.9	26.9	26.2	62%
2	WTA333	39.86	86.5	48.8	80.0	54%
3	WTA500	55.47	96.1	32.2	86.6	42%
4	WTA610	66.18	119.0	36.9	103.0	44%
5	WTA750	80.03	113.6	51.7	93.6	30%
6	WTB333	39.86	90.5	22.6	16.5	56%
7	WTC333	39.86	97.8	45.3	93.4	59%
8	WTF333	39.86	100.4	67.6	108.0	60%
9	WTA333	39.86	82.1	52.1	76.5	51%

The stress and strain values were also recorded for each of the tested beams, where the peak stresses and strains occurred as expected in the center of each tested beam. Table 3-2 outlines the peak stress values calculated by finding the axial force in the bottom flange using the floating flange method and the shear force in the web and converting them to stress values.

Table 3-2: Stress and Strain Values of the Beam in the Center of the Beam

Beam	Web Strain (μstrain)	Web Stress (MPa)	Flange Strain (μstrain)	Flange Stress (MPa)
WTA333-1	0.0013	98.66218	0.00976	394.9622
WTA333-2	0.0054	82.15912	0.00332	328.8975
WTA500	0.00544	78.00368	0.00857	312.2625
WTA610	0.00369	47.7674	0.00635	194.3467
WTA750	0.00631	61.70226	0.0292	251.0422
WTB333	0.00539	47.91776	0.0166	195.6715
WTC333	0.00269	61.37112	0.00688	344.1067
WTF333	0.0032	57.97437	0.00581	371.6732
WTA333-9	0.0038	43.30839	0.0102	381.6542

As shown in Table 3-2 all tested beams did not reach an overall yielding point. This is because a local flange failure occurred rather than a full flange yielding. Additionally, all of these reported strain values are recorded at the center of the beam only, because strain values at other locations of the tested beams were very small, since the load is primarily concentrated at the center of the beam and reduces towards to either end of the beam.

3.2 Individual Test Results

For reference in the following discussions Figure 3-1 and Figure 3-2 will be used in the legends of some of the figures. Figure 3-1 shows the locations of the horizontal displacement and Figure 3-2 shows the locations of the vertical displacement.

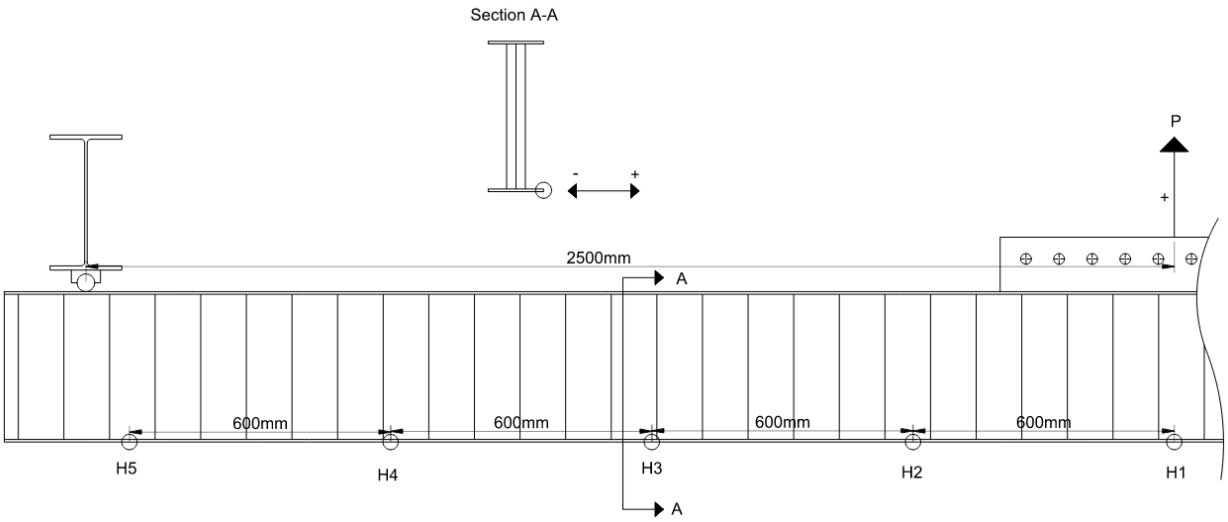

Figure 3-1: Locations of Horizontal Displacement

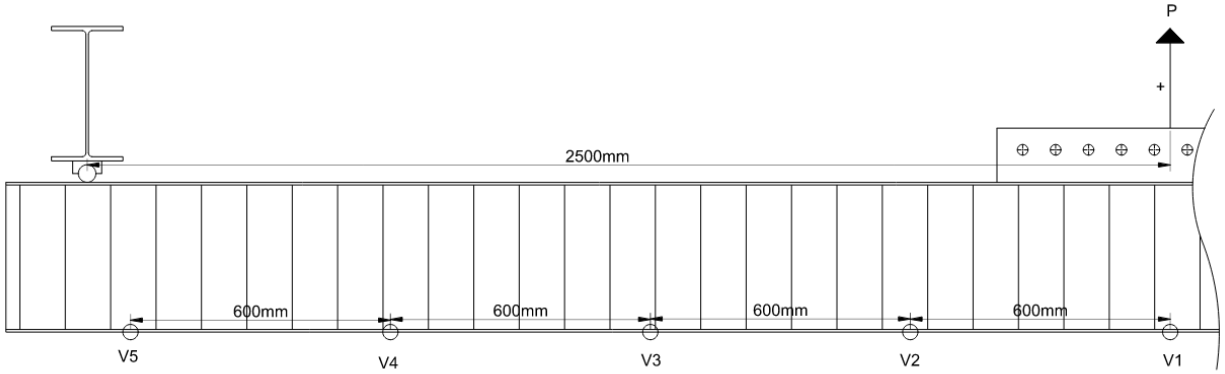

Figure 3-2: Locations of Vertical Displacement

3.2.1 Test #1 - WTA333/127x6 –1

The first test that was completed was a WTA333/127x6 SIN beam. At the center of the first SIN beam significant deflection began to occur at around 80 kNm and a peak moment strength of 103.9 kNm was reached. Significant deflection is defined by the standard code limit (S16-14) of L/360 which equates to around 15mm. This peak load corresponded to a peak horizontal deflection of 26.2 mm. The ultimate strenght of the Test #1 SIN beam is 62% stronger than the theoretically calculated moment strength. Figure 3-3 shows the horizontal deflections along the beam versus the moment force on the SIN beam over the duration of the Test #1 SIN Beam.

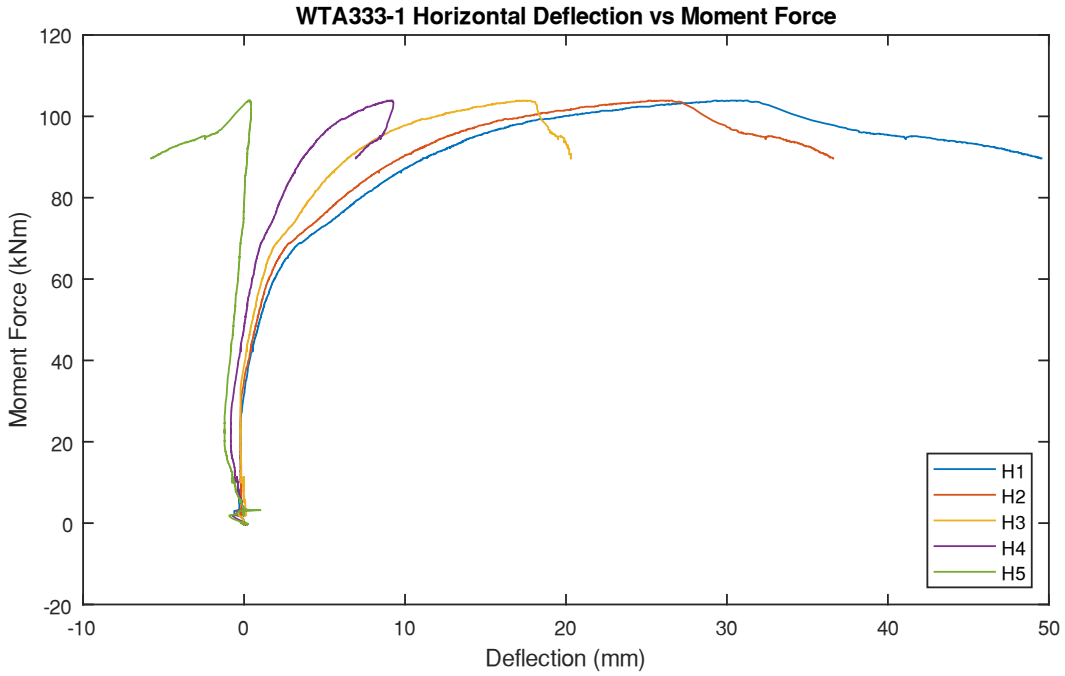

Figure 3-3: WTA333-1 Horizontal Deflection vs Moment Force

As presented in Figure 3-3 the horizontal displacement gauge at the end of the Test #1 SIN beam, H5, had a final deflection in the negative direction. This is because after the beam reached its peak load and underwent local flange buckling it was then unloaded. The negative final value is seen because the residual deformation of the beam pushes the extreme ends back to a negative final position. Inital deflection variations are also noticed early on in the testing this is due to the SIN beam settling into the support location which presents itself as erratic movement in the data. Figure 3-4 shows the vertical deflections along the SIN beam versus the moment force on the beam over the duration of the Test #1.

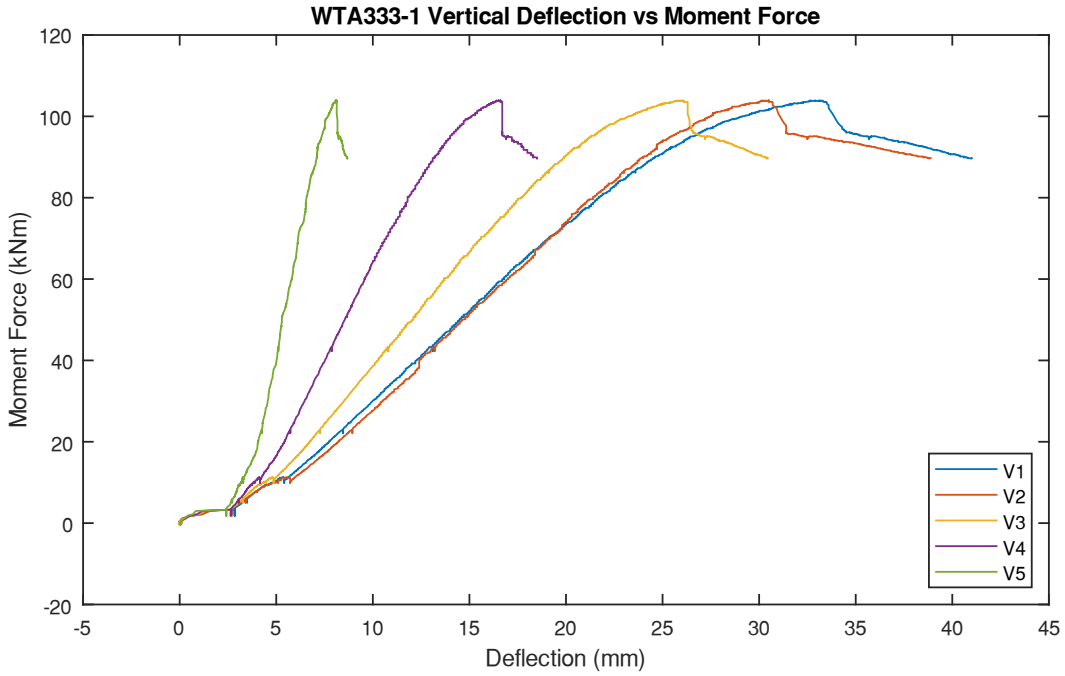

Figure 3-4: WTA333-1 Vertical Deflection vs Moment Force

Similarily, in Figure 3-4 the vertical displacement of the Test #1 SIN beam had erratic initial deflections early in the test which confrims this is due to the SIN beam settling into the support location.

3.2.2 Test #2 - WTA333/127x6 – 2

The second test completed was once again a WTA333/127x6 SIN beam this was chosen to ensure the testing procedure was consistent and repeatable. By using a similar beam, the testing practices could be perfected. Significant horizontal deformation began to occur earlier but still similar in th WTA333/127x6 – 2 (i.e., beginning around the 60 kNm mark) compared to the WTA333/127x6 – 1. Also, Test #2 SIN beam reached an ultimate strength of 86.5 kNm which was much less compared to the peak moment strength of 103.9 kNm that was reached in Test #1. However, the Test #2 SIN beam reached a peak horizontal deflection of 80.0 mm before the local flange buckling occurred, and thus, performing more ductile than the Test #1 SIN beam. The same ductile behavior

was observed comparing the vertical deflections of Test #2 and Test #1 SIN beams. The overstrength observed for the Test #2 SIN beam was 54%. The more ductile behavior and the smaller ultimate capacity is likely due to the testing apparatus being adjusted from test to test. The connection of the beam to the loading apparatus from Test #2 onward was less stiff, this will be discussed further in Section 3.5. Figure 3-5 shows the horizontal deflections along the beam versus the moment force on the beam over the duration of the Test #2.

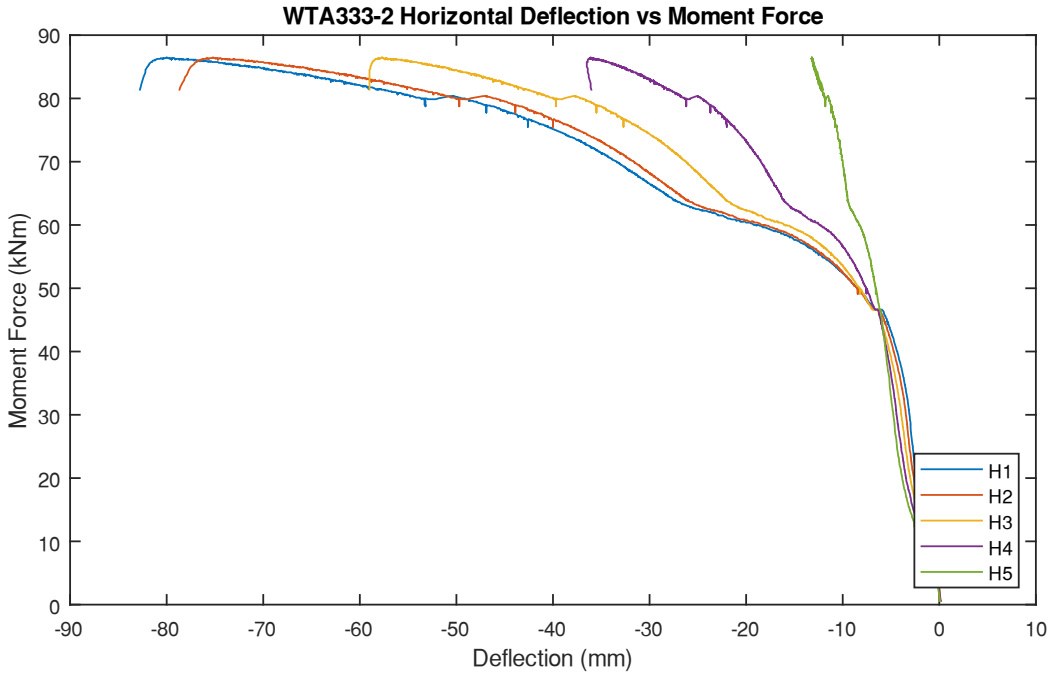

Figure 3-5: WTA333-2 Horizontal Deflection vs Moment Force

This time the Test #2 SIN beam slip at the support location is minimal however during this test the bolts that were placed in the shear tabs of the hold down support beams slipped at the 45 kNm mark. This caused the SIN beam to suddenly deflect by a few millimeters. Figure 3-6 shows the vertical deflections along the beam versus the moment force on the beam over the duration of the Test #2.

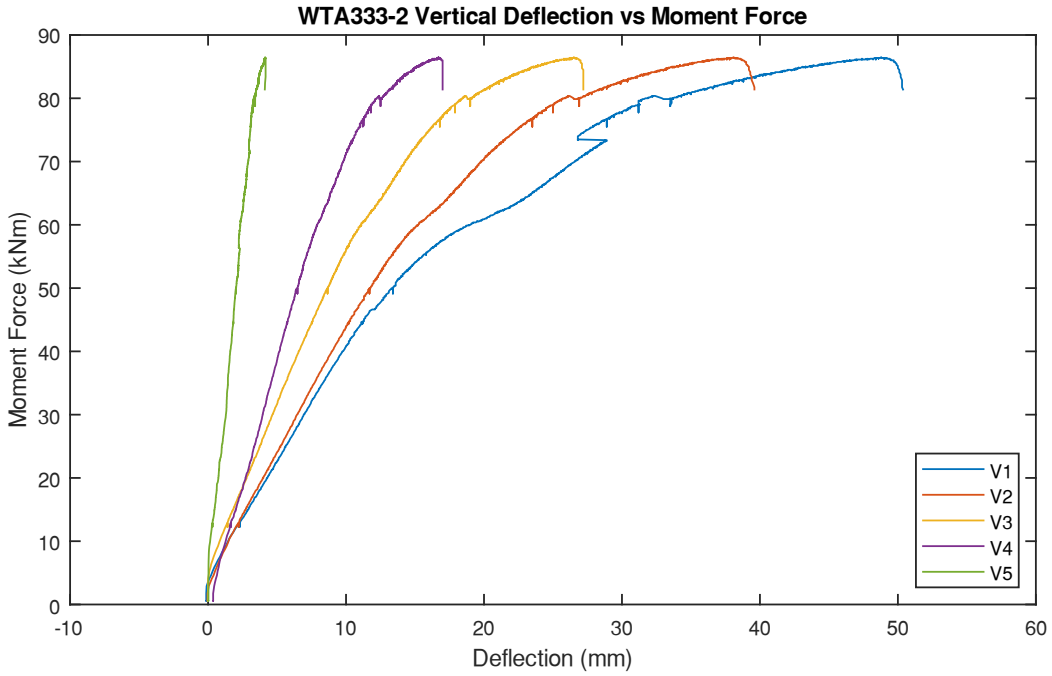

Figure 3-6: WTA333-2 Vertical Deflection vs Moment Force

3.2.3 Test #3 – WTA500/127x6

The third SIN beam that was tested was the WTA500/126x6 SIN beam. As expected, the tested SIN beam had a larger strength compared to the theoretical capacity. Significant deformation began to occur at the 60 kNm mark where after this point the SIN beam reached a peak strength of 96.1 kNm with a corresponding horizontal deflection of 86.6 mm. A hardening trend was also noticed in this Test #3 where the SIN beam reached a load and ceased to resist further load for a short time before continuing to resist more load again. Figure 3-7 shows the horizontal deflections along the beam versus the moment force on the beam over the duration of the Test #3.

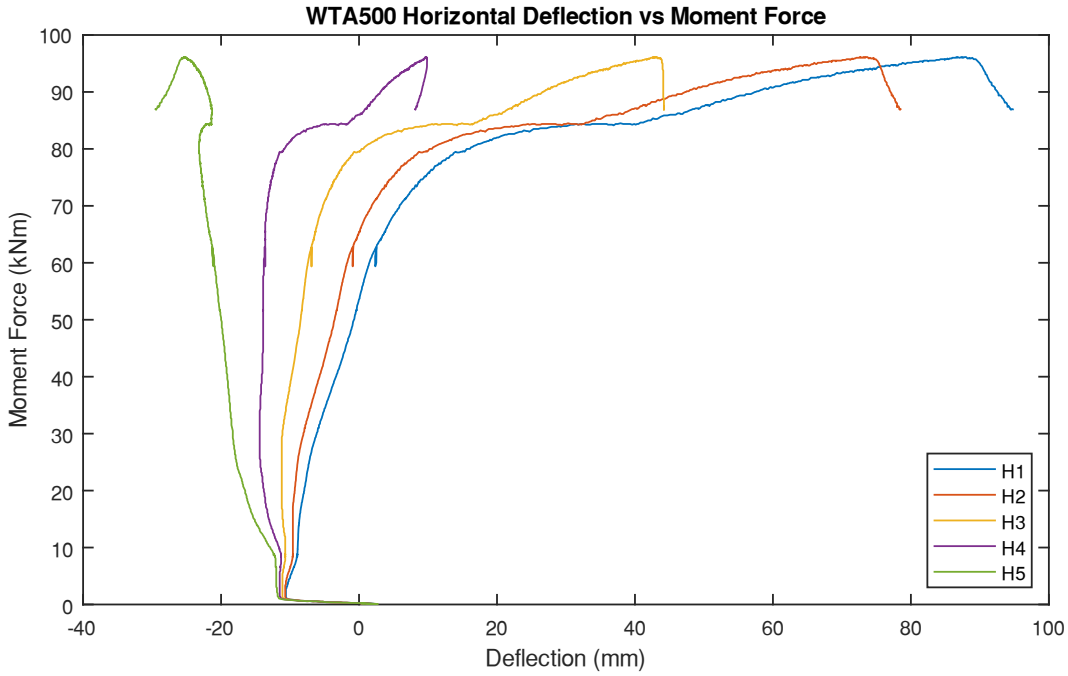

Figure 3-7: WTA500 Horizontal Deflection vs Moment Force

Similar to the Test #1, for the Test #3 SIN beam the settling into the support location is observed at the beginning of the test this time in all five displacement gauges. Figure 3-8 shows the vertical deflections along the SIN beam versus the moment force on the SIN beam over the duration of the Test #3.

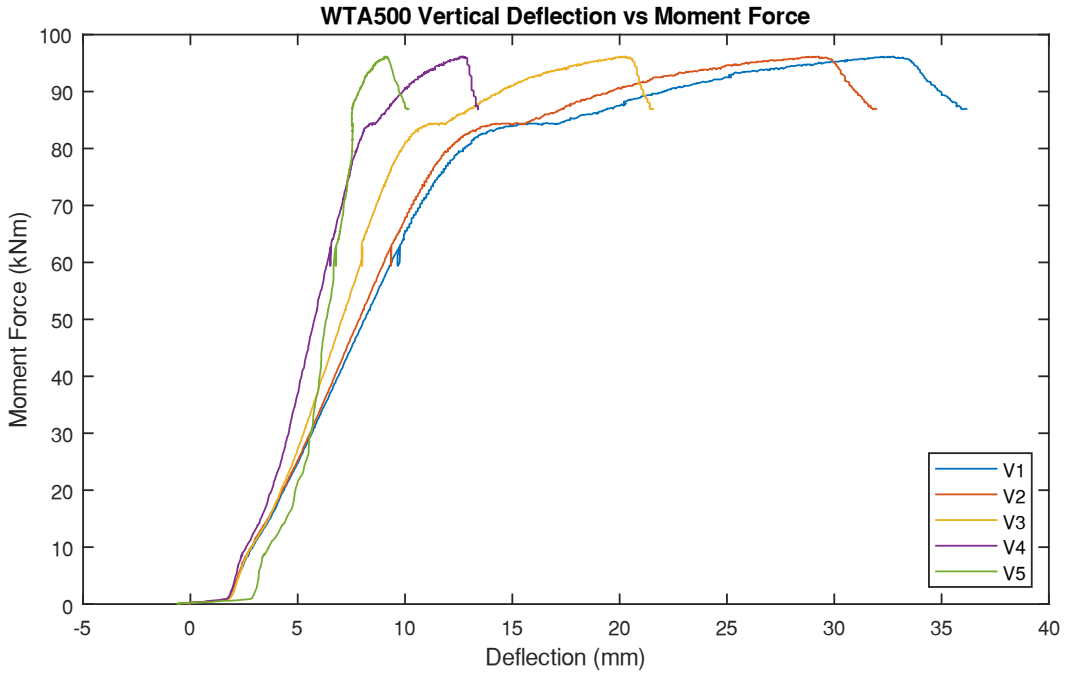

Figure 3-8: WTA500 Vertical Deflection vs Moment Force

3.2.4 Test #4.1 – WTA610/127x6

The Test #4.1 completed was a WTA 610/127x6 SIN beam. Similar to the previous tests (i.e., Test #1, Test #2, Test#3) the Test #4.1 SIN beam was loaded into the apparatus and all the instrumentation discussed in the experimental section was installed on the beam. The test began and the beam started to resist load. Shortly after the start of the test the displacement information being monitored was not following the typical trends of the previous tests (Figure 3-9). It was at this point that a local flange buckling at the support location was observed. The test was immediately ceased, and the beam was unloaded. Figure 3-9 shows the local flange failure.

Figure 3-9: WTA610 Local Flange Failure

With the Test #4.1 SIN beam in the unloaded position there was no observable residual deformation from the test apart from the local flange buckling at the support location. A 13 mm doubler plate was then added to the top of the flange to at either support to prevent further local buckling. Thus, for all of the remaining tests a doubler plate was added as well.

3.2.5 Test #4.2 – WTA610/127x6 (Retest)

With the doubler plates fitted and confirmation that the beam integrity had not been compromised by the initial test a retest of the WTA610/127x6 SIN beam was then completed. Significant deformation began to occur at the 90 kNm mark after this the beam reached a peak strength of 119 kNm with a corresponding horizontal deflection of 103 mm. Figure 3-10 shows the horizontal deflections along the beam versus the moment force on the beam over the duration of the Test #4.2.

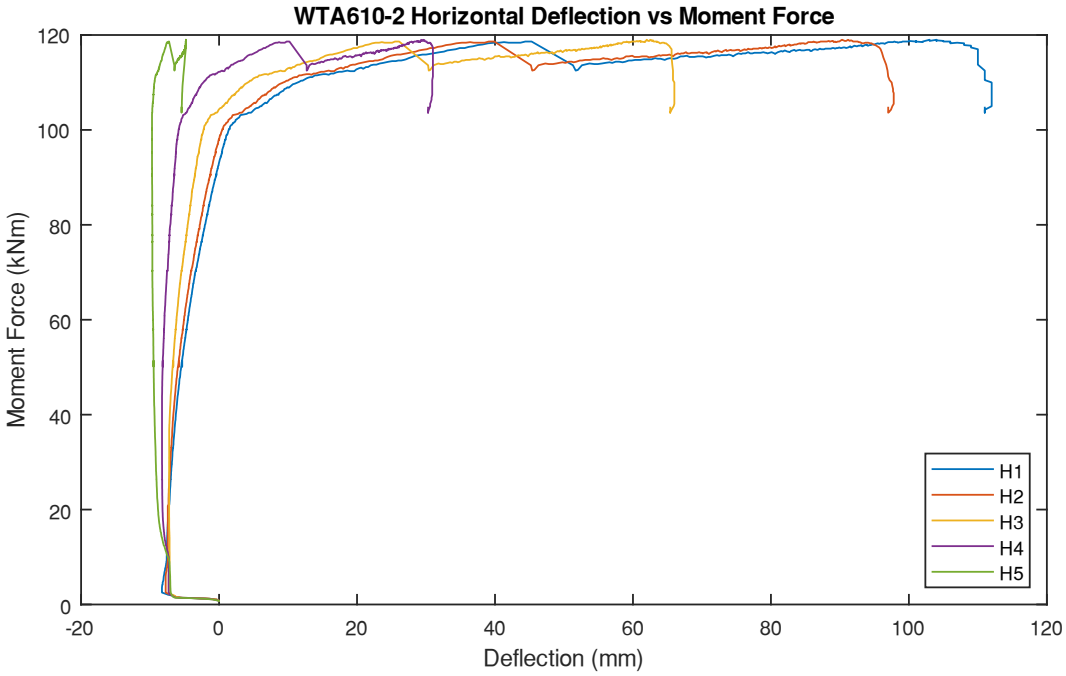

Figure 3-10: WTA610-2 Horizontal Deflection vs Moment Force

Once again, the settling of the Test #4.2 SIN beam into the supports is observed early on and another hardening trend is visible after the 100 kNm mark. Figure 3-11 shows the vertical deflections along the beam versus the moment force on the beam over the duration of the Test #4.2.

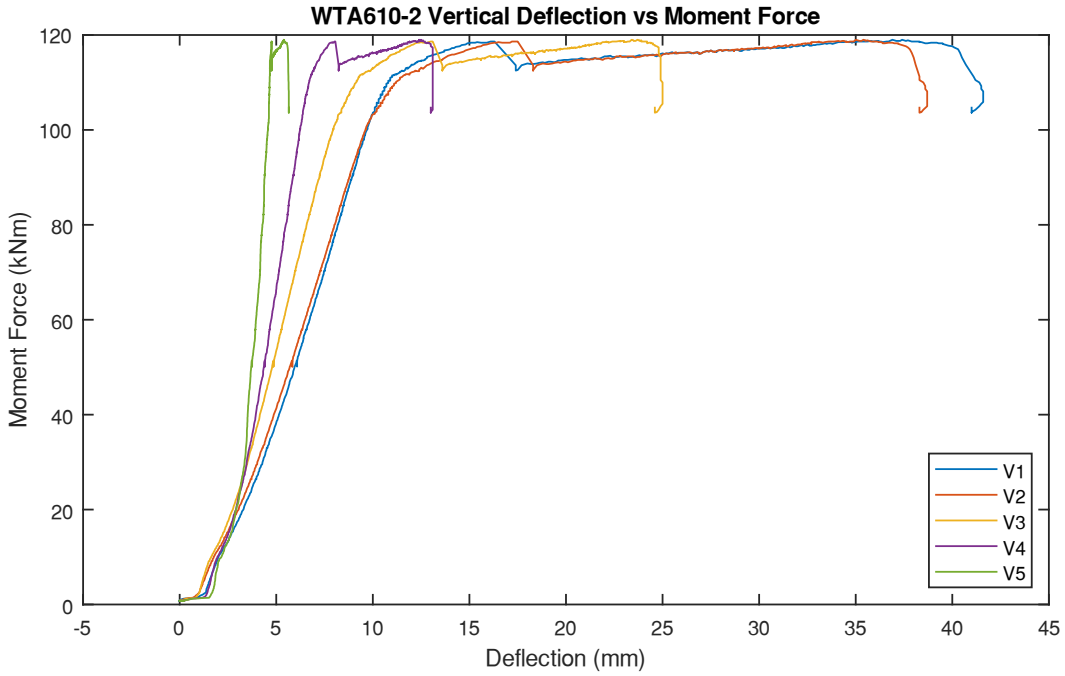

Figure 3-11: WTA610-2 Vertical Deflection vs Moment Force

3.2.6 Test #5 – WTA750/127x6

Test #5 was the deepest selected specimen and it was a WTA750/127x6 SIN beam. Significant deflection on this member began around the 40 kNm mark, i.e., earlier compared to previous tests. This is expected as it is the most slender SIN beam of all the specimens. The beam reached a peak moment strength of 113.6 kNm with a corresponding horizontal deflection of 93.6 mm. The overstrength of the WTA750 was the smallest of all of tests at 30% overstrength. Figure 3-12 shows the horizontal deflections along the beam versus the moment force on the beam over the duration of the Test #5.

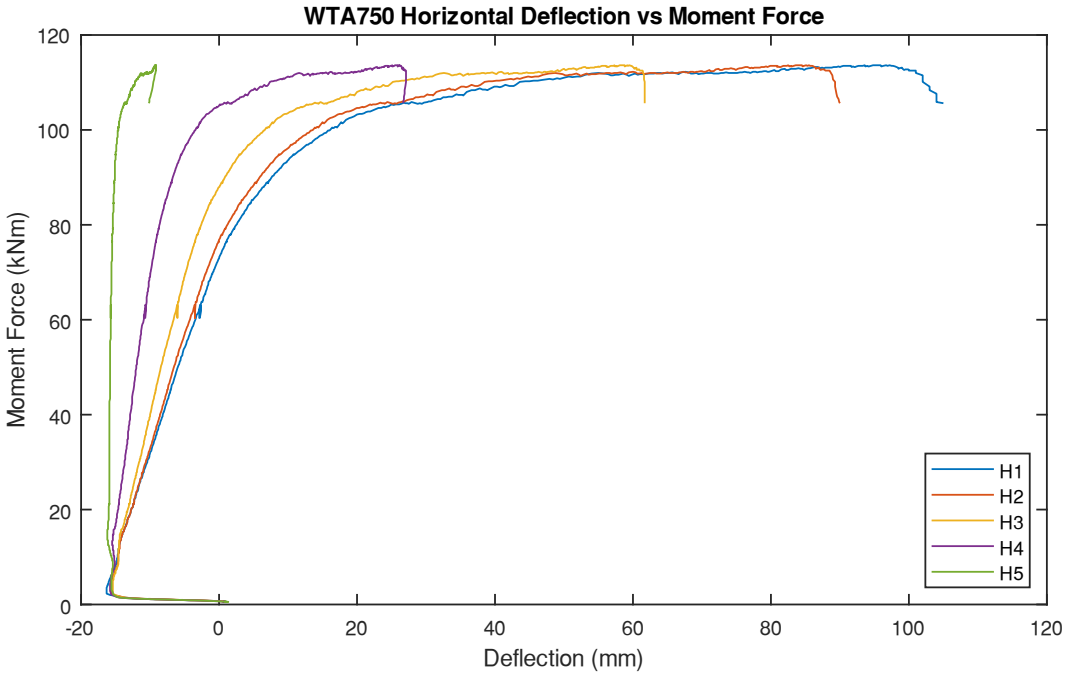

Figure 3-12: WTA750 Horizontal Deflection vs Moment Force

Figure 3-13 shows the vertical deflections along the beam versus the moment force on the beam over the duration of the Test #5.

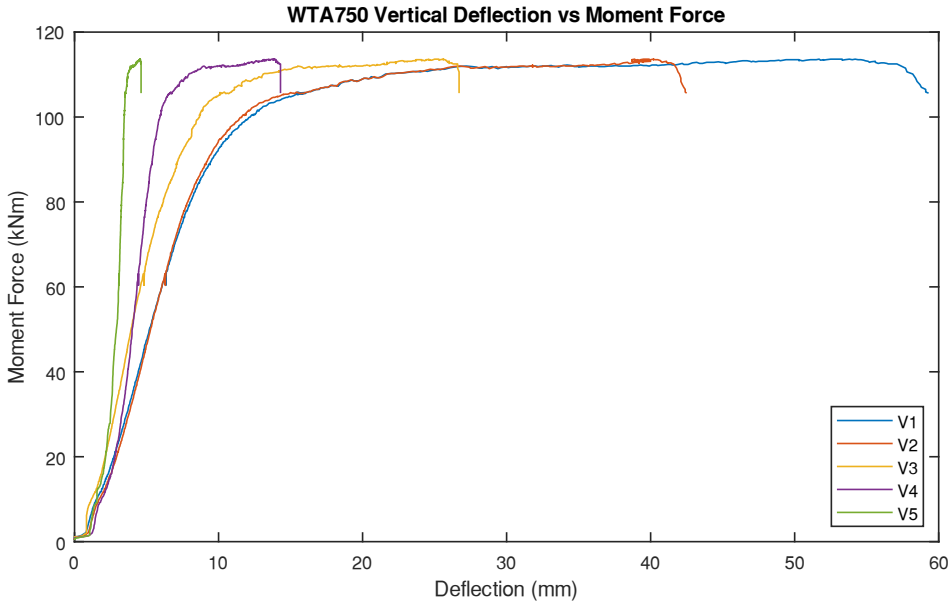

Figure 3-13: WTA750 Vertical Deflection vs Moment Force

The WTA 750/127x6 SIN beam was the only tested beam to be whitewashed to observe the visual yielding of the member. Since the web does not resist axial load induced from the moment force the web did not show any yielding. Therefore, the whitewash on the web did not provide further insight into the web performance. The whitewash on the flanges did indicate the location of yielding in the local flange failure and showed some stress paths at the location where the flange met the web, but minimal yielding was observed.

3.2.7 Test #6 – WTB333/127x6

Test #6 was a WTB333/127x6 SIN beam which was the first beam with a larger web thickness. Significant deflection began to occur at the 80 kNm mark. Shortly after the significant deflection occurred the test reached its peak strength of 90.5 kNm. The corresponding lateral deflection at this point was 16.5mm. This was the only test to reach its peak strength prior to the hardening trend and local flange failure. Figure 3-14 shows the horizontal deflections along the beam versus the moment force on the beam over the duration of the Test #6.

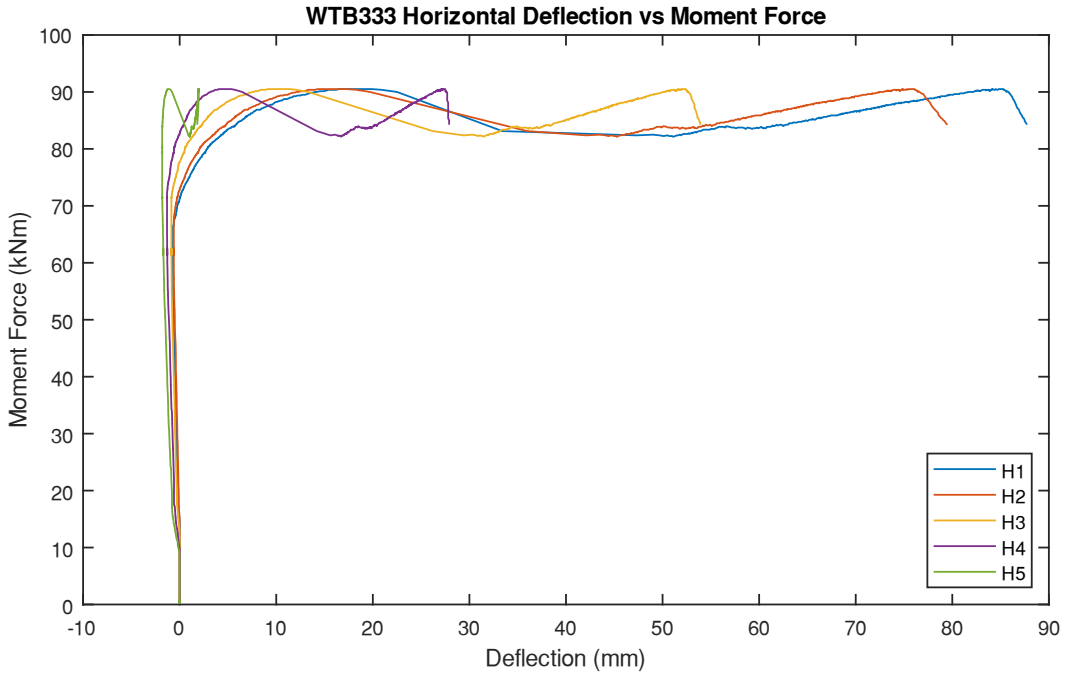

Figure 3-14: WTB333 Horizontal Deflection vs Moment Force

Figure 3-15 shows the vertical deflections along the beam versus the moment force on the beam over the duration of the Test #6.

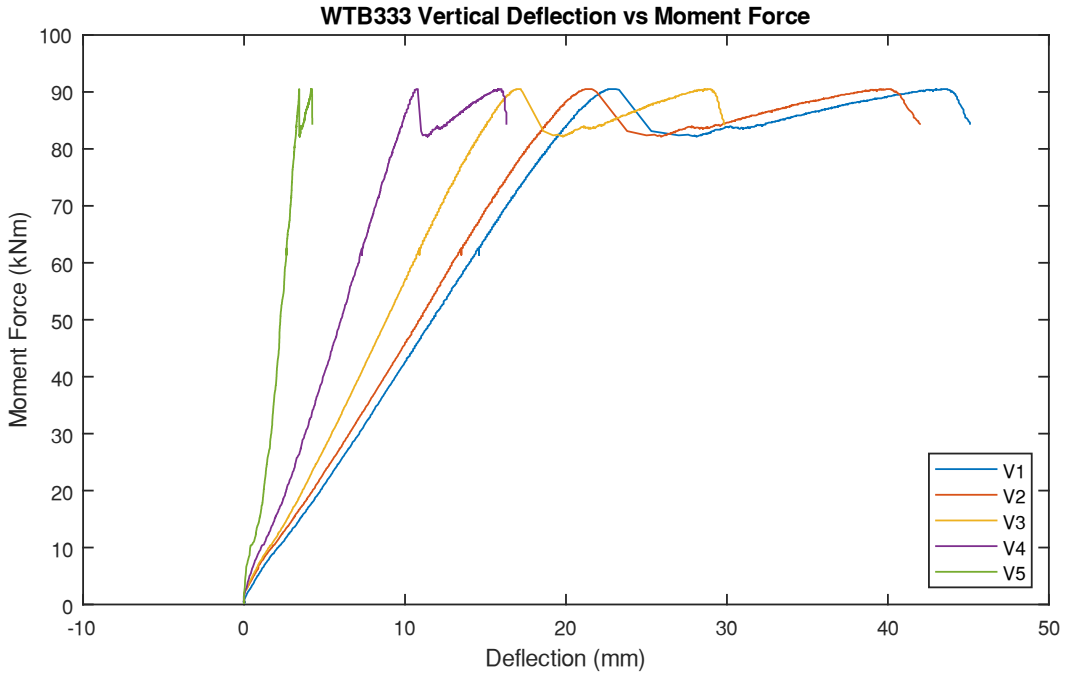

Figure 3-15: WTB333 Vertical Deflection vs Moment Force

3.2.8 Test #7 – WTC333/127x6

Test #7 was a WTC333/127x6 SIN beam. Similar to the WTB333 beam the deflection is very steady until around 80 kNm when significant lateral deflection begins to occur. The beam reached a peak moment strength of 97.8 kNm with a corresponding lateral deflection of 93.4 mm. Similar to the other beams with varying web thickness a hardening trend is very visible in the performance of the beam. Figure 3-16 shows the horizontal deflections along the beam versus the moment force on the beam over the duration of the Test #7.

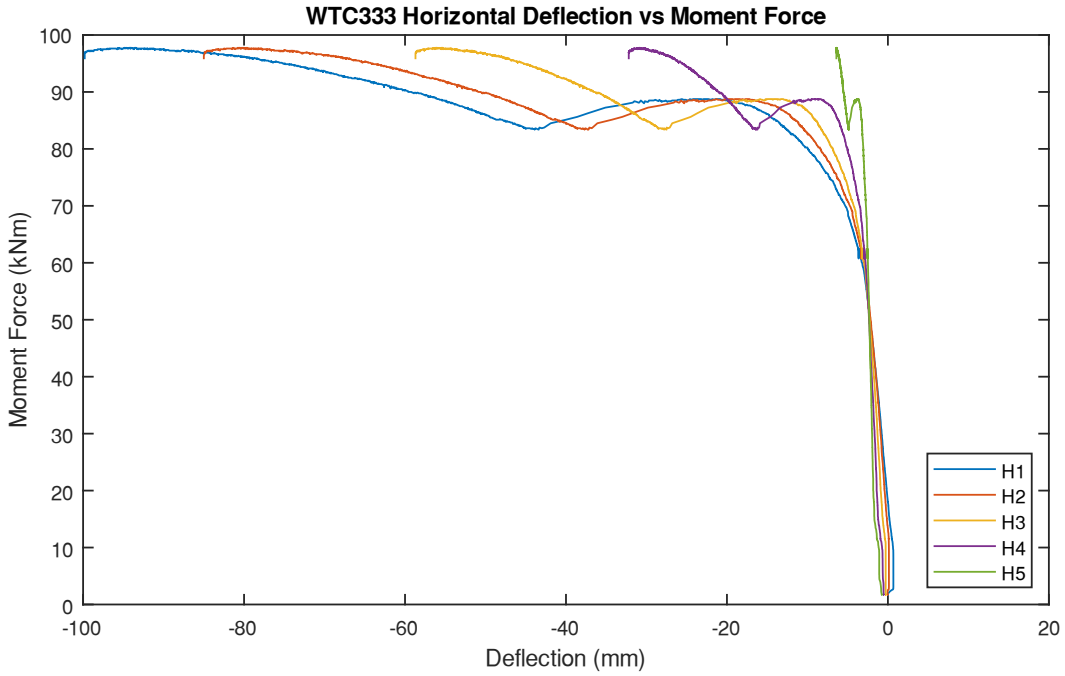

Figure 3-16: WTC333 Horizontal Deflection vs Moment Force

Figure 3-17 shows the vertical deflections along the beam versus the moment force on the beam over the duration of the Test #7.

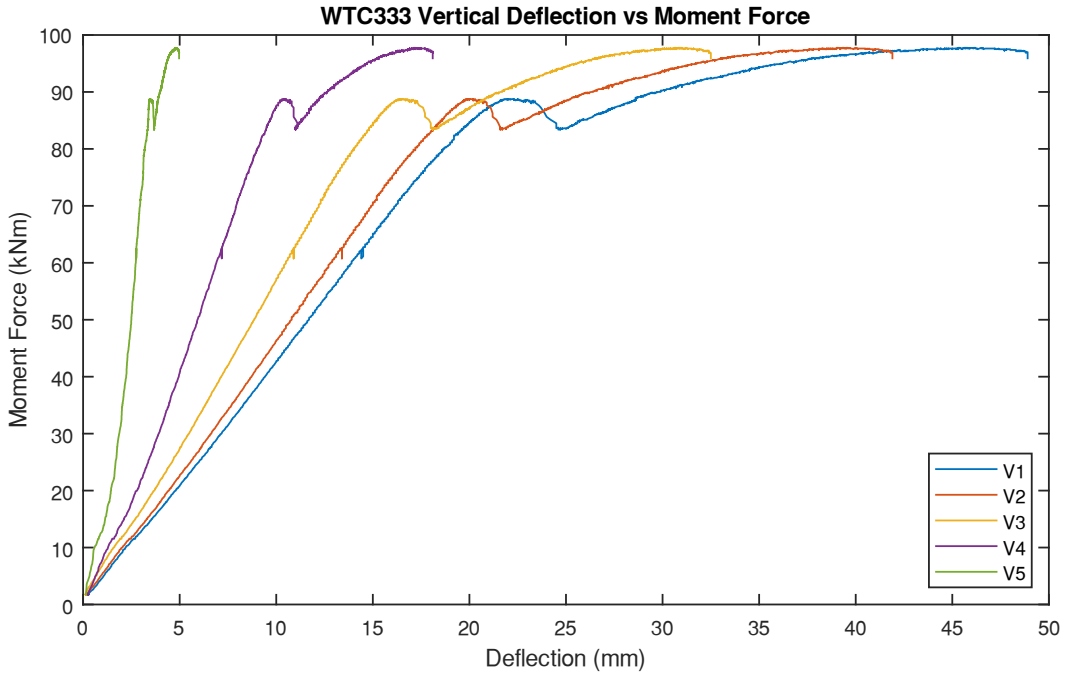

Figure 3-17: WTC333 Vertical Deflection vs Moment Force

3.2.9 Test #8 – WTF333/127x6

Test #8 was the final test of the varying web thickness beams with a WTF333/127x6 SIN beam, and it had the thickest web of all of the specimens. Significant deflection for this test started to be observed at the 50 kNm mark which is earlier than the previous 333 mm deep SIN beams. However, contrary to the other beams the WTF333 reached a peak strength of 100.4 kNm. At this peak point the lateral deflection was 125 mm which was nearing impact with the beam test apparatus. Thus, the test was ceased at this point to prevent damage to the system. This was the largest deflection of all the beams without a local failure and at the point of ceasing the test no signs of reduction in load were imminent. Figure 3-18 shows the horizontal deflections along the beam versus the moment force on the beam over the duration of the Test #8. As presented in this figure all five locations along the web that monitored the lateral deflection indicated a plateau in the resistance of the beam but no reduction in the load can be seen.

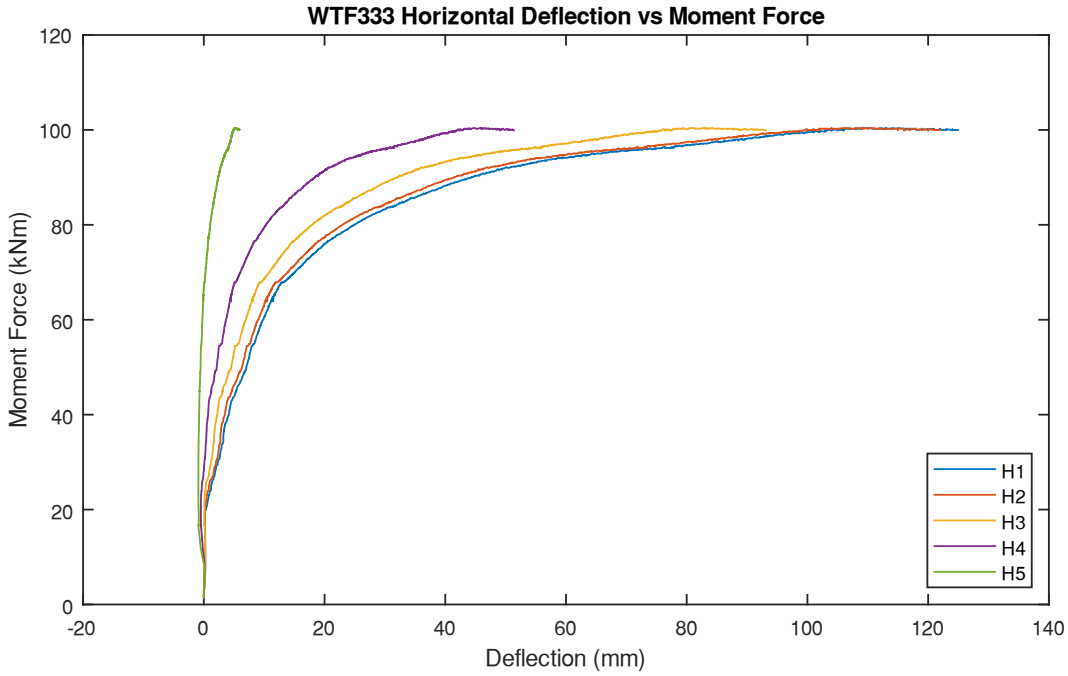

Figure 3-18: WTF333 Horizontal Deflection vs Moment Force

Figure 3-19 shows the vertical deflections along the beam versus the moment force on the beam over the duration of the Test #8.

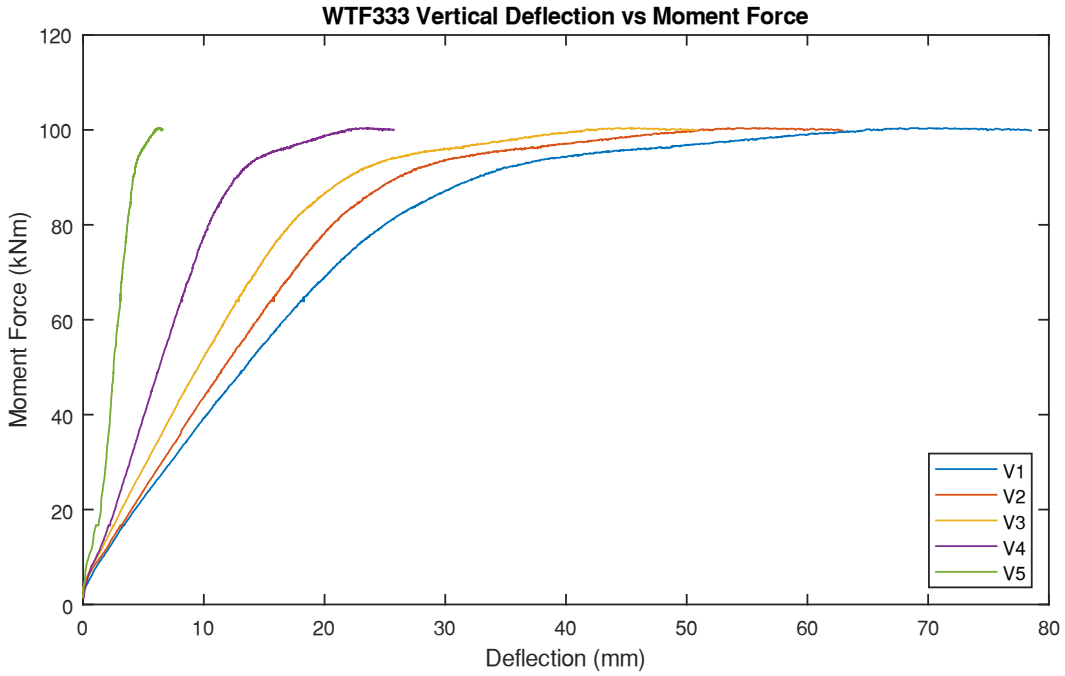

Figure 3-19: WTF333 Vertical Deflection vs Moment Force

3.2.9 Test #9 – WTA333/127x6 – 9

Test #9 was the final test that was completed, it was a WTA333x127x6 SIN beam, and it was the third beam of this size. In this test significant lateral deflection was observed at the 60 kNm mark. The beam reached a peak moment strength of 82.1 kNm which is similar to the second WTA333 test (i.e., Test #2). The corresponding lateral deflection was 76.5 which also closely follows the second WTA333 test. The comparison of the identical test will be discussed further in section 3.5. Figure 3-20 shows the horizontal deflections along the beam versus the moment force on the beam over the duration of the Test #9.

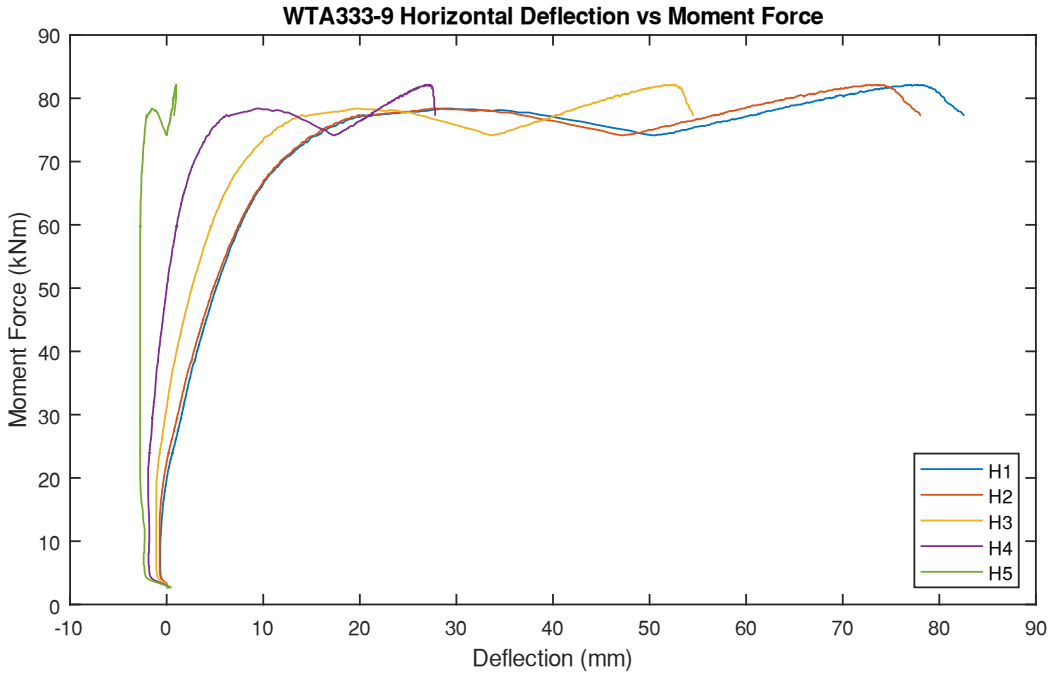

Figure 3-20: WTA333 Horizontal Deflection vs Moment Force

Figure 3-21 shows the vertical deflections along the beam versus the moment force on the beam over the duration of the Test #9.

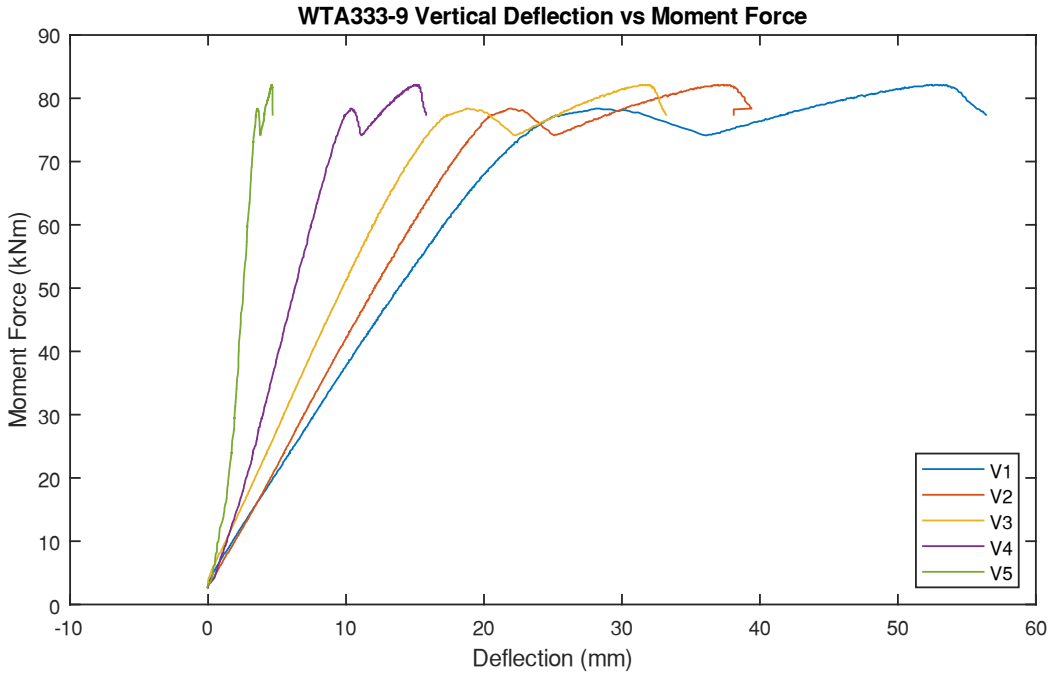

Figure 3-21: WTA333 Vertical Deflection vs Moment Force

3.3 Comparison of Varying Web Depths

Figure 3-22 shows the relationship of the lateral deflection versus the moment force of the four beams with varying web depth. For the WTA333 beams the second test (WTA333/127x6-2 SIN beam) will be used as the representative data. This is because the second tested beam provides results closest the average result of the three identical beams. As shown in the Figure 3-22, the load that can be resisted by the SIN beams increases with the depth of the beam and its web. This equates to an average of 7.2% of strength for every 100 mm of increased depth. The theoretical increase in strength following the conventional method produces a 20% increase per 100 mm. Additionally, with the increase in depth the magnitude of the lateral deflection that occurs prior to local buckling increases. Therefore, this indicates that the deeper the beam is, the higher lateral deflection that it will undergo. It should be noted that the WTA610/127x6 SIN beam reaches a larger peak strength than the deeper WTA750/127x6 SIN beam. As discussed in Section 3.5 there

is some variability from beam to beam which could be concluded as the cause of this inconsistency. It is also possible that because the WTA610/127x6 beam had to be retested that this altered the results in this manner.

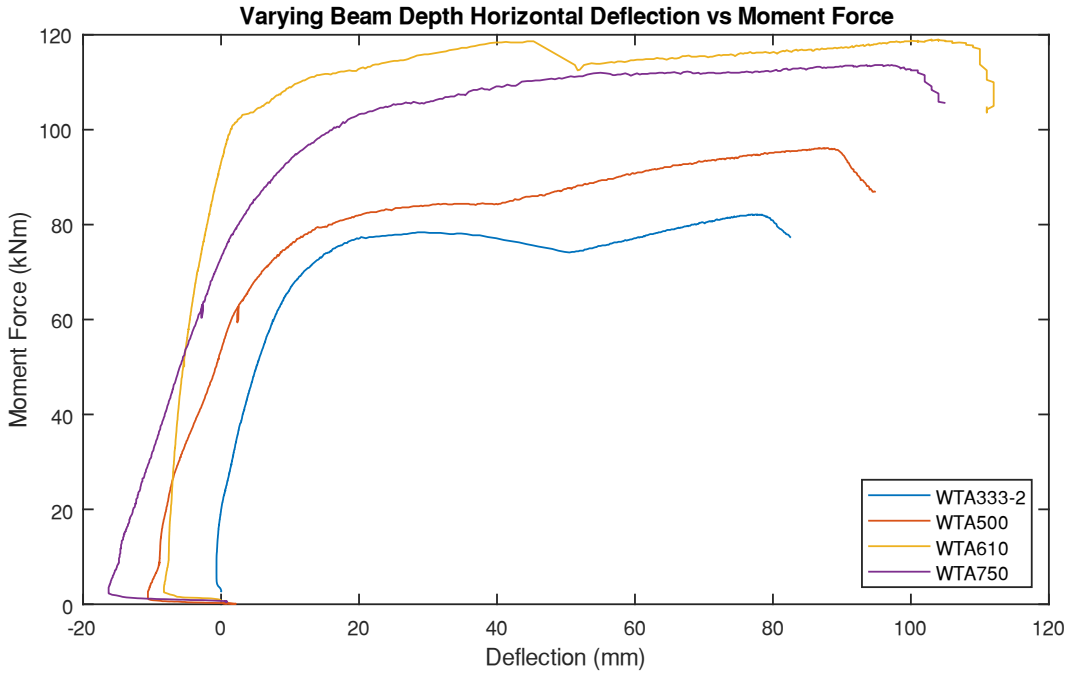

Figure 3-22: Horizontal Deflection vs Moment Load of Varying Depth Beams

3.4 Comparison of Varying Web Thicknesses

Figure 3-23 illustrates the relationship of the horizontal deflection versus the moment force of the four beams with varying web thicknesses. It indicates that as the thickness of the beam web increases, the LTB strength of the beam also increases. Once again, the second WTA333 beam test results were used as these results are the closest to the average result of the three beams. The average increase in strength is 6.7% for every millimeter of web thickness. In these beams a more noticeable hardening trend is visible. The WTA, WTB, and WTC beams all show a very noticeable peak in strength followed by a small dip in strength while increasing in deflection. Finally, the resistance begins to build again before finally reaching local flange failure. This is possibly due to

the beam undergoing an initial deflection before the stiffness of the web begins to restrain the beam from further rotation. The WTF beam is the only outlier; this is because the beam reached a total deflection of 125mm and so the test was ceased to prevent the beam from deflecting further and damaging the testing apparatus. Unlike the beam depth, the web thickness does not seem to have an effect of the lateral deflection of the beam.

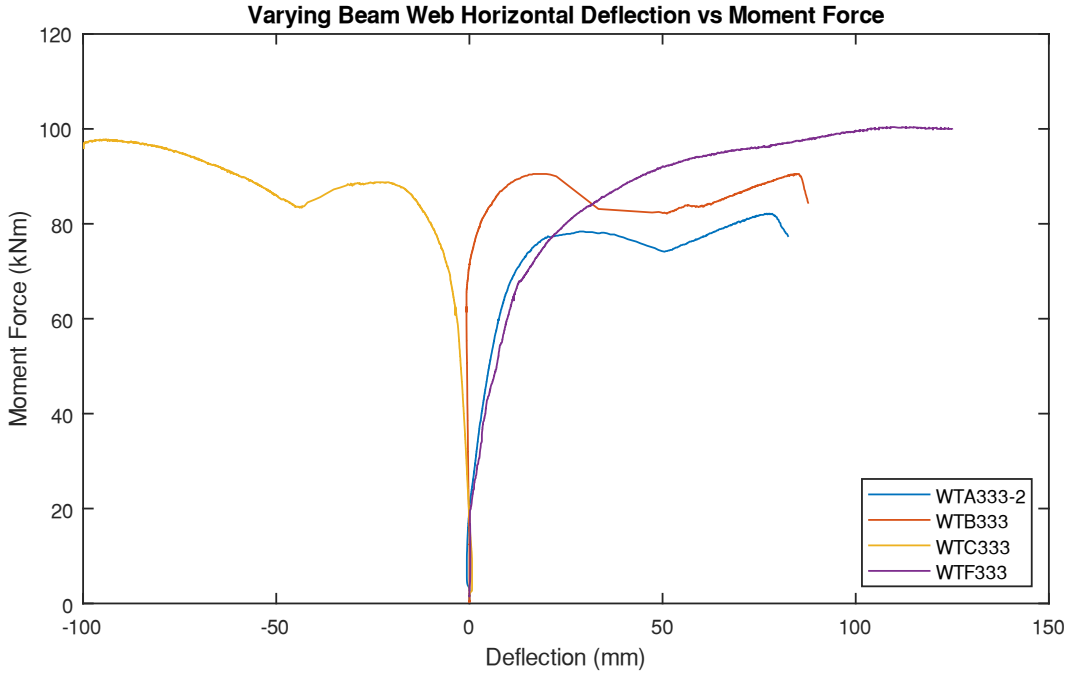

Figure 3-23: Horizontal Deflection vs Moment Force of Beams with Varying Web Thickness

3.5 Comparison of Identical Beams

Figure 3-24 shows the relationship of the moment force and lateral deflection of the three identical WTA333/127x6 SIN beams. This figure indicates that there is some variation in the results of beams with identical geometry. WTA333-1 (i.e., Test #1) had the largest peak strength of 103 kNm while the other two tested WTA333-2 (i.e., Test #2) and WTA333-9 (i.e., Test #9) were more similar in their response with peak strengths of 86.5 kNm and 82.2 kNm, respectively however the shape of the performance curves does vary. The WTA333-1 although produced a higher strength

did not deflect as much only laterally deflecting 26.2 mm before local flange failure in comparison to the 80 mm and 76.5 mm of the WTA333-2 and WTA333-9 respectively. This equates to an average strength of 90.8kNm with a coefficient of variation (COV) of 12.68%. With the outlying results of the first test this does indicate a high variation from beam to beam; however, since only three measurements were recorded for this statistic, it may not reflect the variation in a larger sample of members. Additionally, all three of the beams exceeded the theoretical conventional moment resistance by an average of 64%. Therefore, even considering this variation it still places the strength above the theoretically calculated strength. A number of factors could cause this variation, the most likely being the testing procedure. One testing practice that was adjusted was the tightening of the shear tab bolts. For the first test an impact wrench was used to tighten all 10 bolts locking the beam and actuator together. During the test the rotation and buckling of the beam was cause the actuator to undergo lateral stress. In order to avoid this issue, the bolts were only hand tightened for the remaining tests this allowed the top flange to rotate more free and note impact the actuator. This added rigidity in the WTA333-1 (i.e., Test #1) is a strong possible explanation and accounts for both the reduced horizontal deflection and the increased ultimate capacity. This means that for subsequent testing the procedure was more consistent from test to test. Additionally, it could be due to the steel being from an alternate batch. However, this is less likely as material testing reports were provided from the supplier and they show the material for the flanges and webs all came from similar steel batches.

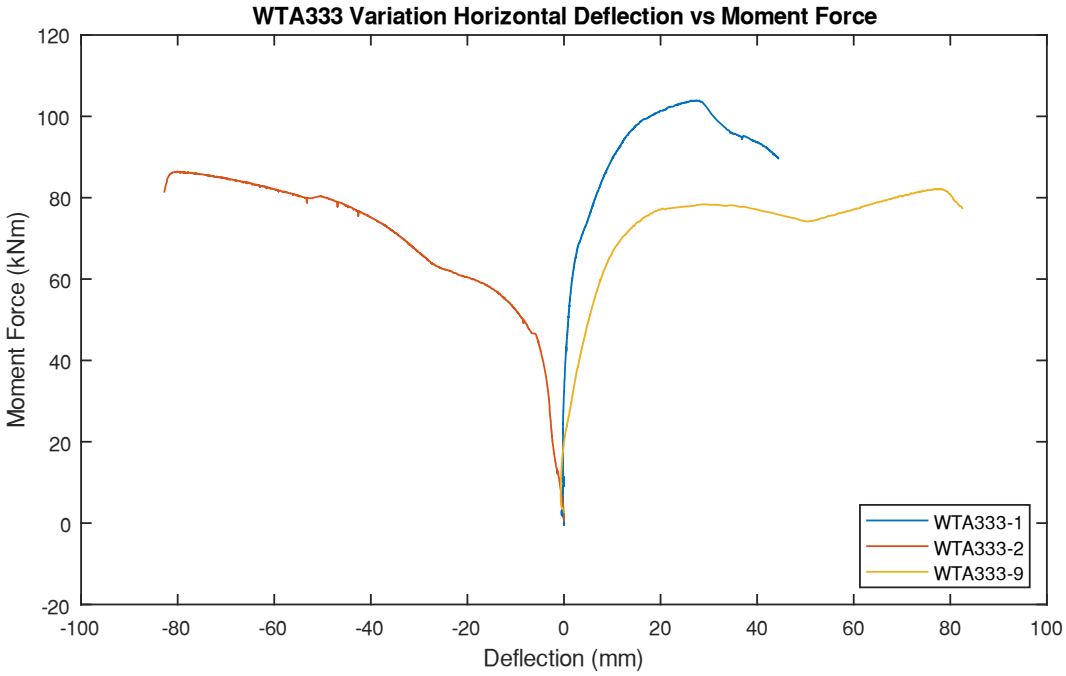

Figure 3-24: Horizontal Deflection vs Moment Force of WTA333 Beam Tests

Chapter 4: Numerical Analyses

4.1 Development of Equivalent Web Thickness Equation and Method

Based on the observations and results discussed in Chapter 3, the current method for calculating the LTB resistance of a CWPG provides conservative estimates, i.e., the theoretical LTB strength is anywhere from 30% to 60% less than the experimental LTB strength. This difference in the LTB strength is due to the corrugated web providing additional stiffness to the flange. The depth of the web had no observable impact on the LTB strength increase apart from what is gained by increasing the distance of the flanges. The web thickness did affect the LTB strength of the beam, and as such, having a thicker web produced a stronger beam. The experimental results were compared to the previous proposed calculation method to determine if a previous method would fit to quantify this increased stiffness or if a new method needs to be proposed. Table 4-1 shows the beams calculated LTB resistances from the various procedures mentioned in the literature review.

Table 4-1: LTB Resistances of Previous Proposed Calculation Methods

Beam	Mr Conventional	Mr Experimental	Mr Lindner (1990)	Mr Moon (2009)	Mr Sayed - Ahmed (2005)
WTA333/127x6	39.86	90.83333	93.21	27.63	40.18
WTA500/127x6	55.47	96.125	139.93	33.33	55.81
WTA610/127x6	66.18	119	170.70	37.63	66.53
WTA750/127x6	80.03	113.625	209.87	43.48	80.39
WTB333/127x6	39.86	90.5	93.21	27.63	40.72
WTC333/127x6	39.86	97.75	93.21	27.63	41.14
WTF333/127x6	39.86	100.375	93.21	27.63	43.10

The proposed method by Lindner to adjust the torsional constant provides an adequate value for 333 mm deep beams; however, similar to the conventional beams the change in thickness of the web does not affect the beam strength (Lindner 1990). But as discussed in the experimental results the thickness of the web increases the strength of the beam by 6.7% per millimeter of web

thickness. Additionally, for the other depth beams the resistance calculated is larger than the experimentally observed values. The method proposed by Moon et al. does not provide adequate design strengths. All of the calculated values are smaller than the conventional method this indicates that the beam is less strong than the floating flange method which was not observed experimentally (Moon et al. 2009). Finally, the method proposed by Sayed-Ahmed does increase the strength for both the depth and the web thicknesses; however the magnitude of increase is minimal (Sayed-Ahmed 2005). Thus, based on the precious observations, a better method for adjustment could be the equivalent web thickness method; however, the equation suggested by this method needs to be adjusted to suit sinusoidal shaped webs and to better fit the magnitude of increase. Therefore, Eq. (13) was developed to be utilized in calculating the LTB moment resistance.

$$w_{eq} = t_w + \left(\frac{3 * a_3}{s}\right) * t_w \tag{13}$$

Where w_{eq} is the equivalent web thickness, t_w is the actual web material thickness, a_3 is the amplitude of corrugation and *s* is the length of one corrugation wave. Eq. (13) uses the geometric parameters of the corrugation and the thickness of the web material to increase the value of the web. From there the geometric constants I_y, C_w, and J can be calculated using an I-Shape. Eq. (14), Eq. (15) and Eq. (16) outline how to calculate each geometric constant and Figure 4-1 outlines the geometric properties of the beam.

$$I_y = \frac{1}{12}(2tb^3 + (d - 2t){w_{eq}}^3) \tag{14}$$

$$C_w = \frac{1}{24}(d - t)^2 b^3 t \tag{15}$$

$$J = \frac{1}{3}(2tb^3 + (d-t){w_{eq}}^3) \tag{16}$$

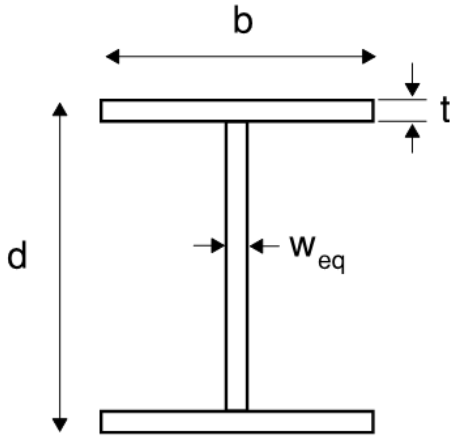

Figure 4-1: Geometric Section of the Beam with Equivalent Width

Using the geometric constants calculated with the new equivalent web thickness the calculation for bending of unsupported members can be completed following clause 13.6 of S16-14 (Canadian Standards Association 2014). The process of the proposed method can be found in Appendix B.

4.1 Numerical Analysis of Proposed Equation and Method

To evaluate the new proposed equivalent thickness equation, 112 SIN beams were chosen from the SIN beam technical guide including the sizes used in the experimental tests. (Steelcon Fabrication Inc. 2019b) and the hypothetical LTB strength was calculated and compared to the previously presented experimental results. 28 beams were chosen for each web thickness, WTA, WTB, WTC, and WTF. Web thicknesses of WTH and WTK were omitted from this analysis as there is no experimental data of these sizes to compare to. Within the sets of 28 beams different sizes are chosen with depths ranging from 333 mm to 750 mm and flange sizes ranging from 127 mm wide by 6 mm thick up to 203 mm wide by 19 mm thick. A full list of all of the members can

be found in Appendix C. Table 4-1 shows the average moment strengths of the different SIN beam groups, where theoretical strength stands for the strength calculated using the current design code, proposed stands for the strength calculated using the proposed method, average LTB strength increase is the percentage of strength increase from the theoretical strength to the proposed strength and LTB strength max increase is the largest percentage of strength increase out of the beams in that SIN beam group.

Table 4-2: Average Moment Strengths for SIN Beam Groups

Web Thickness	Average Theoretical LTB Moment Strength (kNm)	Average Proposed LTB Moment Strength (kNm)	Average LTB Strength Increase	Maximum LTB Strength Increase
WTA	283.23	304.34	4.99%	16.26%
WTB	285.23	315.38	7.40%	20.88%
WTC	286.16	324.11	10.29%	25.70%
WTF	286.16	349.46	18.81%	51.46%

The LTB strength increases for the WTA, WTB, WTC, and WTF groups from the theoretical procedure to the proposed procedure is on average 4.99%, 7.40%, 10.29% and 18.81% respectively. This translates to an average of 6.02% strength increase per millimeter of thickness added. This is slightly lower than the 6.7% average increase observed in the experimental results. Figure 4-2, Figure 4-3, Figure 4-4, and Figure 4-5 show all of the beams and their associated strength increases for comparison.

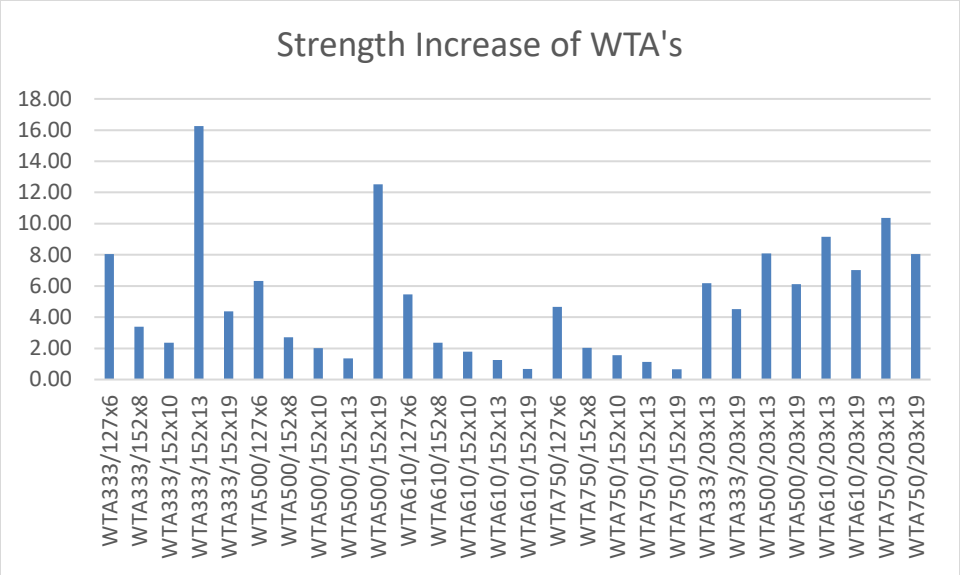

Figure 4-2: Strength Increase of the WTA Beams

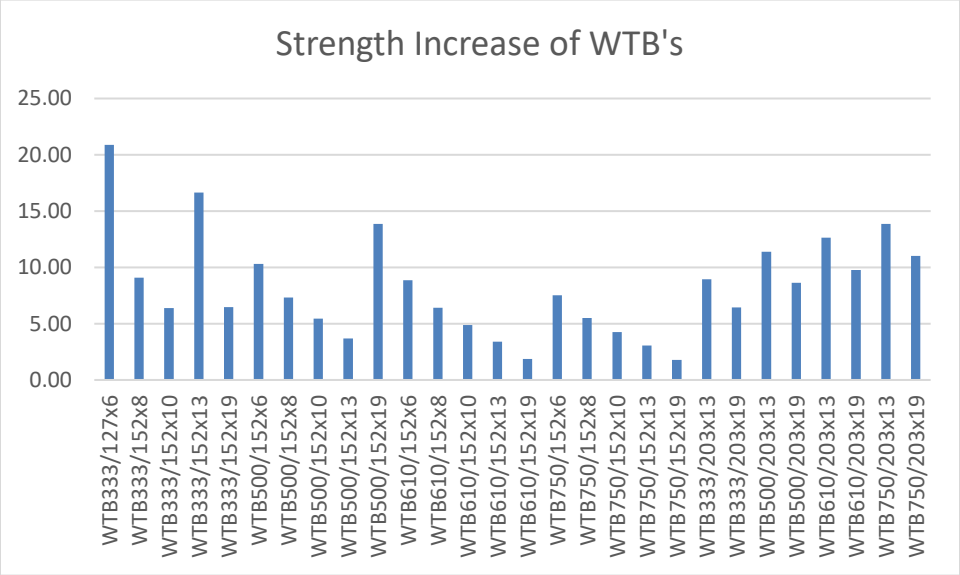

Figure 4-3: Strength Increase of the WTB Beams

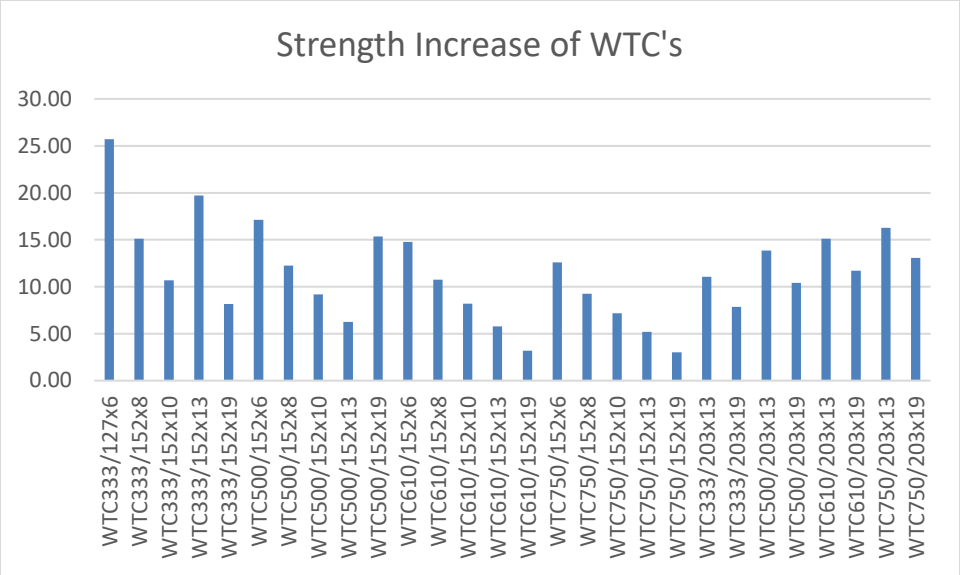

Figure 4-4: Strength Increase of the WTC Beams

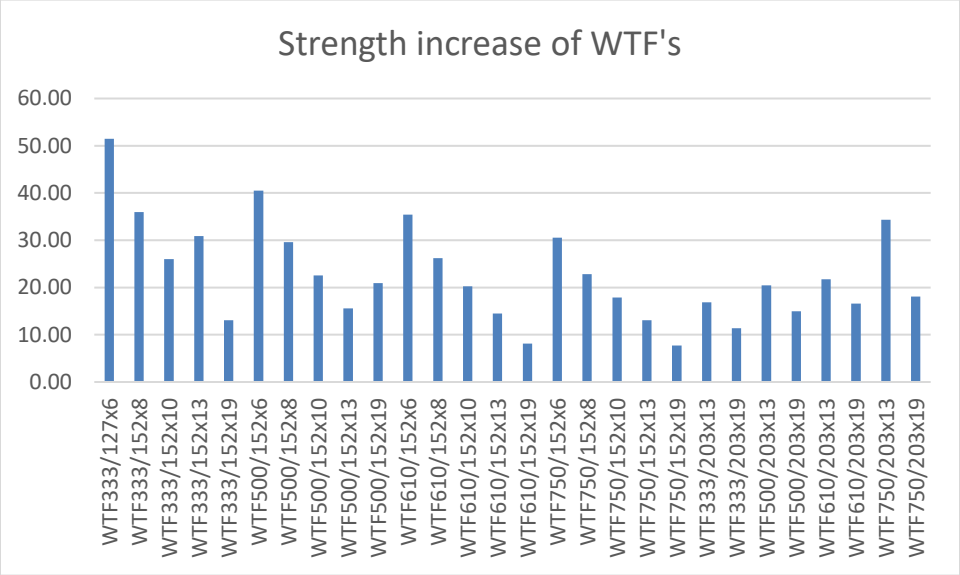

Figure 4-5: Strength Increase of the WTF Beams

Therefore, this new proposed method and the equivalent width equation remains conservative compared to the experimental results. In some configurations where the thickness of the web and the beam height are both large the increase in LTB strength has a possibility of exceeding what was observed in the experiments. In order to prevent an under designed beam a limitation condition should be applied. Based on the average increase and the variation observed in the experimental

results, it is proposed that the LTB strength of the SIN beam calculated using the equivalent web thickness shall not exceed 1.3 times the LTB strength calculated using the flange material alone (Eq. (17)).

$$Mr_{hyp} < 1.3 * Mr_{theoretical} \quad (17)$$

This limitation will prevent the design from exceeding the lowest probable resistance including the possible variation in beam-to-beam performance. Based on the analysis of the proposed process the results show a satisfactory conformance to the real LTB strength of the SIN beams and further analysis can be completed.

The proposed method was intended to be run on the beams used in Hannebauers (2008) experiments. Out of the four beams that were tested two were identical so that leaves three sizes that can be compared to the test results. All beams have flanges that are 20 mm by 250 mm and a depth of 1000 mm and all had unbraced lengths of 6000 mm. Table 4-3 outlines the LTB resistances observed and calculated for the three beams.

Table 4-3: Experimental Results Comparison of Previous Research

Beam #	Beam Web Thickness	$Mr_{Theoretical}$ (kNm)	Mr_{Exp} (kNm)
1	2.6	1363	1215
2	3.1	1363	1170
3	3.2	1363	1193

As shown the experimental results of Hannebauers (2008) research are below the theoretical calculated value. This is due to limited information on the corrugation and other beam parameters. Therefore Hannebauers (2008) research cannot be used in comparison of the proposed method.

4.2 Monte Carlo Simulation

With the applicability of the calculation method proposed in Section 4.1a further investigation of the method should be done in the future. The framework of a Monte Carlo Simulation (MCS) was run using the steel yield strength (F_y) as the variable parameter. Several parameters were considered for the variable parameter; however, since the geometric dimensions of the beam are not subject to large variations F_y was chosen as the only parameter with potential variability. The yield strength is assumed to fit a lognormal distribution with an average value of 350 MPa and a standard deviation of 60.1 MPa (Sadowski et al. 2015). Seven separate MCS's with 10000 cycles per simulation were run. A simulation was run for each beam size used in the experimental program. The simulations were run using a beam length of 5000mm similar to the experimental program. However, when run with this unbraced length the calculation is governed by S16 clause 13.6-b (i.e., Eq. (18)). It states that the moment resistance of the beam is to be equal to the elastic critical moment multiplied by the safety factor phi (ϕ) when the elastic critical moment (M_u) is less than 0.67 times the yield moment (M_y) (Canadian Standards Association 2014). For all of the MCS analyses the safety factor phi is set equal to 1.

$$When \quad M_u \leq 0.67 * M_y \quad Then \quad M_r = \phi M_u \tag{18}$$

Since the equation for M_u does not include steel yield capacity (the variable parameter), the simulation produces a single value for all 10000 iterations. To provide a useful simulation the length of the beam was adjusted to 2500 mm which allows the results not to be limited by the S16 clause 13.6-b mentioned above. Figure 4-6 shows the histograms of the four beams with varying web thicknesses for comparison with the experimental results. The remaining histograms can be found in the Appendix D.

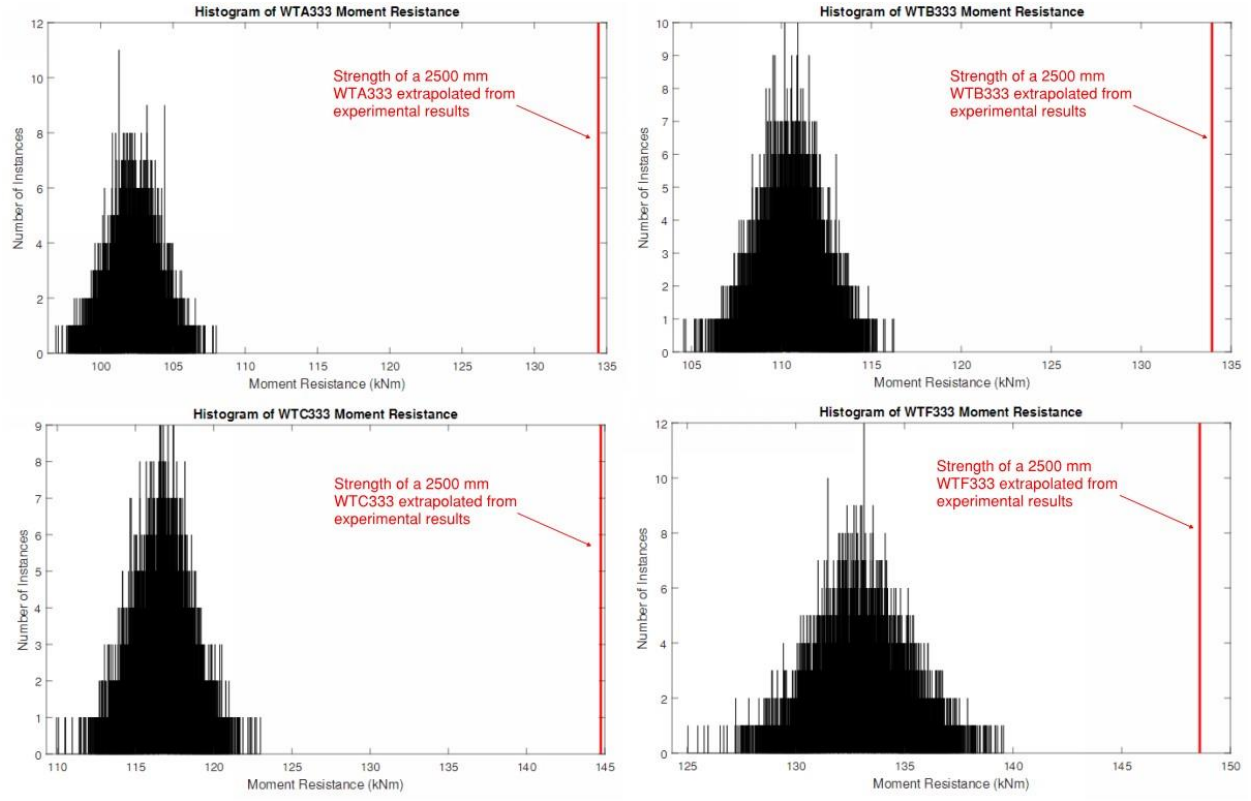

Figure 4-6: Histograms of Moment Resistance

Since the simulation beams are half as long as the experimental results the results are extrapolated by using the overstrength percentage to scale the results to a smaller beam length. Table 4-4 outlines the results from each analysis.

Table 4-4: Summary of Monte Carlo Simulations

SIN Beam Size	Average Moment Resistance (kNm)	Coefficient of Variation of Moment Resistance	Probability of beam LTB strength under design
WTA333	102.3	1.48%	<1%
WTB333	110.5	1.41%	<1%
WTC333	116.7	1.39%	<1%
WTF333	133.0	1.41%	<1%
WTA500	163.8	1.28%	75%
WTA610	207.3	1.17%	<1%
WTA750	264.8	0.99%	>99%

Five out of the seven MCS simulations produced a near 0% probability of being under designed using the proposed method. But two out of the seven MCS simulations produced a near 100%

(WTA750) and 75% (WTA500) probability of being under designed. This does not necessarily mean that the WTA750 and WTA500 SIN beams are being under designed. The limit used to test if the beam is under designed was based on the assumption that the data collected in the experiments with 5000 mm beams can be accurately scaled to a shorter beam. When comparing the simulation results with the theoretically calculated LTB moment strengths of the beams the overstrength percentage is within the range of potential increase that was observed in the physical testing. Additionally, WTA750 and WTA500 SIN beams designed at such a short length are actually governed by sectional capacity rather than LTB strength which reduces the possibility of under designing them further. As mentioned, the primary objective of this section is just to lay the foundation of future research because the more data that can be collected the more useful the Monte Carlo simulation (MCS) can become.

4.3 Preliminary Finite Element Analysis

Similarly to the MCS to continue the development of the proposed method for calculating LTB resistance, a finite element analysis (FEA) model was developed using the software package ABAQUS (Dassault Systemes Simulia Corp. 2014). The model was developed with the intent of running a parametric study on a wide range of beam sizes to compare to the new calculation method proposed in Section 4.1. However, with timeline constraints the scope of this section was reduced to provide a start for the FEA modelling that will be completed in the future. Thus, only the WTA333/127x6 SIN beam has been modelled in ABAQUS (Dassault Systemes Simulia Corp. 2014) and compared to the experimental results., i.e., a beam with identical geometric properties and configuration to the experimental Test #1, #2 and #9 beams. Test #2 results will be used for a similar reason as Sections 3.3 and 3.4 because it is closest to the average results of the three

identical beams. Figure 4-7 shows the WTA333/127x6 SIN beam model in ABAQUS that was modelled as a 5250 mm long beam with a 1000 mm shear tab on the top flange.

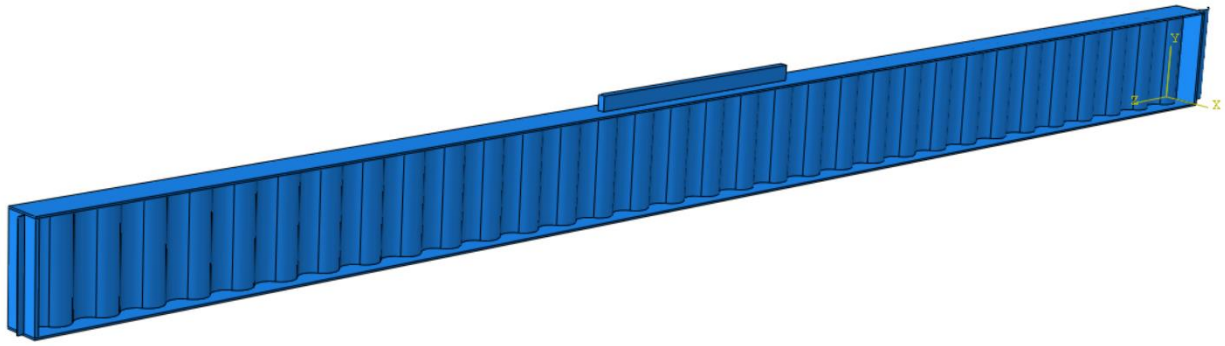

Figure 4-7: FEA Model of WTA333/127x6 SIN Beam

The web of the WTA333/127x6 SIN beam is modelled with 8-noded quadrilateral elements with an approximate size of 30 mm and ranging the whole thickness of the web. This size of mesh keeps the computing cost low while still accurately depicting the curvature of the corrugated web. A smaller mesh of 20 mm and a larger mesh of 40 mm sizes were also run producing identical results confirming the validity of the mesh size. For the flange and shear tab elements a tetrahedral mesh with 4 nodes was used. This was chosen over an 8-noded quadrilateral element in order to model the connection of the flange to the web since the curvature of the web prevents simple elements being used. Figure 4-8 shows the mesh of the part in the FEA software.

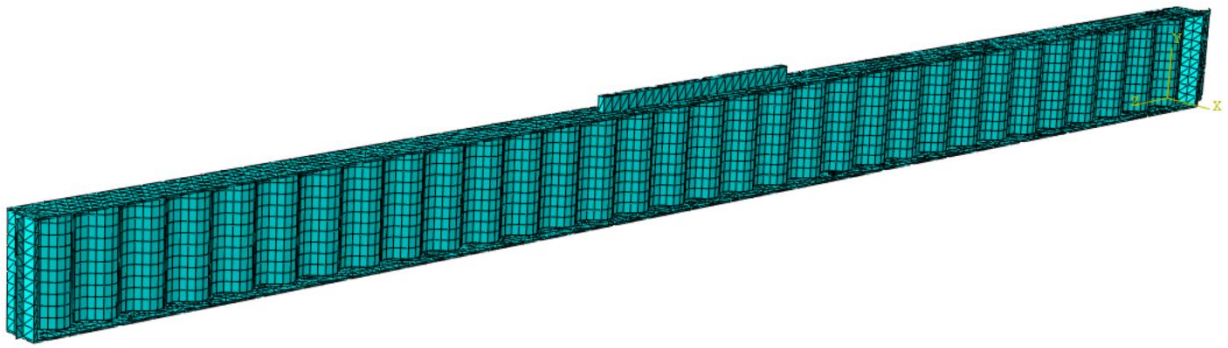

Figure 4-8: Mesh of WTA333/127x6 SIN Beam

The material of the WTA333/127x6 SIN beam was modelled using a simple plastic isotropic steel material with Young's modulus of 200GPa and Poisson's ratio of 0.3. The section of the of the WTA333/127x6 SIN beam was modelled as a solid homogenous section using the previously mentioned material properties. To quantify the plastic properties of the steel, stress and strain values from an Abaqus video tutorial were used and then scaled up to match the yield and ultimate strength of the experimentally tested beams (Dassault Systemes Simulia Corp. 2019). These values will eventually be replaced with properties based on coupon testing of the steel that was experimentally tested. Three boundary conditions are applied to restrict the movement of the beam and to mimic the experimental setup. The top ends of the beam are restricted from translation in the x, y and z directions while allowing rotation. In addition to those two edges being restricted, the top shear tab is restricted to only translate in the y directions simulating a similar function to the load cell pulling on the beam. For the loading procedure a displacement control is used to displace the shear tab in a vertical direction similar to the experimental test. A static loading procedure is used to apply the displacement over a specified length of time. The maximum number of steps was limited to 100 steps in order to keep a low computational cost.

The analysis was successful in producing results that generally follow the experimental results. Initial observations show that the beam does buckle in a form similar to the experiment as can be seen in Figure 4-9.

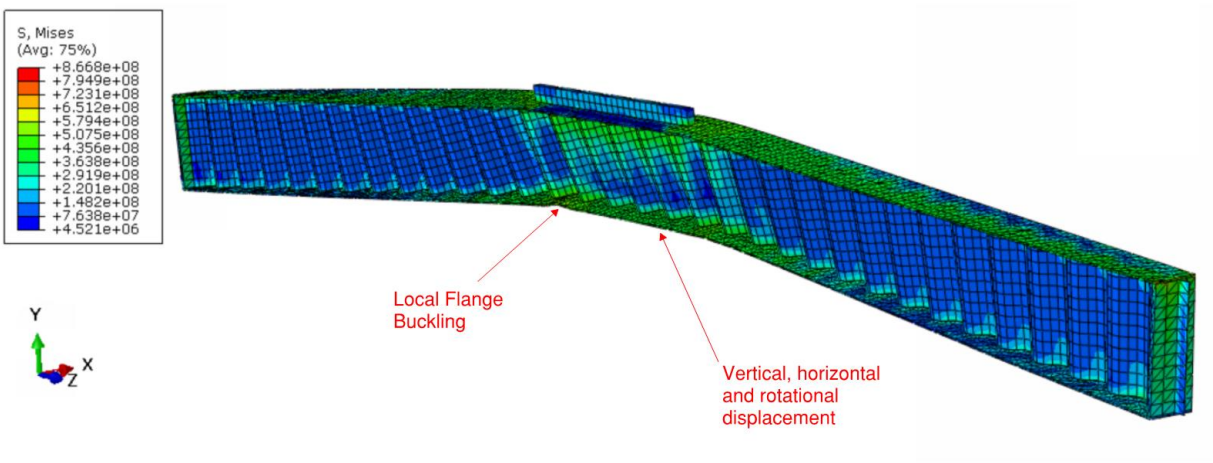

Figure 4-9: Von Mises Stress Distribution of the SIN Beam

Similar to the experimental testing a local flange buckling can be noticed in the compression flange in a similar location. The beam deflects similarly as well, under the 60mm vertical displacement control a horizontal deflection of 54 mm can be observed. The stress and strain values do not follow similarly to the experimental tests. Figure 4-10 shows the stress strain curve of the FEA analysis and the experimental Test #2 (i.e., WTA333-2) at the center of the lower flange.

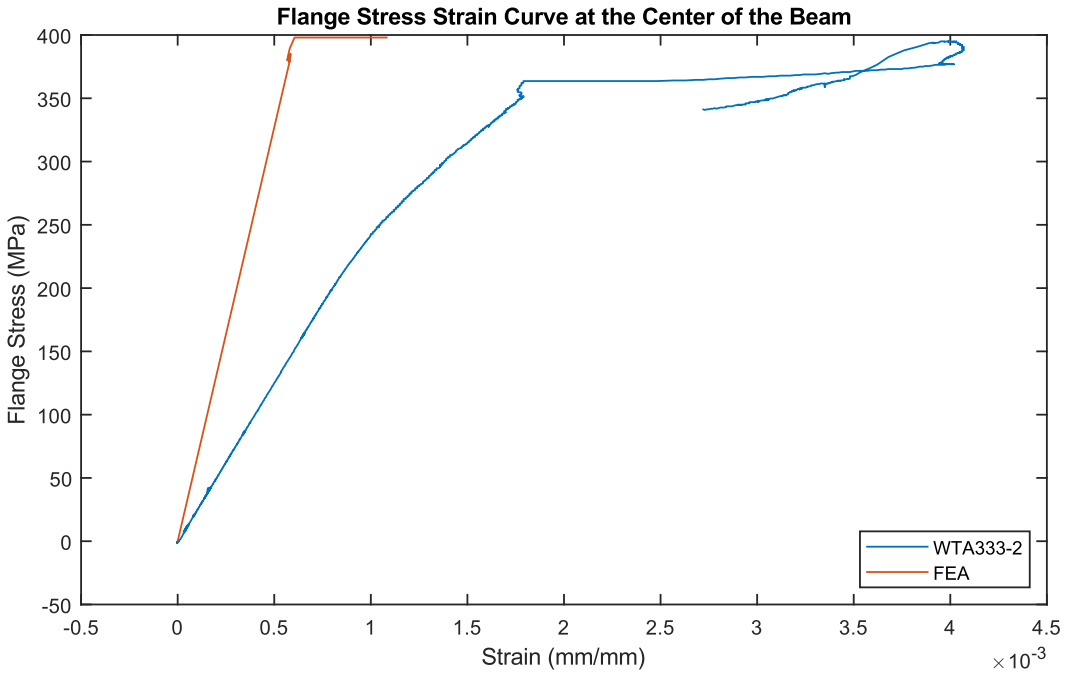

Figure 4-10: Stress Strain Curve of the Center of the Lower Flange

The Test #2 SIN Beam was chosen for the comparison of the FEA to the experimental results because the Test #2 SIN Beam most closely adhered to the average results of the three beams in the identical beam group. The FEA analysis as expected follows a more elastic and perfectly plastic pattern this is because there is only a small amount of information about the actual steel properties which causes the nonlinearity of the curve to only occur at a few points. The FEA stress strain curve also does not follow the slope that steel should showing the material properties are not correct. Finally, the force applied to the top of the beam equated to a final force of about 93 kNm which matches the beams slight increased strength in comparison to the experimental test. Overall, the FEA model provides an adequate preliminary representation with much room for improvement.

To improve the FEA model a few issues need to be addressed. Firstly, the material assumed for the model needs to be adjusted. Coupon testing should be done to obtain all the material data on the steel used in the experiments. This would provide a material more similar to the experimental

tests and a more accurate deformation and stress response. Second, for the FEA model to provide useful information it will need to be expanded to a parametric study. The model could be created using input variables for the section parameter and then a wide range of beam types and beam lengths could be analyzed to review if the proposed equation for LTB strength is suitable.

Chapter 5: Conclusion and Future Work

5.1 Summary of Thesis

This thesis investigated the lateral torsional buckling (LTB) strength of corrugated web plate girders (CWPGs) with sinusoidally profiled webs, also called SIN beams. Nine CWPGs were experimentally tested in a configuration that favoured LTB failure. The nine specimens were chosen with a varying range of web depths and thicknesses to investigate the effect that each web parameter had on the LTB strength of each member. All nine beams produced an ultimate strength greater than the theoretical LTB strength showing that the current design procedure is conservative. The results of the tests showed that the web thickness does affect the LTB strength while the depth of the web does not provide any additional strength to the beam apart from what is gained by having larger distance between flanges.

From the experimental results a new proposed method for calculating the LTB strength of CWPG was developed and proposed. The proposed method utilized an equivalent web thickness model and was configured to account for the web geometry. It was then numerically tested to determine its reliability and applicability when applied to a wide range of beam configurations in addition to what was a part of the experimental program. Then a Monte Carlo simulation (MCS) was run to lay the foundation of the risk of adopting the new method in a design scenario.

Finally, a preliminary FEA model was developed to simulate the experimental testing. The FEA model simulated the experimental testing confirming the viability of its use in the future to investigate a large population of beams with some adjustments required.

5.2 Conclusions

Based on the research completed in this thesis the following conclusion can be derived.

- The experimental results show that the conventional design method for calculating LTB resistance of CWPGs with sinusoidally shaped webs is conservative and a more precise method is possible.
- When comparing the SIN beams from the experimental program it is evident that the web thickness does affect the LTB strength of the beam, as the thickness increases so does the LTB resistance. The web depth however does not affect the strength of the beam apart from what is gained by increasing the distance of the flanges.
- The proposed method for calculating the LTB resistance utilizing Eq. (13) to calculate the equivalent web thickness does provide an adequate strength increase within the limitations provided. The average increase in strength fits within the increase that was observed in experimental testing which indicates that it could be a viable design method.

5.3 Future Work

The experimental testing completed on CWPGs in this thesis has been limited by the constraints of the testing facilities. Along with those constraints brings limits to the data that can be gathered and utilized in numerical analysis. To strengthen and expand the research completed in this thesis the following could be completed in the future.

- Experimental testing of beams with varying unbraced lengths would provide insight into the effect of long and short spans on the LTB capacity of CWPG's. This information would prove additionally useful in the risk analysis to further strengthen the proposed calculation method.
- Larger scale testing on similar beams would also provide further information into the variability of strength from identical beams and the reliability of the beams' strength.

- Finally, expanding the FEA analysis to utilize plastic material properties of the tested CWPG's and creating a parametric study on a wide range of sections and a range of unbraced lengths would confirm the ability of the proposed calculation method to estimate a CWPG's LTB strength.

Notations

The following symbols are used in this paper:

α = Angle of diagonal portion of the trapezoidal web profile;
ϕ = Safety Factor;
a = Length of flat portion of the trapezoidal web profile;
a_3 = Sinusoidal wave amplitude;
b = Horizontal length of diagonal portion of the trapezoidal web profile;
b = Flange width;
b_f = Flange width;
c = Full length of diagonal portion of the trapezoidal web profile;
COV = Coefficient of variation;
C_w = Warping torsional constant;
$CWPG$ = Corrugated web plate girder;
d = Beam depth;
d_1 = Flange distance;
E = Elastic Modulus;
FEA = Finite element analysis;
F_y = Yield Strength;
G = Shear modulus;
G_{co} = Adjusted shear modulus;
h_w = Web depth;
I_w = Warping torsional constant;
I_w^* = Adjusted warping torsional constant;
$\overline{I_w}$ = Adjusted warping torsional constant;
I_y = Second moment of inertia about the weak axis;
J = Torsional constant;
kN = Kilonewtons;
kNm = Kilonewton meters;
L = Unbraced Length;
LTB = Lateral torsional buckling;
mm = Millimeters;
M_{cr} = Elastic critical moment capacity;
MCS = Monte Carlo Simulation;
MPa = Megapascals;
M_r = Moment resistance;
Mr_{exp} = Experimentally obtained moment resistance;
$Mr_{theoretical}$ = Theoretically calculated moment resistance;
Mr_{hyp} = Moment resistance calculated using the proposed equation;
M_u = Elastic critical moment capacity;
M_y = Yield moment capacity;
s = Half of the sinusoidal wavelength;

S_x = Elastic section modulus about the strong axis;
t = Flange thickness;
t_f = Flange thickness;
t_w = Web thickness;
u_x = Torsional adjustment factor;
W = Torsional Adjustment;
w_{eq} = Equivalent web thickness;
Z_x = Plastic section modulus about the strong axis;

References

Canadian Standards Association. 2014. *Design of steel structures.*

Dassault Systemes Simulia Corp. 2014. "ABAQUS Analysis User's Manual."

Dassault Systemes Simulia Corp. 2019. *SIMULIA How-to Tutorial for Abaqus | Material Plasticity and Restart Analysis*.

Driver, R. G., H. H. Abbas, and R. Sause. 2006. "Shear Behavior of Corrugated Web Bridge Girders." *J. Struct. Eng.*, 132 (2): 195–203. https://doi.org/10.1061/(ASCE)0733-9445(2006)132:2(195).

Elgaaly, M., A. Seshadri, and R. W. Hamilton. 1997. "Bending Strength of Steel Beams with Corrugated Webs." *J. Struct. Eng.*, 123 (6): 772–782. https://doi.org/10.1061/(ASCE)0733-9445(1997)123:6(772).

Elkawas, A. A., M. F. Hassanein, and M. Elchalakani. 2018. "Lateral-torsional buckling strength and behaviour of high-strength steel corrugated web girders for bridge construction." *Thin-Walled Struct.*, 122: 112–123. https://doi.org/10.1016/j.tws.2017.10.021.

Feng, Y., L. Jiang, W. Zhou, and J. Han. 2019. "Lateral-torsional buckling of box beam with corrugated steel webs." *J. Cent. South Univ.*, 26 (7): 1946–1957. https://doi.org/10.1007/s11771-019-4122-0.

Hannebauer, D. 2008. "Zur Querschnitts- und Stabtragfähigkeit von Trägern mit profilierten Stegen."

Ibrahim, S. A. 2014. "Lateral torsional buckling strength of unsymmetrical plate girders with corrugated webs." *Eng. Struct.*, 81: 123–134. https://doi.org/10.1016/j.engstruct.2014.09.040.

Lindner, J. 1990. "Lateral torsional buckling of beams with trapezoidally corrugated webs." *Stab Steel Struct Bp. Hung.*

Moon, J., J.-W. Yi, B. H. Choi, and H.-E. Lee. 2009. "Lateral–torsional buckling of I-girder with corrugated webs under uniform bending." *Thin-Walled Struct.*, 47 (1): 21–30. https://doi.org/10.1016/j.tws.2008.04.005.

Nguyen, N. D., S. N. Kim, S.-R. Han, and Y.-J. Kang. 2010. "Elastic lateral-torsional buckling strength of I-girder with trapezoidal web corrugations using a new warping constant under uniform moment." *Eng. Struct.*, 32 (8): 2157–2165. https://doi.org/10.1016/j.engstruct.2010.03.018.

Pasternak, H., and G. Kubieniec. 2010. "PLATE GIRDERS WITH CORRUGATED WEBS." *J. Civ. Eng. Manag.*, 16 (2): 166–171. https://doi.org/10.3846/jcem.2010.17.

Sadowski, A. J., J. M. Rotter, T. Reinke, and T. Ummenhofer. 2015. "Statistical analysis of the material properties of selected structural carbon steels." *Struct. Saf.*, 53: 26–35. https://doi.org/10.1016/j.strusafe.2014.12.002.

Sause, R., H. H. Abbas, W. G. Wassef, R. G. Driver, and M. Elgaaly. 2003. "Corrugated Web Girder Shape and Strength Criteria." (03): 72.

Sayed-Ahmed, E. Y. 2005. "Lateral torsion-flexure buckling of corrugated web steel girders." *Proc. Inst. Civ. Eng. - Struct. Build.*, 158 (1): 53–69. https://doi.org/10.1680/stbu.2005.158.1.53.

Steelcon Fabrication Inc. 2015. *SIN Beam Video.*

Steelcon Fabrication Inc. 2019a. "Steelcon SIN Beam Projects." *Steelcon.ca*. Accessed November 9, 2021. https://steelcon.ca/sin-beam-projects/.

Steelcon Fabrication Inc. 2019b. “SIN Beam - Technical Guide v14.”
Zhang, Z., G. Li, and F. Sun. 2011. “Flexural-torsional buckling of H-beams with corrugated webs.”

Appendix A: Additional Experimental Results

Test #1 – WTA333/127x6 – 1

Figure A-1: End Profile of the Deformed WTA333/127x6 – 1

Figure A-2: Side Profile of the Deformed WTA333/127x6 – 1

Test #2 – WTA333/127x6 – 2

Figure A-3: Compression Flange of the Deformed WTA333/127x6 – 2

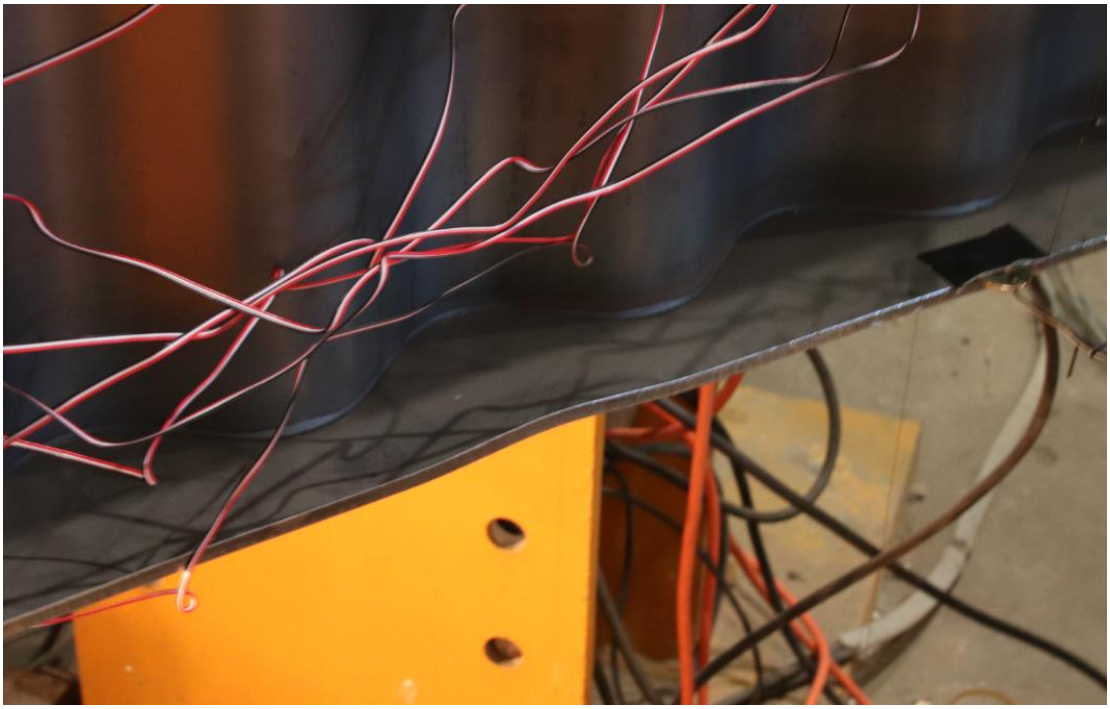

Figure A-4: Local Flange Buckling of the Deformed WTA333/127x6 – 2

Test #3 – WTA500/127x6

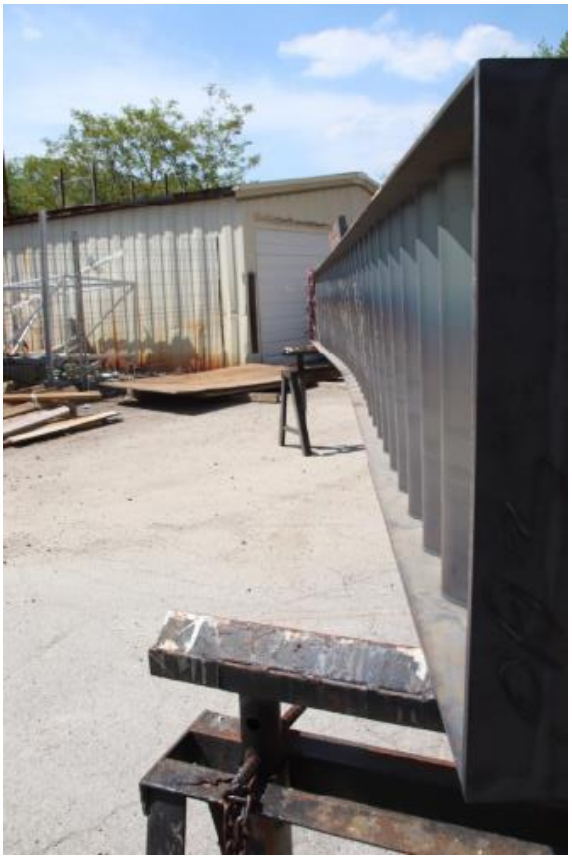

Figure A-5: End Profile of the Deformed WTA500/127x6

Figure A-6: Local Flange Buckling of the Deformed WTA500/127x6

Test #4.1 – WTA610/127x6

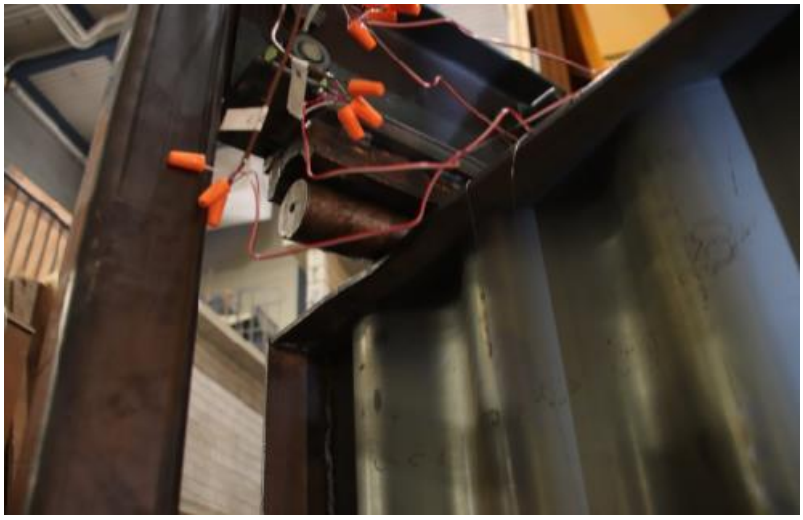

Figure A-7: Local Flange Buckling at Support of the WTA610/127x6

Test #4.2 – WTA610/127x6 (Retest)

Figure A-8: End Profile of the Deformed WTA610/127x6

Figure A-9: Local Flange Buckling of the Deformed WTA610/127x6

Test #5 – WTA750/127x6

Figure A-10: End Profile of the Deformed WTA750/127x6

Figure A-11: Local Flange Buckling and Yielding of the Deformed WTA750/127x6

Test #6 – WTB333/127x6

Figure A-12: End Profile of the Deformed WTB333/127x6

Figure A-13: Local Flange Buckling of the Deformed WTB333/127x6

Test #7 – WTC333/127x6

Figure A-14: End Profile of the Deformed WTC333/127x6

Figure A-15: Local Flange Buckling of the Deformed WTC333/127x6

Test #8 – WTF333/127x6

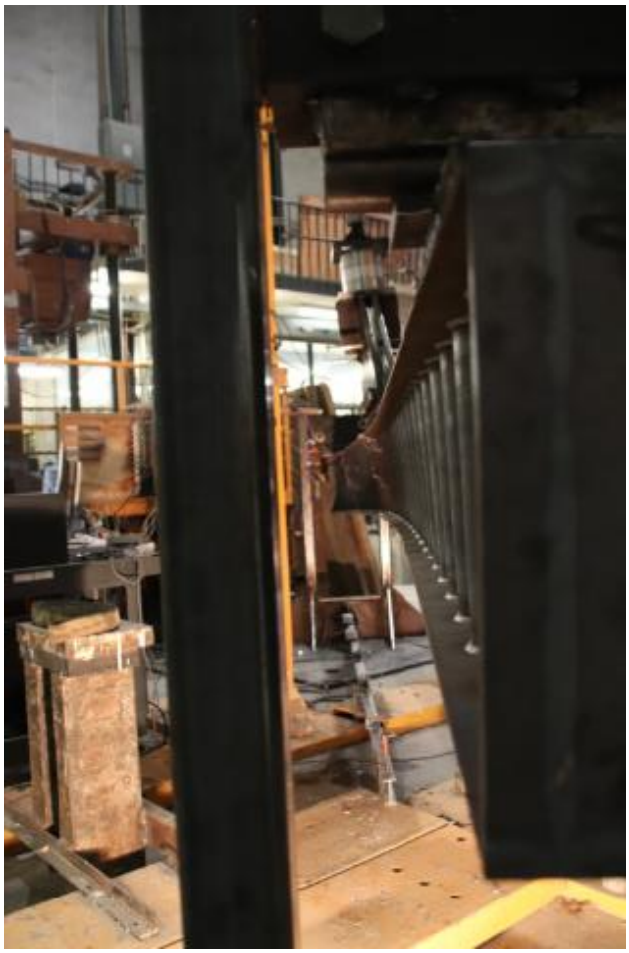

Figure A-16: End Profile of the Deformed WTF333/127x6

Figure A-17: Faint Local Flange Buckling of the Deformed WTF333/127x6

Test #9 – WTA333/127x6 – 9

Figure A-18: End Profile of the Deformed WTA333/127x6 – 9

Figure A-19: Faint Local Flange Buckling of the Deformed WTA333/127x6 – 9

Appendix B: Sample LTB Resistance Calculations

Conventional Method

The following calculation outlines the conventional process for obtaining LTB resistance of a WTA333/127x6 that is 5000 mm long under a simply supported span. This process uses two floating flanges to calculate all of the geometric properties. It then follows the S16-14 clause 13.6 (Canadian Standards Association 2014). Figure B-20 shows the Loading configuration and the bending moment and shear diagrams using a unit load.

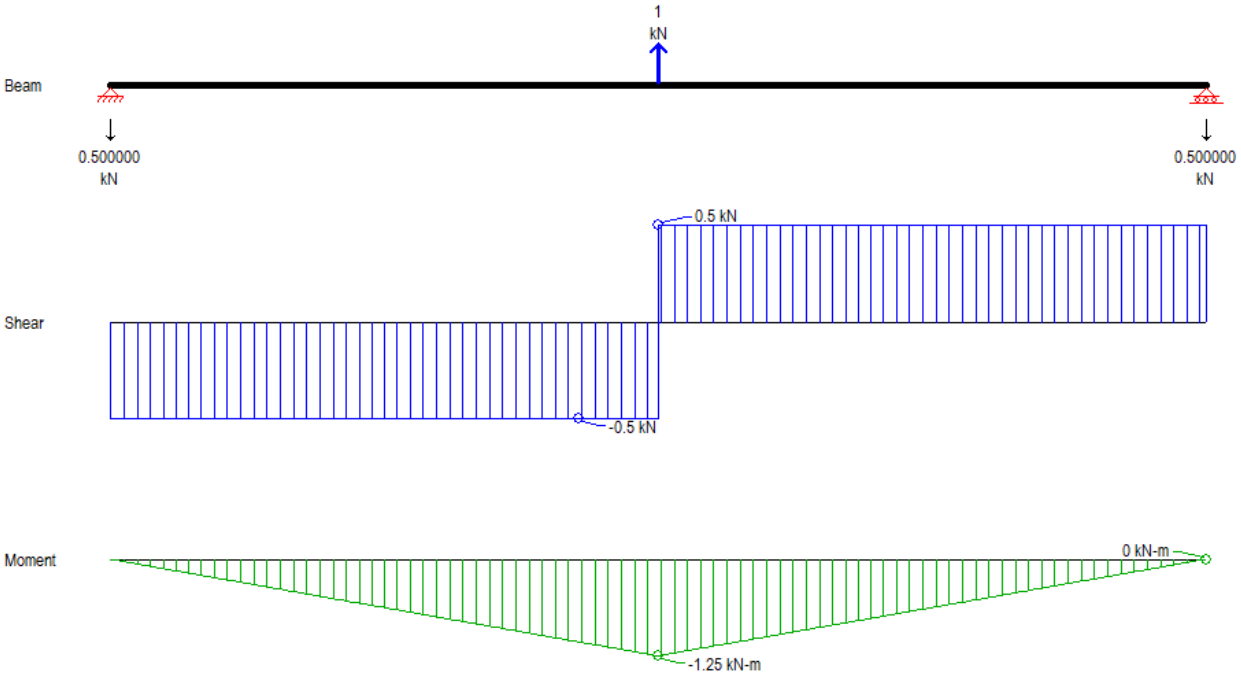

Figure B-20: Simply Supported beam Bending Moment and Shear Diagrams

First, the ω_2 Value is calculated based on the moment distribution on the beam.

$$\omega_2 = \frac{4M_{Max}}{\sqrt{M_{Max}^2 + 4M_a^2 + 7M_b^2 + 4M_c^2}} \leq 2.5 \qquad (13.6.a.ii)$$

$$\omega_2 = \frac{4 * 1.25kNm}{\sqrt{(1.25kNm)^2 + 4 * (0.62kNm)^2 + 7 * (1.25kNm)^2 + 4 * (0.62kNm^2}} = 1.27$$

Where M_{Max} is the maximum bending moment, M_a is the bending moment at the quarter point along the length of the beam, M_b is the bending moment at the halfway point along the beam and M_c is the bending moment at the three quarter point along the beam.

Next I_y, C_w, and J are calculated.

$$C_w = \frac{(d-t)^2 b^3 t}{24}$$ (Steelcon Fabrication Inc. 2019b)

$$C_w = \frac{(345-6)^2 (127)^3 (6)}{24} = 58850555686\ mm^6$$

$$J = \frac{2bt^3}{3}$$ (Steelcon Fabrication Inc. 2019b)

$$J = \frac{2(127)(6)^3}{3} = 18288\ mm^4$$

$$I_y = \frac{tb^3}{6}$$ (Steelcon Fabrication Inc. 2019b)

$$I_y = \frac{(6)(127)^3}{6} = 2048383\ mm^4$$

Now the critical elastic moment M_u can be calculated.

$$M_u = \frac{\omega_2 \pi}{L} \sqrt{EI_y GJ + \left(\frac{\pi E}{L}\right)^2 I_y C_w} \quad (13.6.a.ii)$$

$$M_u =$$

$$\frac{(1.27)\pi}{(5000)} \sqrt{(200000)(2048383)(77000)(18288) + \left(\frac{\pi(200000)}{5000}\right)^2 (2048383)(5.89 * 10^{10})}$$

$$M_u = 39.9\ kNm$$

Since most SIN beams are classified as class three sections based on the flange properties especially the ones utilized in this these the yield moment is calculated next. In order to do so the elastic section modulus S_x is used.

$$S_x = \frac{b(d^3 - d_1^3)}{6d} \quad \text{(CISC p7-83)}$$

$$S_x = \frac{(127)((345)^3 - (333)^3)}{6(345)} = 253852\ mm^3$$

$$M_y = S_x F_y \quad (13.5.b)$$

$$M_y = (253852)(408) = 103.57\ kNm$$

Then based on the comparison of the critical elastic moment to the elastic moment the LTB resistance can be calculated.

$$When\ \ M_u > 0.67 M_y \quad (13.6.b)$$

$$Then\ M_r = 1.15\emptyset M_y \left[1 - \frac{0.28M_y}{M_u}\right]$$

$$When\ \ M_u \leq 0.67M_y$$

$$Then\ \ M_r = \emptyset M_u$$

$$39.9\ kNm < 0.67(103.57) = 69.39\ kNm$$

$$M_r = (1)(39.9) = 39.9kNm$$

Proposed Method

The proposed method follows a similar procedure to the conventional method however it uses an equivalent thickness equation to use an I shaped geometry to calculate the various constants. First the equivalent thickness is calculated.

$$w_{eq} = t_w + \left(\frac{3 * a_3}{s}\right) * t_w$$

$$w_{eq} = (1.897) + \left(\frac{3 * (40)}{(77.5)}\right) * (1.897) = 4.83\ mm$$

Then using the equivalent thickness the remainder of the calculation follows the standard outlined in S16-14 clause 13.6 using standard I shape for geometric constant calculation

$$C_w = \frac{1}{24}(d - t)^2 b^3 t) \qquad \text{(CISC p7-88)}$$

$$C_w = \frac{1}{24}\big((345) - (6)\big)^2 (127)^3 (6)) = \ 58850555686\ mm^6$$

$$J = \frac{1}{3}(2tb^3 + (d-t){w_{eff}}^3) \quad \text{(CISC p7-88)}$$

$$J = \frac{1}{3}\big(2(6)(127)^3 + \big((345) - (6)\big)(4.83)^3\big) = 31054\ mm^4$$

$$I_y = \frac{1}{12}(2tb^3 + (d-2t){w_{eff}}^3) \quad \text{(CISC p7-88)}$$

$$I_y = \frac{1}{12}\big(2(6)(127)^3 + \big((345) - 2(6)\big)(4.83)^3\big) = 2051613\ mm^4$$

Now the critical elastic moment M_u can be calculated.

$$M_u = \frac{\omega_2 \pi}{L}\sqrt{EI_yGJ + \left(\frac{\pi E}{L}\right)^2 I_y C_w} \quad \text{(13.6.a.ii)}$$

$$M_u =$$

$$\frac{(1.27)\pi}{(5000)}\sqrt{(200000)(2051613)(77000)(31054) + \left(\frac{\pi(200000)}{5000}\right)^2 (2051613)(5.89 * 10^{10})}$$

$$M_u = 43.07\ kNm$$

Just as before because the beam is class three the yield moment is calculated next. In order to do so the elastic section modulus S_x is used.

$$S_x = \frac{1}{6d}\big[bd^3 - \big(b - w_{eq}\big)(d-2t)^3\big] \quad \text{(CISC p7-87)}$$

$$S_x = \frac{1}{6(345)}[(127)(345)^3 - ((127) - (4.83))((345) - 2(6))^3] = 340089\ mm^3$$

$$M_y = S_x F_y \quad (13.5.b)$$

$$M_y = (340089)(408) = 138.75\ kNm$$

It should be noted that this elastic moment value calculated is strictly for the purpose of the LTB calculation process. This does not reflect the beams actual elastic moment strength as the flanges cannot withstand axial load. The conventional approach of using two floating flanges to calculate the moment strength is the correct method when calculating sectional moment strength.

Now based on the comparison of the critical elastic moment to the elastic moment the LTB resistance can be calculated.

$$When\ \ M_u > 0.67M_y \quad (13.6.b)$$

$$Then\ M_r = 1.15\emptyset M_y \left[1 - \frac{0.28M_y}{M_u}\right]$$

$$When\ \ M_u \leq 0.67M_y$$

$$Then\ \ M_r = \emptyset M_u$$

$$43.07kNm < 0.67(138.75) = 92.96\ kNm$$

$$M_r = (1)(43.07) = 43.07kNm$$

Appendix C: List of Beam Sizes Used in the Numerical Analysis

Table C-1: List of Beam Sizes Used in the Numerical Analysis

Designation	Web Thickness	Web Height	Flange Width	Flange Thickness	Depth	Mr Conventional	Mr Hypthetical
WTA	1.897	333	127	6	345	29.09	32.10
WTA	1.897	333	152	8	349	69.19	72.19
WTA	1.897	333	152	10	353	95.02	97.79
WTA	1.897	333	152	13	359	142.26	144.70
WTA	1.897	333	152	19	371	226.91	235.74
WTA	1.897	500	152	6	512	39.55	42.91
WTA	1.897	500	152	8	516	92.50	95.87
WTA	1.897	500	152	10	520	122.25	125.48
WTA	1.897	500	152	13	526	174.09	177.07
WTA	1.897	500	152	19	538	307.22	309.75
WTA	1.897	610	152	6	622	46.82	50.31
WTA	1.897	610	152	8	626	108.85	112.36
WTA	1.897	610	152	10	630	141.80	145.20
WTA	1.897	610	152	13	636	197.68	200.89
WTA	1.897	610	152	19	648	336.63	339.44
WTA	1.897	750	127	6	762	56.29	59.91
WTA	1.897	750	152	8	766	130.26	133.90
WTA	1.897	750	152	10	770	167.72	171.28
WTA	1.897	750	152	13	776	229.55	232.97
WTA	1.897	750	152	19	788	377.70	380.80
WTA	1.897	333	203	13	359	224.73	237.27
WTA	1.897	333	203	19	371	354.98	370.22
WTA	1.897	500	203	13	526	314.36	334.56
WTA	1.897	500	203	19	538	490.59	517.04
WTA	1.897	610	203	13	636	373.41	441.88
WTA	1.897	610	203	19	648	577.04	610.63
WTA	1.897	750	203	13	776	449.17	522.74
WTA	1.897	750	203	19	788	686.55	728.79
WTB	2.657	333	127	6	345	29.09	36.80
WTB	2.657	333	152	8	349	69.19	77.16
WTB	2.657	333	152	10	353	95.02	102.46
WTB	2.657	333	152	13	359	142.26	148.89
WTB	2.657	333	152	19	371	226.91	240.32
WTB	2.657	500	152	6	512	66.07	75.31
WTB	2.657	500	152	8	516	92.50	101.52

WTB	2.657	500	152	10	520	122.25	130.93
WTB	2.657	500	152	13	526	174.09	182.17
WTB	2.657	500	152	19	538	307.22	314.14
WTB	2.657	610	152	6	622	78.80	88.37
WTB	2.657	610	152	8	626	108.85	118.27
WTB	2.657	610	152	10	630	141.80	150.98
WTB	2.657	610	152	13	636	197.68	206.39
WTB	2.657	610	152	19	648	336.63	344.32
WTB	2.657	750	152	6	762	95.30	105.18
WTB	2.657	750	152	8	766	130.26	140.06
WTB	2.657	750	152	10	770	167.72	177.35
WTB	2.657	750	152	13	776	229.55	238.83
WTB	2.657	750	152	19	788	377.70	386.16
WTB	2.657	333	203	13	359	224.73	243.42
WTB	2.657	333	203	19	371	354.98	376.89
WTB	2.657	500	203	13	526	314.36	343.62
WTB	2.657	500	203	19	538	490.59	528.27
WTB	2.657	610	203	13	636	373.41	447.85
WTB	2.657	610	203	19	648	577.04	624.24
WTB	2.657	750	203	13	776	449.17	528.97
WTB	2.657	750	203	19	788	686.55	744.35
WTC	3.038	333	152	6	345	47.49	61.17
WTC	3.038	333	152	8	349	69.19	82.36
WTC	3.038	333	152	10	353	95.02	107.43
WTC	3.038	333	152	13	359	142.26	153.42
WTC	3.038	333	152	19	371	226.91	244.18
WTC	3.038	500	152	6	512	66.07	81.25
WTC	3.038	500	152	8	516	92.50	107.47
WTC	3.038	500	152	10	520	122.25	136.77
WTC	3.038	500	152	13	526	174.09	187.71
WTC	3.038	500	152	19	538	307.22	318.95
WTC	3.038	610	152	6	622	78.80	94.61
WTC	3.038	610	152	8	626	108.85	124.56
WTC	3.038	610	152	10	630	141.80	157.19
WTC	3.038	610	152	13	636	197.68	212.36
WTC	3.038	610	152	19	648	336.63	349.67
WTC	3.038	750	152	6	762	95.30	111.71
WTC	3.038	750	152	8	766	130.26	146.65
WTC	3.038	750	152	10	770	167.72	183.91
WTC	3.038	750	152	13	776	229.55	245.23
WTC	3.038	750	152	19	788	377.70	392.05

WTC	3.038	333	203	13	359	224.73	248.38
WTC	3.038	333	203	19	371	354.98	381.86
WTC	3.038	500	203	13	526	314.36	350.97
WTC	3.038	500	203	19	538	490.59	536.66
WTC	3.038	610	203	13	636	373.41	454.42
WTC	3.038	610	203	19	648	577.04	634.30
WTC	3.038	750	203	13	776	449.17	535.84
WTC	3.038	750	203	19	788	686.55	837.23
WTF	4.176	333	152	6	345	47.49	78.38
WTF	4.176	333	152	8	349	69.19	99.98
WTF	4.176	333	152	10	353	95.02	124.81
WTF	4.176	333	152	13	359	142.26	169.82
WTF	4.176	333	152	19	371	226.91	255.99
WTF	4.176	500	152	6	512	66.07	101.17
WTF	4.176	500	152	8	516	92.50	128.03
WTF	4.176	500	152	10	520	122.25	157.39
WTF	4.176	500	152	13	526	174.09	207.77
WTF	4.176	500	152	19	538	307.22	336.94
WTF	4.176	610	152	6	622	78.80	115.84
WTF	4.176	610	152	8	626	108.85	146.48
WTF	4.176	610	152	10	630	141.80	179.28
WTF	4.176	610	152	13	636	197.68	234.11
WTF	4.176	610	152	19	648	336.63	369.69
WTF	4.176	750	152	6	762	95.30	134.31
WTF	4.176	750	152	8	766	130.26	169.97
WTF	4.176	750	152	10	770	167.72	207.47
WTF	4.176	750	152	13	776	229.55	268.62
WTF	4.176	750	152	19	788	377.70	414.10
WTF	4.176	333	203	13	359	224.73	262.74
WTF	4.176	333	203	19	371	354.98	394.88
WTF	4.176	500	203	13	526	314.36	373.15
WTF	4.176	500	203	19	538	490.59	559.19
WTF	4.176	610	203	13	636	373.41	478.93
WTF	4.176	610	203	19	648	577.04	661.50
WTF	4.176	750	203	13	776	449.17	561.62
WTF	4.176	750	203	19	788	686.55	861.84

Appendix D: Histograms Of Monte Carlo Simulations

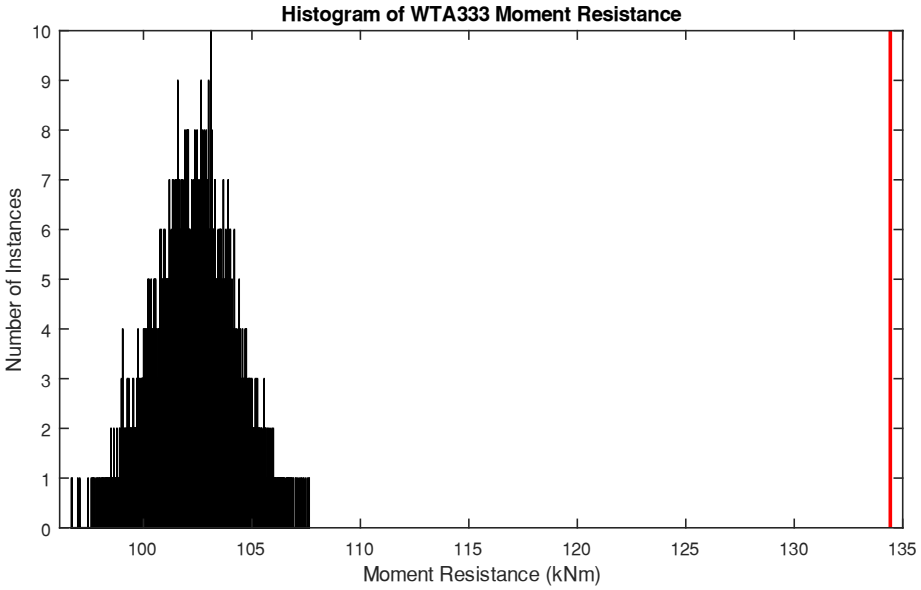

Figure D-21: Histogram of WTA333 Moment Resistance

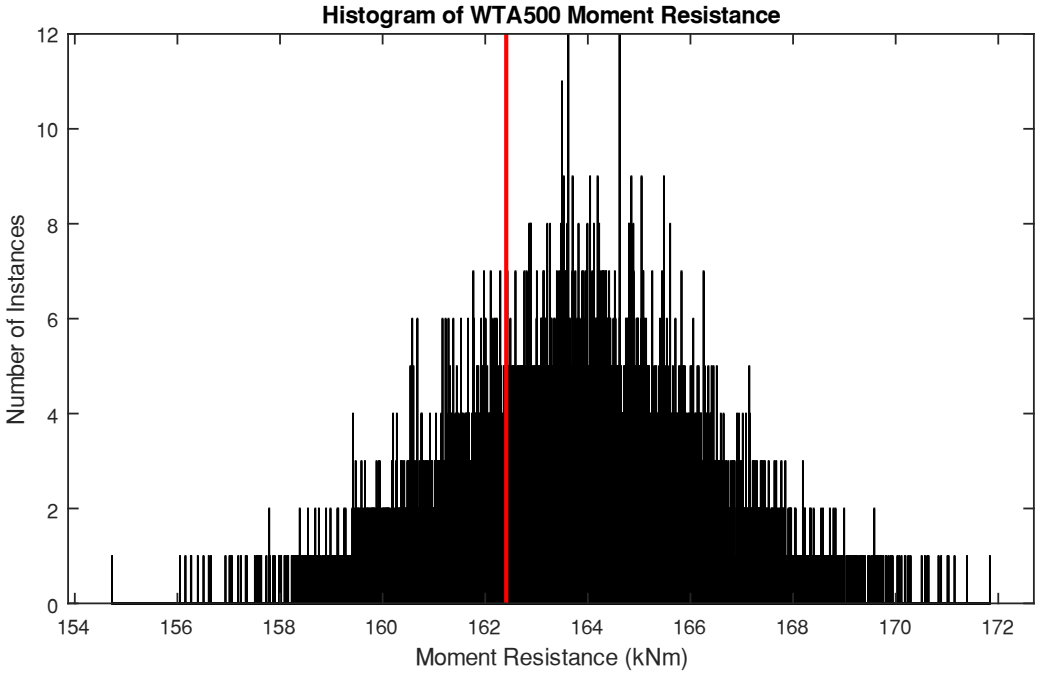

Figure D-22: Histogram of WTA500 Moment Resistance

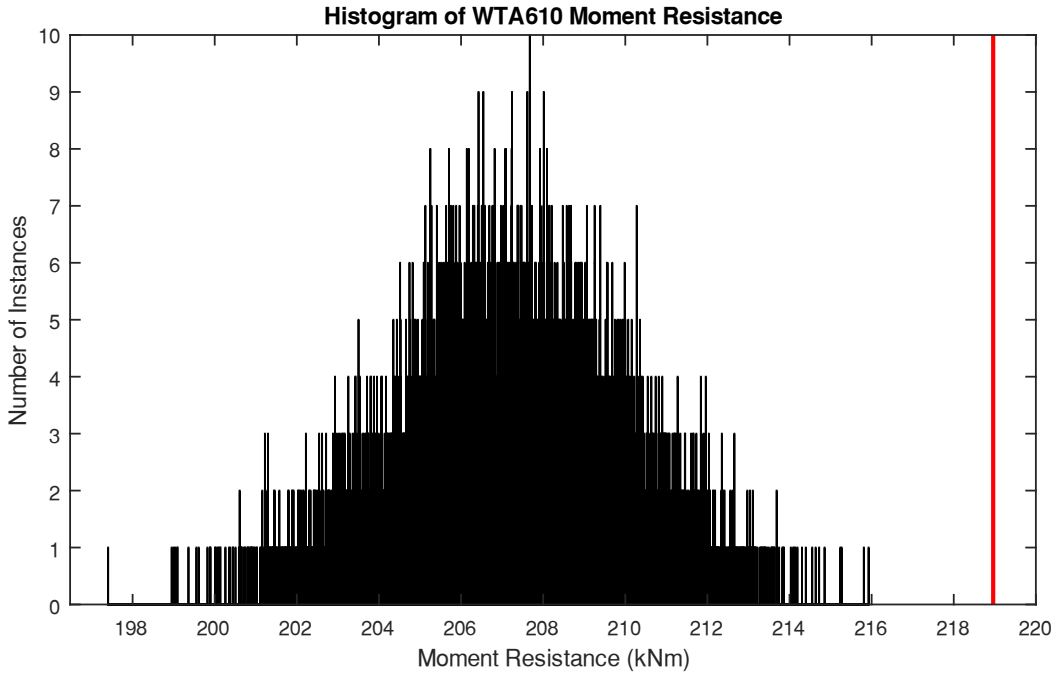

Figure D-23: Histogram of WTA610 Moment Resistance

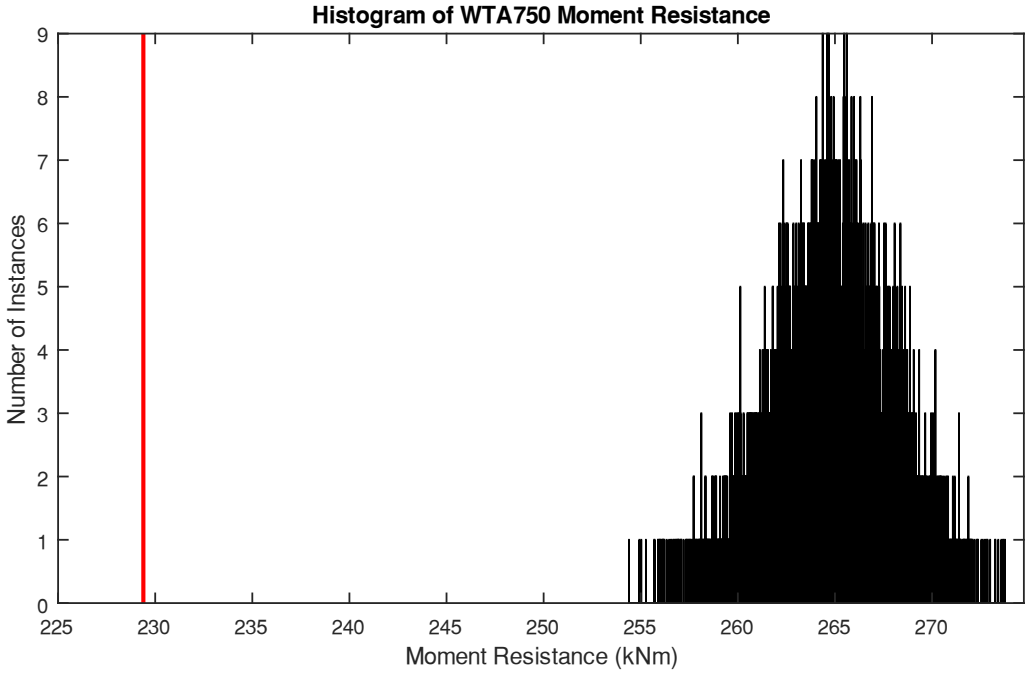

Figure D-24: Histogram of WTA750 Moment Resistance

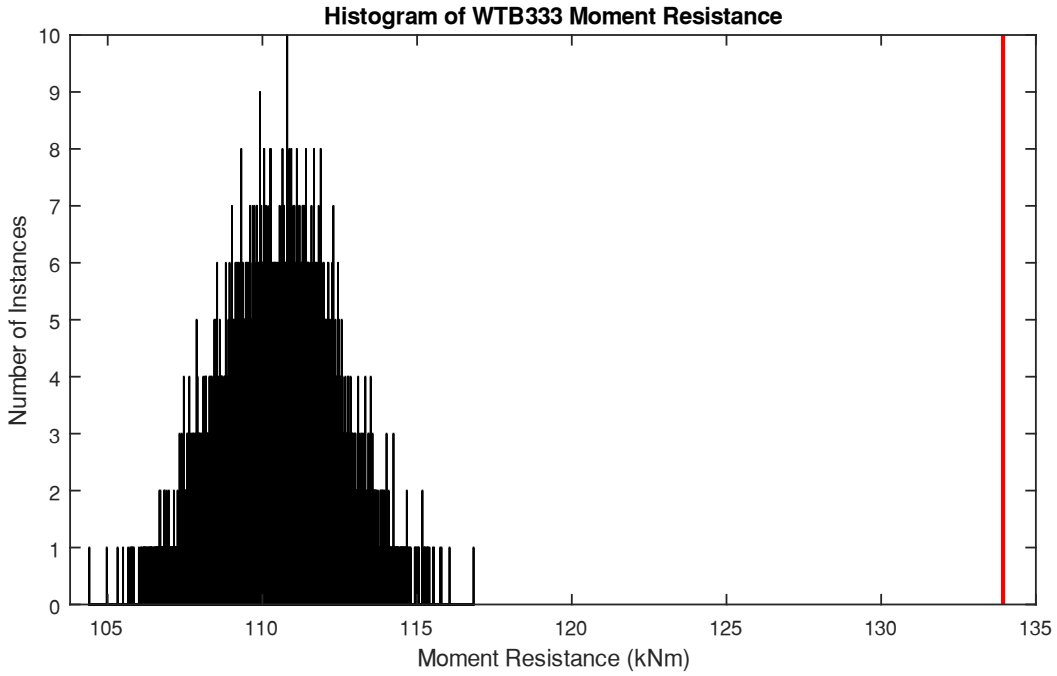

Figure D-25: Histogram of WTB333 Moment Resistance

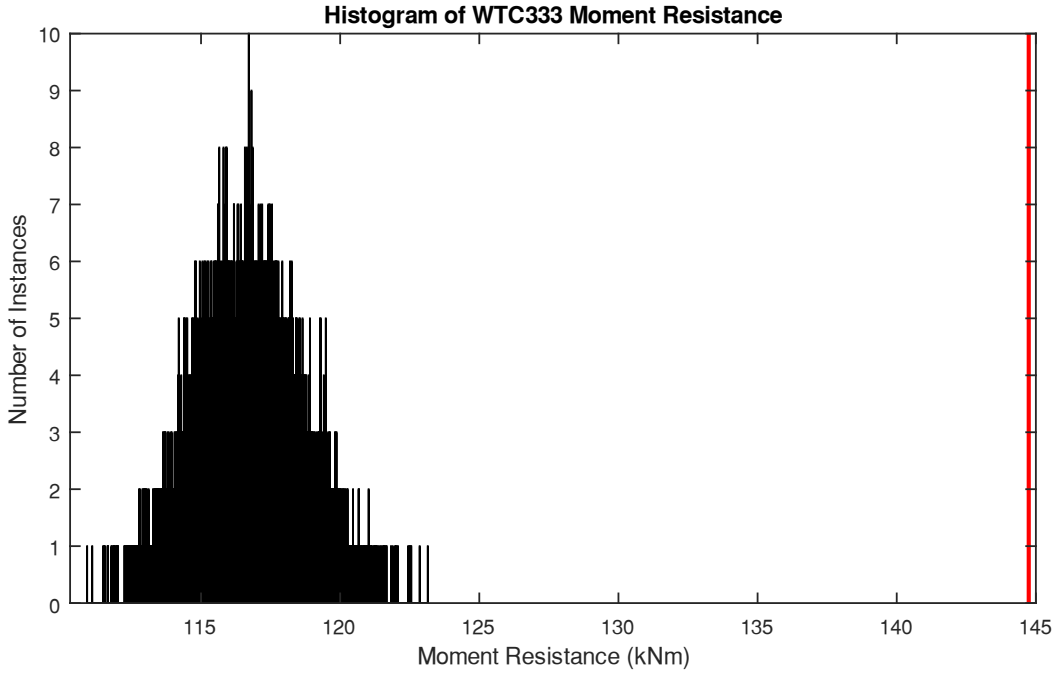

Figure D-26: Histogram of WTC333 Moment Resistance

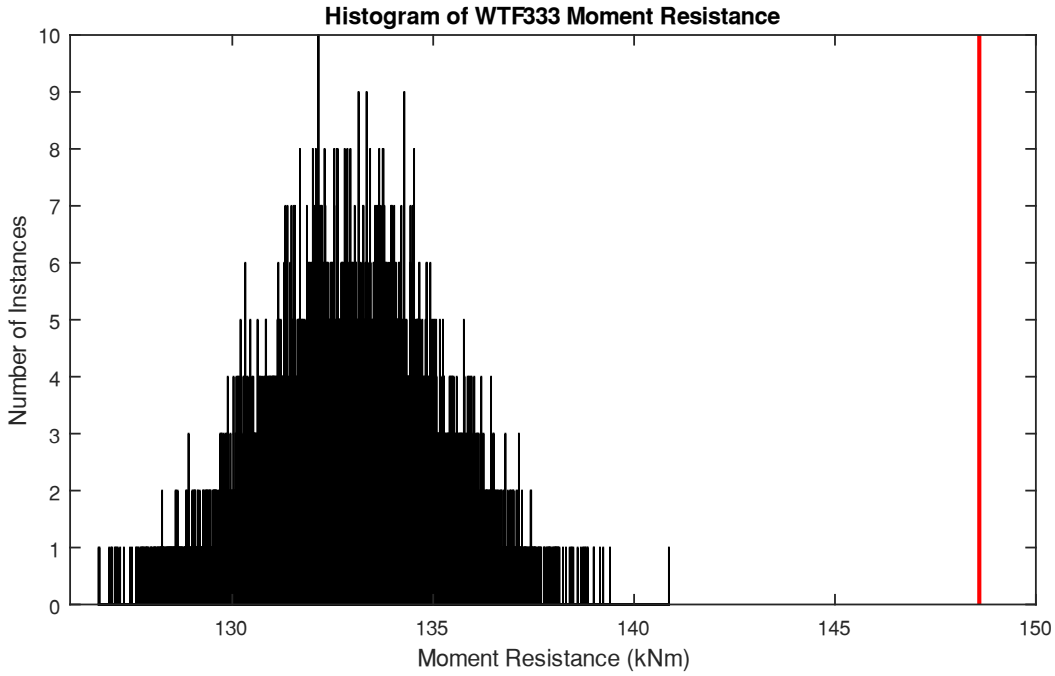

Figure D-27: Histogram of WTF333 Moment Resistance

Appendix E: Experiment Drawings

The following pages outline the drawings used in the construction of the testing apparatus.

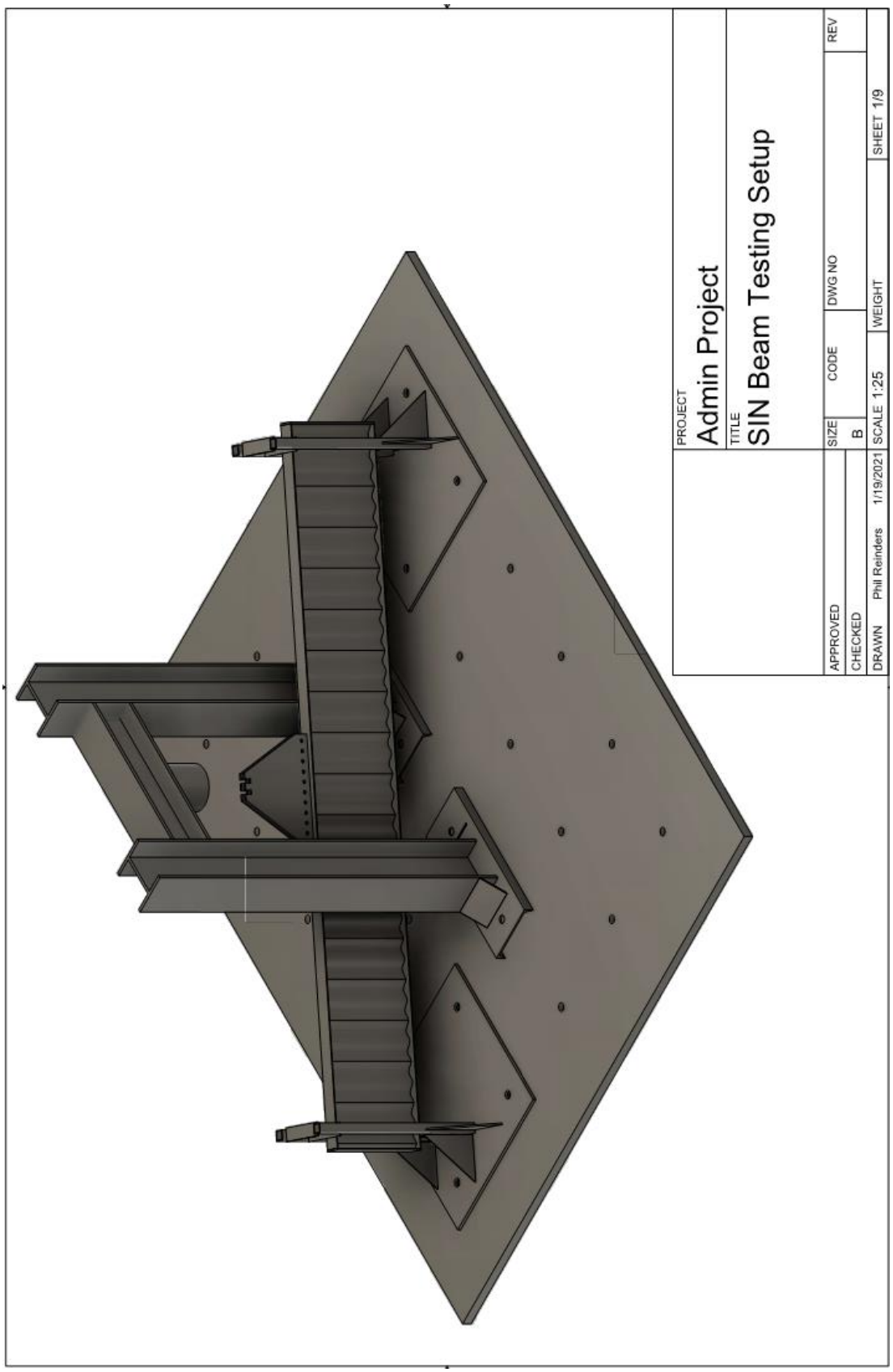
PROJECT
Admin Project
TITLE
SIN Beam Testing Setup
SIZE
B
CODE
DWG NO
REV
APPROVED
CHECKED
DRAWN Phil Reinders 1/19/2021
SCALE 1:25
WEIGHT
SHEET 1/9

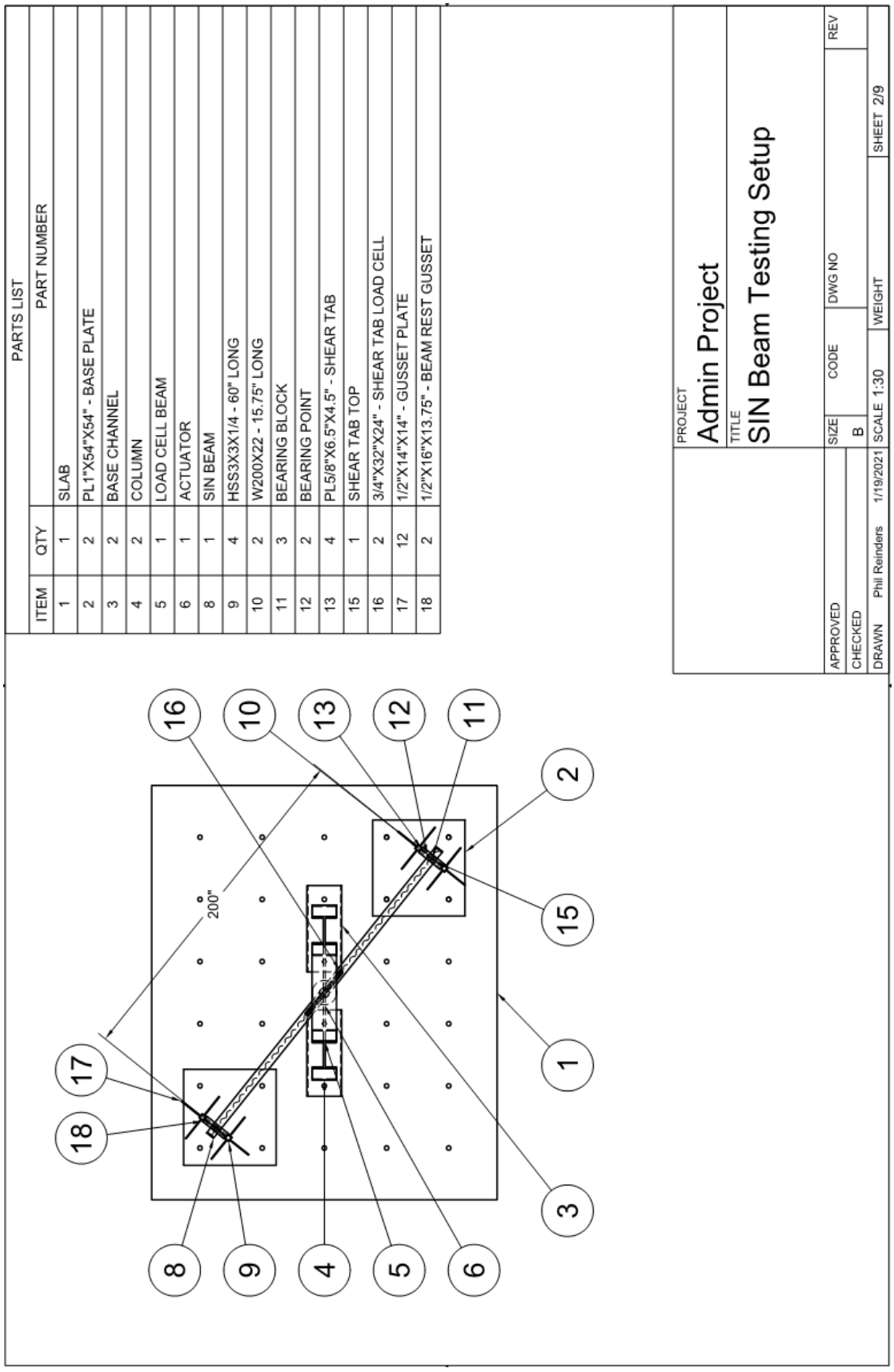
PARTS LIST
ITEM QTY PART NUMBER
1 1 SLAB
2 2 PL1"X54"X54" - BASE PLATE
3 2 BASE CHANNEL
4 2 COLUMN
5 1 LOAD CELL BEAM
6 1 ACTUATOR
8 1 SIN BEAM
9 4 HSS3X3X1/4 - 60" LONG
10 2 W200X22 - 15.75" LONG
11 3 BEARING BLOCK
12 2 BEARING POINT
13 4 PL5/8"X6.5"X4.5" - SHEAR TAB
15 1 SHEAR TAB TOP
16 2 3/4"X32"X24" - SHEAR TAB LOAD CELL
17 12 1/2"X14"X14" - GUSSET PLATE
18 2 1/2"X16"X13.75" - BEAM REST GUSSET
200"
PROJECT
Admin Project
TITLE
SIN Beam Testing Setup
APPROVED
CHECKED
DRAWN Phil Reinders 1/19/2021
SIZE B
CODE
DWG NO
REV
SCALE 1:30
WEIGHT
SHEET 2/9

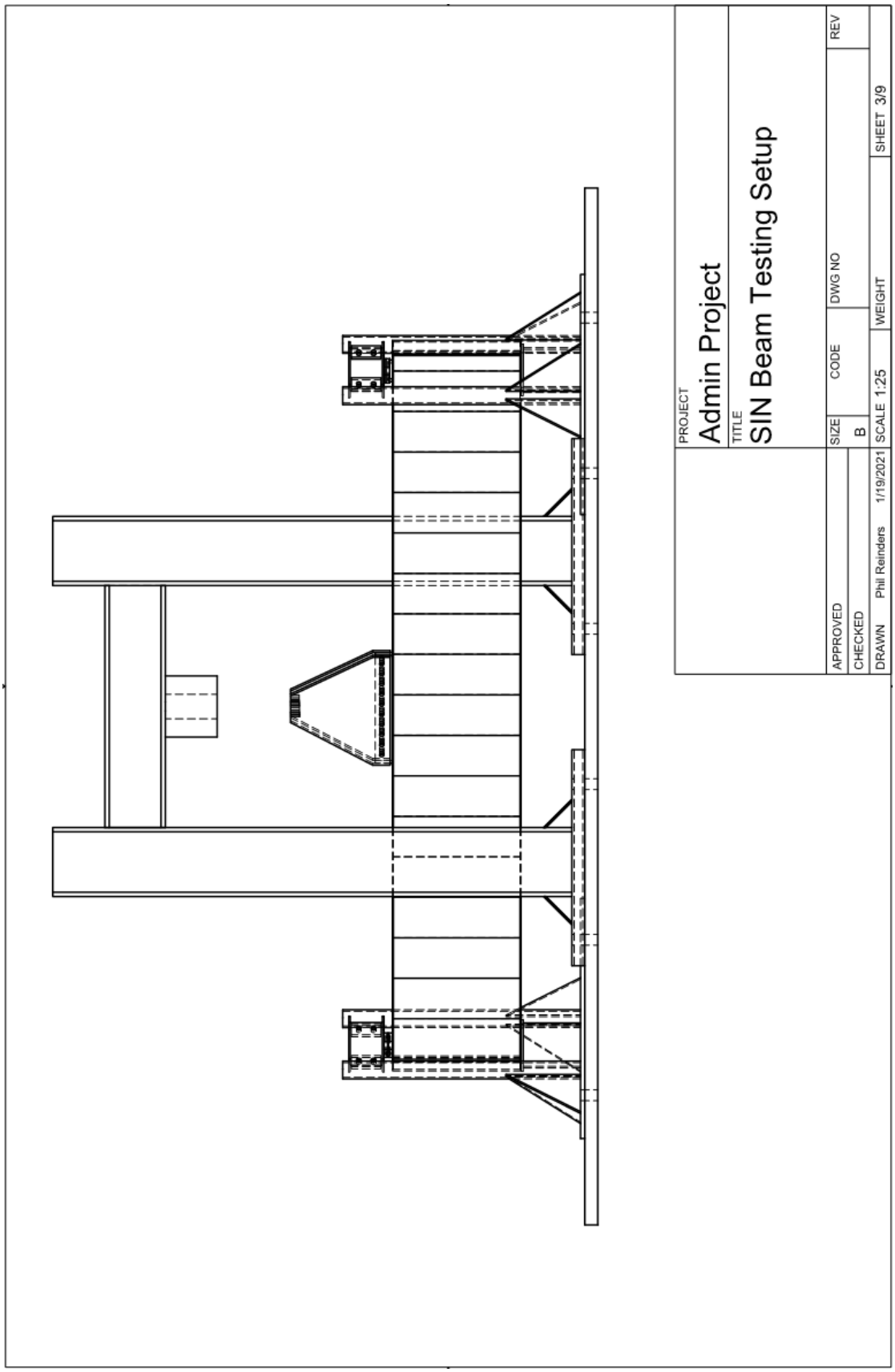
PROJECT
Admin Project
TITLE
SIN Beam Testing Setup
SIZE
B
CODE
DWG NO
REV
APPROVED
CHECKED
DRAWN
Phil Reinders
1/19/2021
SCALE 1:25
WEIGHT
SHEET 3/9

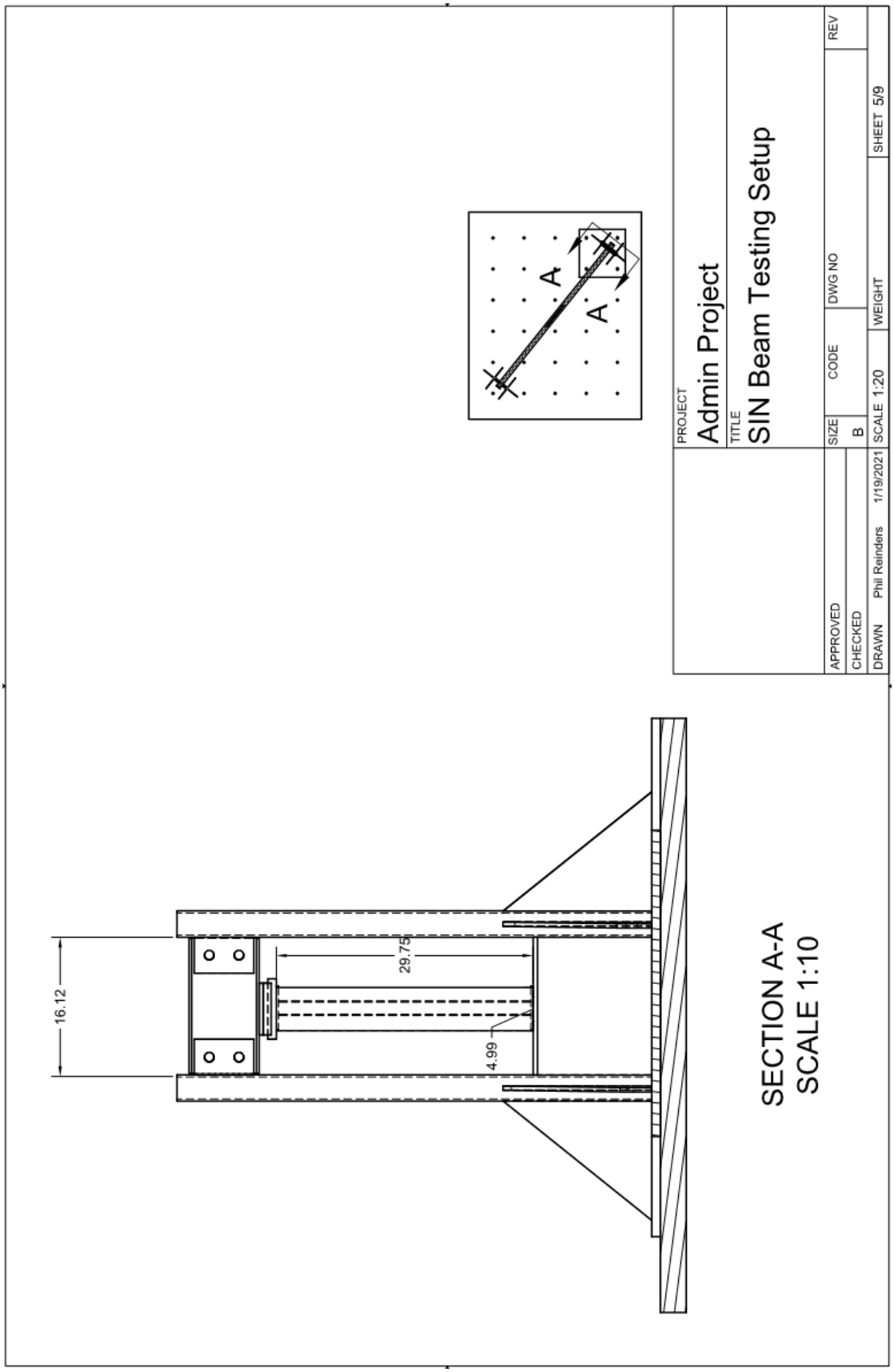
A
A
16.12
29.75
4.99
SECTION A-A
SCALE 1:10
PROJECT
Admin Project
TITLE
SIN Beam Testing Setup
SIZE
B
CODE
DWG NO
REV
SCALE 1:20
WEIGHT
SHEET 5/9
APPROVED
CHECKED
DRAWN
Phil Reinders
1/19/2021

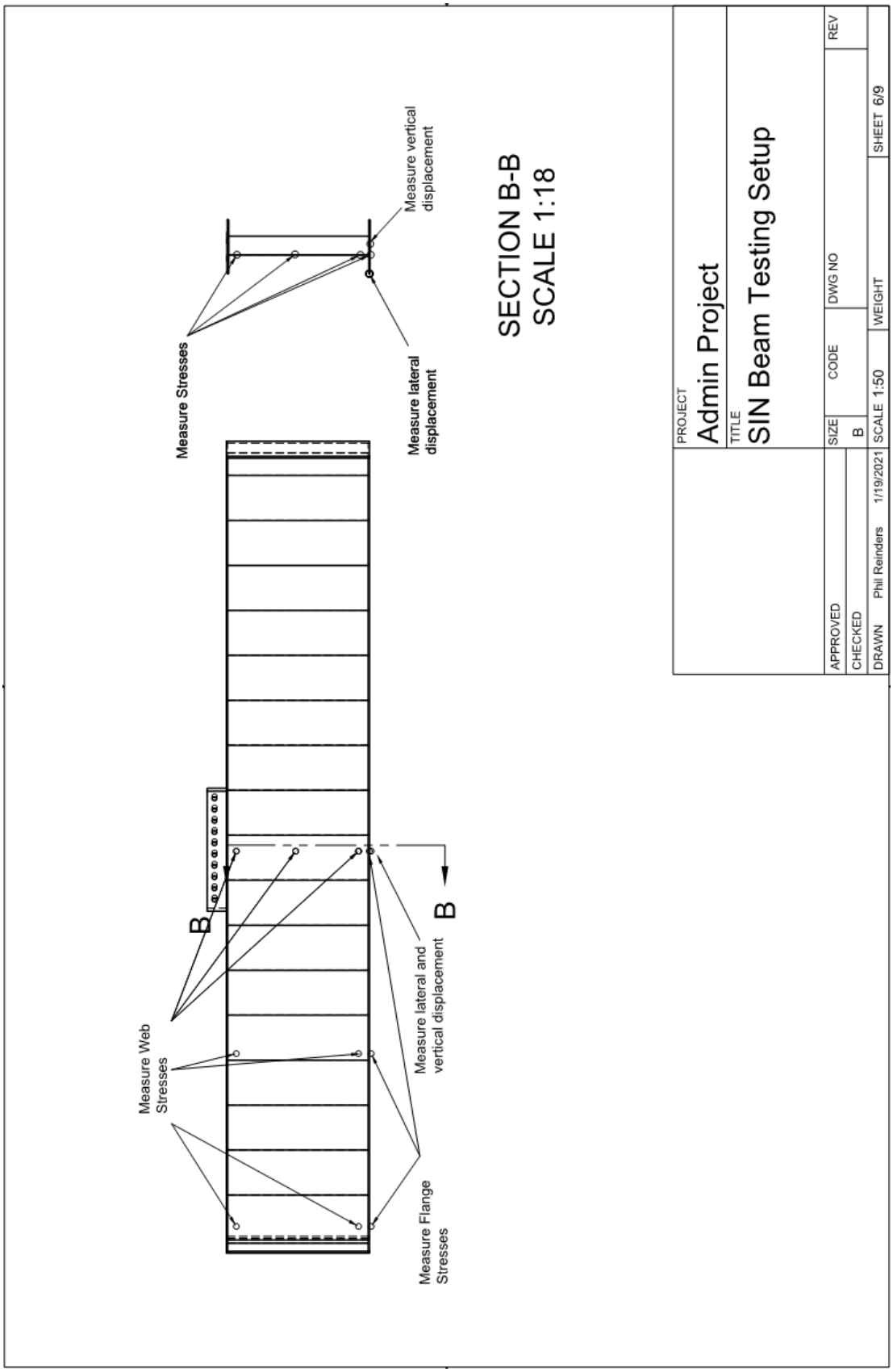
SECTION B-B
SCALE 1:18
Measure vertical displacement
Measure Stresses
Measure lateral displacement
B
B
Measure Web Stresses
Measure lateral and vertical displacement
Measure Flange Stresses
PROJECT
Admin Project
TITLE
SIN Beam Testing Setup
SIZE
B
CODE
DWG NO
REV
APPROVED
CHECKED
DRAWN Phil Reinders 1/19/2021
SCALE 1:50
WEIGHT
SHEET 6/9

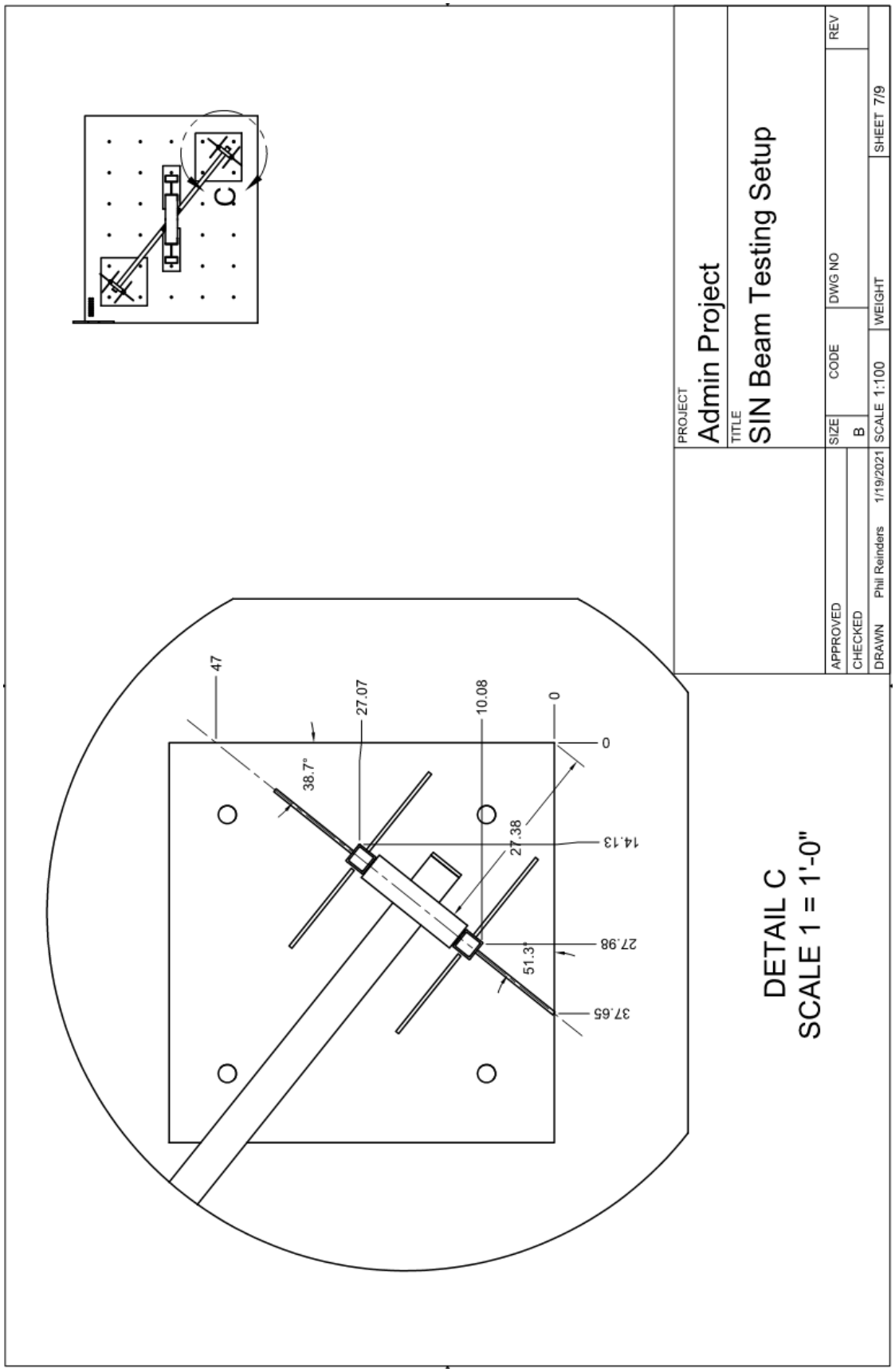
C
47
27.07
10.08
0
0
38.7°
27.38
14.13
27.98
51.3°
37.65
DETAIL C
SCALE 1 = 1'-0"
PROJECT
Admin Project
TITLE
SIN Beam Testing Setup
SIZE
B
CODE
DWG NO
REV
APPROVED
CHECKED
DRAWN
Phil Reinders
1/19/2021
SCALE 1:100
WEIGHT
SHEET 7/9

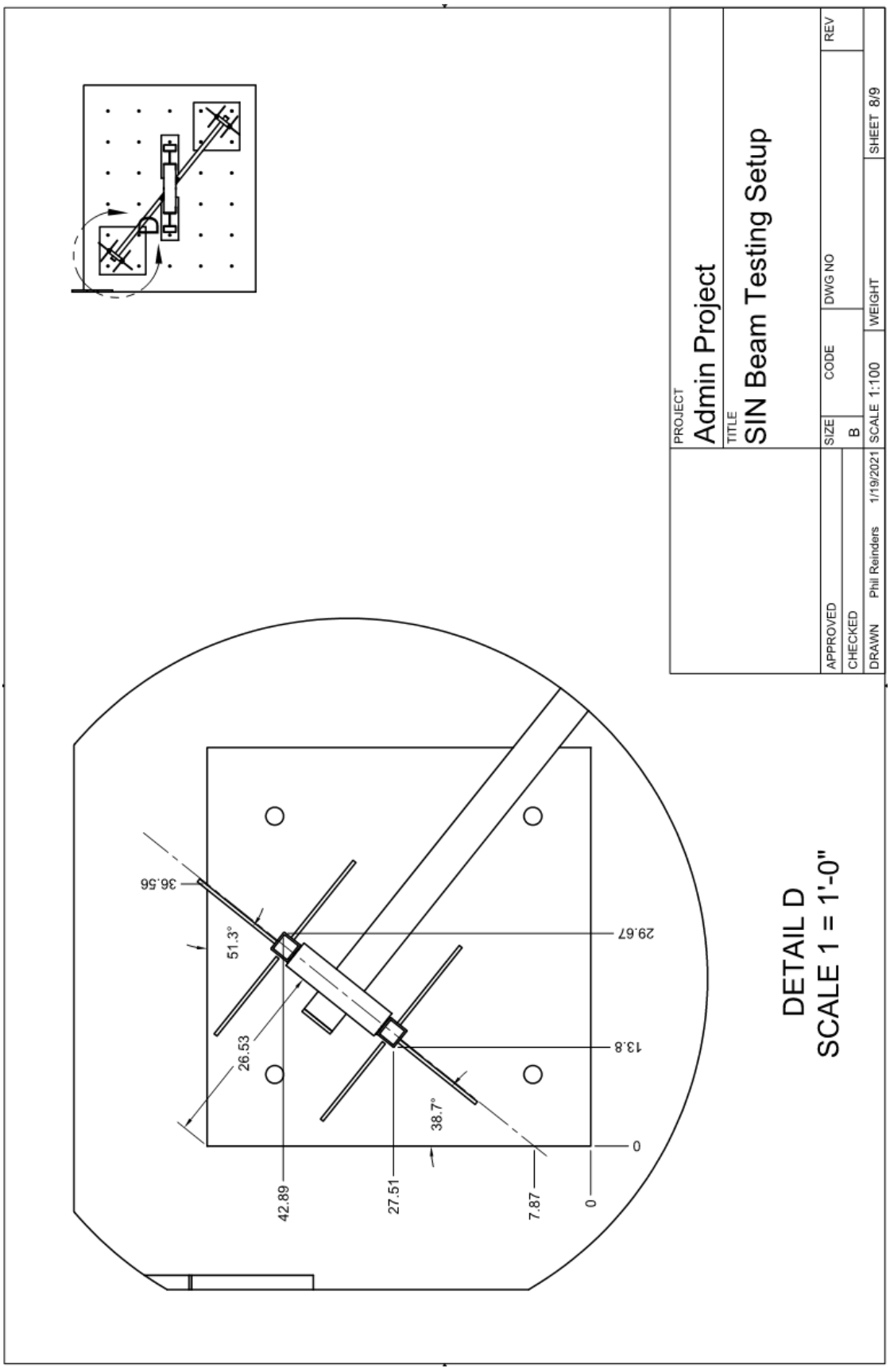
PROJECT
Admin Project
TITLE
SIN Beam Testing Setup
SIZE
B
CODE
DWG NO
REV
SCALE 1:100
WEIGHT
SHEET 8/9
APPROVED
CHECKED
DRAWN Phil Reinders 1/19/2021
DETAIL D
SCALE 1 = 1'-0"
36.56
51.3°
29.67
26.53
13.8
38.7°
0
42.89
27.51
7.87
0

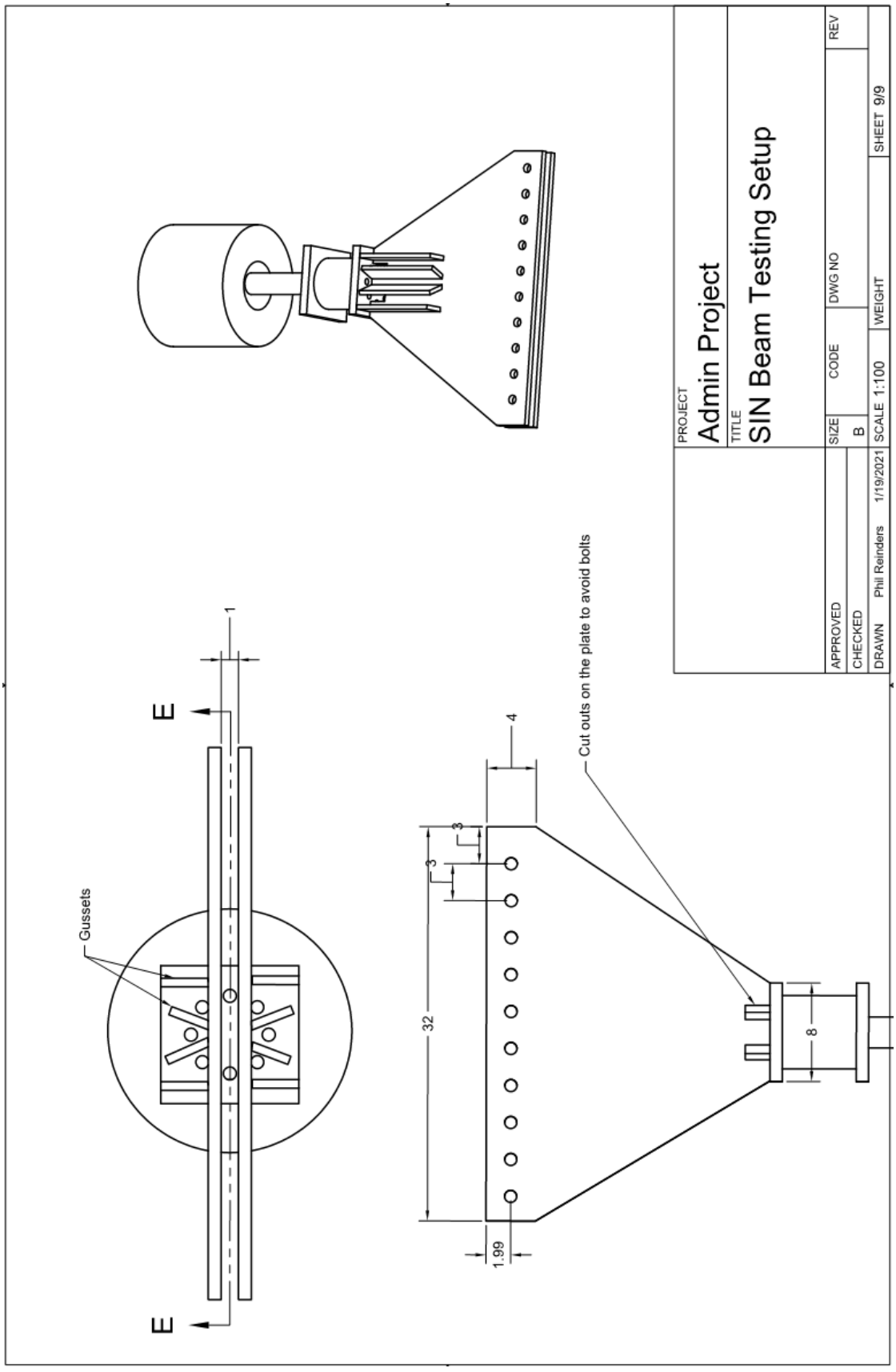
PROJECT
Admin Project
TITLE
SIN Beam Testing Setup
SIZE
B
CODE
DWG NO
REV
SCALE 1:100
WEIGHT
SHEET 9/9
APPROVED
CHECKED
DRAWN Phil Reinders 1/19/2021
E
E
Gussets
1
4
3
3
32
1.99
8
Cut outs on the plate to avoid bolts